OPTIMAL VOIDAGE REPLACEMENT RATIO FOR VISCOUS AND HEAVY OIL RESERVOIRS

A REPORT SUBMITTED TO THE DEPARTMENT OF ENERGY RESOURCES ENGINEERING

OF STANFORD UNIVERSITY

IN PARTIAL FULFILLMENT OF THE REQUIREMENTS FOR THE DEGREE OF MASTER OF SCIENCE

By
David Emilio Delgado
June 2012

I certify that I have read this report and that in my opinion it is fully adequate, in scope and in quality, as partial fulfillment of the degree of Master of Science in [Energy Resources] [Petroleum] Engineering.

_____

Prof. Anthony R. Kovscek
(Principal Advisor)

Abstract

Historically a voidage replacement ratio (VRR) of 1 is assumed to be optimal for oil recovery regardless of whether recovery is occurring from an unconventional heavy oil reservoir or a conventional oil reservoir. That is, it is assumed that of all scenarios, the most oil recovery occurs when the amount of fluids injected into the subsurface equals the amount that comes out. Recently, work has been published that analyzed both field and core-scale data to conclude a VRR of 1 is suboptimal for certain kinds of viscous and heavy oil reservoirs. We seek to understand the conditions under which a VRR of 1 is suboptimal using simulation models. On core-scale models, we tested the sensitivity of the optimal VRR to the curvature of our relative permeability relationships, the critical gas saturation, the chemistry of our oil, the permeability distribution of our model, high and low permeability streaks, permeability cul-de-sacs, the reference scale at which we compare results, and our three-phase model. Realistic relative permeability curves based off rock and fluid interactions observed in the literature were developed and used in the majority of our simulations. We have found that gas mobility is an influential parameter in determining the optimal VRR. The heterogeneity in our model also influenced the optimal VRR to a lesser extent.

Using a geological model of a deep-water, channelized reservoir, we observed at reservoir-scale the influence of heterogeneity and connectivity on the optimal VRR. We found connectivity plays a large role in influencing the optimal VRR on a reservoir-scale. Our results confirm earlier observations made using our core-scale models.

Flow simulations using the reservoir model show that gas mobility and reservoir connectivity have the most influence over the optimal VRR. As the gas mobility decreases and/or the reservoir heterogeneity increases, a VRR below 1 becomes more favorable. Using realistic oil properties and relative permeability curves, we found cases where a VRR below 1 is optimal. In order to predict the optimal VRR using numerical simulation, one must properly characterize the relative permeability curves of the reservoir fluids and the connectivity of the reservoir.

Acknowledgments

Firstly, I would like to thank the Heavy Oil Flagship of BP. This work and all of the research associated with it would not have been possible without their financial support. Within BP, I would also like to thank Steven Vittoratos whose insightful advice pushed the project forward. Without his work to build upon, and his insistence to allocate money to this project, this work would not have been possible. Zhouyuan Zhu both acted as a friend and an advisor who helped build our simulation models. Brian Vanderheyden provided the inspiration for the cul-de-sac model that greatly helped build our understanding of the role of heterogeneity.

My advisor Anthony R. Kovscek is the brain behind this work- the painter behind the painting. Without him, this work would be a mere semblance of what it is now. I have known Prof. Kovscek longer than any professor at Stanford. Six years ago when I attended Stanford's Admit Weekend, I sat in one of his classes, and he was part of the reason I decided on Stanford and majoring in Energy Resources Engineering. He was my advisor throughout my undergraduate education. He acted as both friend and mentor throughout my entire Stanford career. I would not have stayed for a M.S. had he not found me funding. This work represents his vision; his guidance was what drove this project to completion. His knowledge will never cease to amaze me.

I would like to thank every member of SUPRI-A for offering their friendship and advise. I will miss you all. I would also like to thank everyone else in the Energy Resources Engineering Department who I have had the pleasure of interacting with, faculty, staff, and students alike. You are part of the reason leaving Stanford will be so difficult.

Within Stanford, I would specifically like to thank Mac Sriyanong, Orhun Aydin, and Manish Kumar Choudhary who not only offered their friendship, but helped provide new inspiration on how to tackle some particular problem. Jeff Caers and Hongmei Li provided their reservoir-scale model- a model instrumental to understanding implications of our work on a much large scale.

I would like thank CMG support who offered prompt and informative responses whenever I used their services. If anyone wonders why I used CMG's software over a certain other company's software, it is because of the people who work in CMG's support team.

Stanford, I owe you much. You gave me 5-years of education and never charged me a dime, a B.S. and M.S., and the chance to study and live abroad in two wonderful countries through Mrs. Helen Bing's generous support. The skills and values you have taught me will not be forgotten. I will always remember my alma mater.

Lastly, I would like to thank my mother, Linda Cruz Delgado. She juggled being a single-mother, going to school, and working. What little we had she put toward my pre-college

education, so that I was eventually able to get into the school of my dreams. She is the very model of perseverance and determination.

Contents

List of Tables

List of Figures

Chapter 1

1.Introduction

The concept of using solution-gas drive to assist in waterflooding is certainly not new. Such concepts were observed previously in the literature (Dyes 1954). Operating below the bubblepoint pressure so that some gas evolves from the oil solution has been shown to improve recovery during waterflooding by 7 to 12% compared to operating at or above the bubblepoint. It was suggested there is an optimum reservoir pressure at which to operate a waterflood and that speeding up production rates can get to this optimum pressure.

Even with some experimental evidence pointing to increased recovery with the assistance of solution-gas drive, many disadvantages are prescribed to dropping the pressure of a reservoir below the bubblepoint pressure. In heavy-oil reservoirs, when the reservoir pressure is dropped below the bubblepoint, gas evolves from oil and the oil-phase viscosity increases greatly, making the oil less mobile. This problem is compounded by the fact the gas flows easily out of the reservoir, reducing reservoir pressure at a much faster rate than when above the bubblepoint. Further problems occur if the rock compressibility is relatively large, in which case subsidence occurs. For this reason, some countries mandate whatever liquid volume is produced much be matched by an equal volume of fluids injected within a reservoir (Vittoratos and West 2010).

It is erroneous to compare the performance of conventional with unconventional reservoirs. The differences between conventional oil recovery and heavy-oil recovery have been discussed extensively in the literature (Firoozabadi and Anderson 1994, Tang et al. 2006a, Vittoratos et al. 2006). Due to the unfavorable mobility of heavy oil relative to water, a substantial fraction of oil is only recovered after water breakthrough (Tang and Kovscek 2011, Vittoratos et al. 2007). The characteristic high viscosity of heavy oil and foamy oil effects, or gas emulsions in the liquid oil, retard gas flow, substantially extending the solution-gas-drive process in time (Tang et al. 2006 a,b).

Recently, observations have led to further consideration of the interaction between the three phase system of oil, water and gas. Production data taken from numerous Canadian waterfloods showed a correlation between a reduced voidage replacement ratio (VRR) and increased oil recovery (Brice and Renouf 2008). VRR measures the ratio of injected to produced fluids at reservoir conditions. It is purely a volumetric ratio. Traditional waterfloods are conducted at a VRR of 1 to maintain a steady-state mass balance in the reservoir. The absence of a waterflood, i.e., primary depletion, implies a VRR of 0. It is also possible to have a VRR between these two values. A summary of these scenarios is shown in the diagram in Figure 1-1. A VRR greater than 1 implies more fluid is injected than produced; this scenario is usually conducted to raise the reservoir pressure (Vittoratos and West 2010).

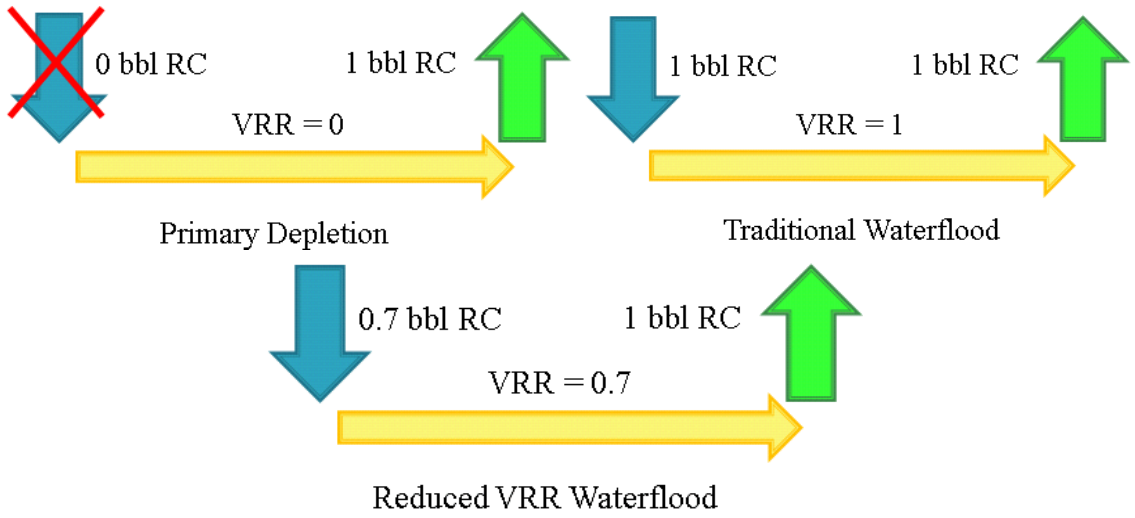

Figure 1-1: Diagram displaying a VRR of 0, 1, and 0.7.

The examiners of the Canadian waterfloods concluded performing primary depletion until recovery of a certain fraction of oil followed by a waterflood is optimal for heavy-oil reservoirs (Brice and Renouf 2008). They also concluded periods of reduced VRR are beneficial. The effectiveness of these recommendations was shown to depend on the oil properties, specifically an oil's API gravity, indicating such a recovery process is unique to heavy oils. The observations imply a correlation between reservoir pressure reduction and heavy-oil mobility.

A later paper takes a much more aggressive stance on the issue of recovery at a VRR less than 1 (Vittoratos and West 2010). The hypothesis presented in the paper by Vittoratos and West builds upon the idea that when the pressure of the heavy oil is reduced to some point below the bubblepoint pressure, gas bubbles evolve within the oil and oil emulsifies with water, greatly increasing the relative mobility of the oil mixture. These bubbles only form given certain oil properties; i.e., the oil must lie within a certain API range for the effect to be significant. If the API is too low, the oil remains virtually immobile even with the aid of any emulsions; if the API is too high, the chemistry of the oil will not allow "partial" immiscibility between the dissolved gas and oil. This novel theory purports that this kind of "foamy" oil is beneficial to oil recovery due to percolation effects. If a conventional waterflood sweeps the "backbone" of the reservoir, i.e., some preferred path by which the water will travel, then a substantial fraction of oil will be left behind in so called "dangling ends," or permeability cul-de-sacs. Given the right oil properties, if the pressure in these regions is reduced to some level that allows the presence of a foamy oil or oil emulsions in these cul-de-sacs, then the oil's mobility is greatly increased, to the point it will flow into the backbone of the reservoir and be produced. Such occurrences appreciably increase oil recovery depending on the heterogeneity of the reservoir and the amount of "dangling ends." The authors of this novel process further claim that to achieve the optimal benefit, one must maintain a VRR of 0.7, that should yield recovery equal to primary depletion and a secondary waterflood combined.

There is still much uncertainty as to how heavy oil behaves under a VRR less than 1. Thus, a comprehensive understanding of the three-phase behavior between the heavy oil, the dissolved gas and water is required. We seek to see if such a recovery process can be modeled using numerical simulation, and to gauge if the process is as advantageous as authors claim. We consider the fluid dynamics of viscous oil, water and gas under a number of situations, building upon the concepts of oil chemistry and reservoir heterogeneity via dangling ends brought up in the paper by Vittoratos and West (2010). We shall develop a list of the primary factors influencing the effectiveness of recovery at a VRR below 1 and test our constructions against a field scale model.

Chapter 2

2.Development of a Base Case

In order to test the sensitivity of recovery to a particular influencing factor, we needed to develop a base case model to have consistent grounds for comparison. We chose to model our base case after a homogeneous, rectangular core with dimensions listed in Table 2-1. The reasons for using a core-sized model as our base case are plentiful. An analogue is easily extended to actual experiments; one would start with core experiments before moving to a field study. We want to observe how the factors influencing the optimal VRR act at core scale in isolation from one another, before implementing simulations on a large scale model where a number of the factors are thrown into the mix and allowed to influence one another. This process allows us to fine tune our understanding of the underlying mechanisms before launching into a full-scale reservoir model. For a discussion of field-scale simulations, see Chapter 4.

Table 2-1: Base case grid dimensions.

Parameter	Base Case
Grid Size	91 × 9 × 9
Block Size	0.065 × 0.087 × 0.087 in^3
Total Volume	4.97e-4 in^3 (60 cm3)
Producer Cell	91,5,5
Injector Cell	1,5,5

2.1. Description of Base Case

The parameters used to construct a base model with which to simulate a reduced VRR waterflood were derived from papers compiling data from various areas of Schrader Bluff and Ugnu (Strycker et al. 1999, Stryker and Wang 2000, Mohanty 2004, Rangel-German et al. 2004). Similarly, we constructed relative permeability values for oil, water, and gas matching curvature characteristics similar to those used to model fluid-rock interactions in the Schrader Bluff field (Strycker et al. 1999, Stryker and Wang 2000). Relative permeability curves were made through the use of Corey curves using the equations described in Corey's paper (1956). We chose a reasonable connate water saturation and residual oil saturation based on the literature. The oil-water relative permeability curves are shown in Figure 2-1, and the liquid-gas curves are shown in Figure 2-2. These relative permeability curves are characteristic of a somewhat medium gravity and slightly viscous oil, say for an oil with a viscosity only around 27 times larger than that of water at reservoir conditions.

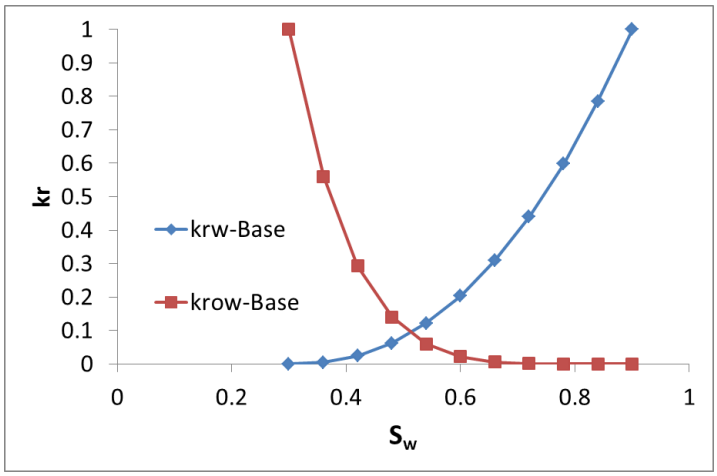

Figure 2-1: Oil-water relative permeability curves for the base case.

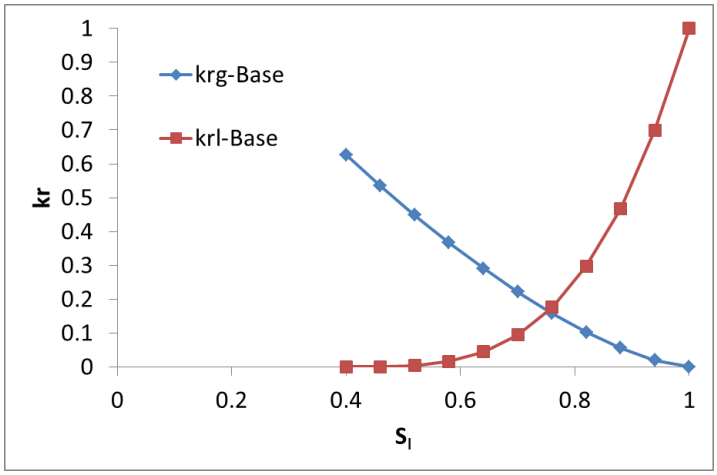

Figure 2-2: Liquid-gas relative permeability curves for the base case.

Fluid properties and K-values were derived to represent an oil characteristic to one found in the Schrader Bluff formation to be consistent with our other parameters. The solution gas oil ratio and oil formation volume factor are shown for reference at an initial temperature in Figure 2-3 and 2-4, respectively. The initial molar and mass fractions of each component in the oil were also determined by these K-values. The proportion of gas components and heavy-oil components is consistent with the literature (Mohanty 2004, Rangel-German et al. 2004, Strycker et al. 1999; Strycker and Wang 2000). A summary of other parameters used is given in Table 2-2. A plot of oil viscosity as a function of pressure is given in Figure 2-5. Fluid data is given in Table 2-3.These base case values were modified as described later in this paper.

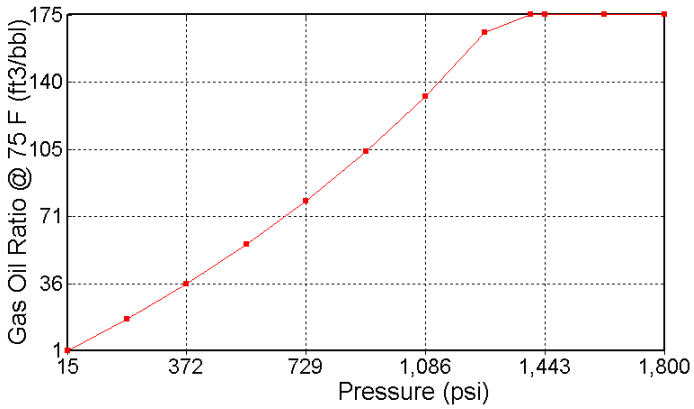

Figure 2-3: Solution gas-oil ratio for the base case.

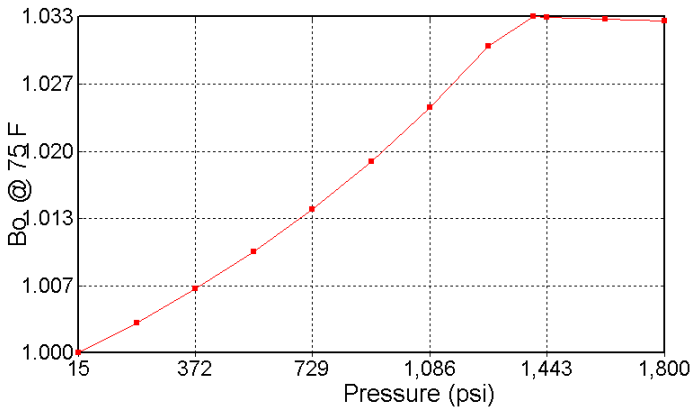

Figure 2-4: Oil formation volume for the base case.

Table 2-2: Base case parameters.

Parameter	Base Case
Porosity	0.25
Permeability	$k_x=k_y=k_z$ = 250 md
Initial Temperature	75 ˚F
Initial Pressure	1500 psi
Bubblepoint Pressure	1400 psi
Initial Water Saturation	30%
Residual Gas Saturation	40%
Residual Oil Saturation	10%

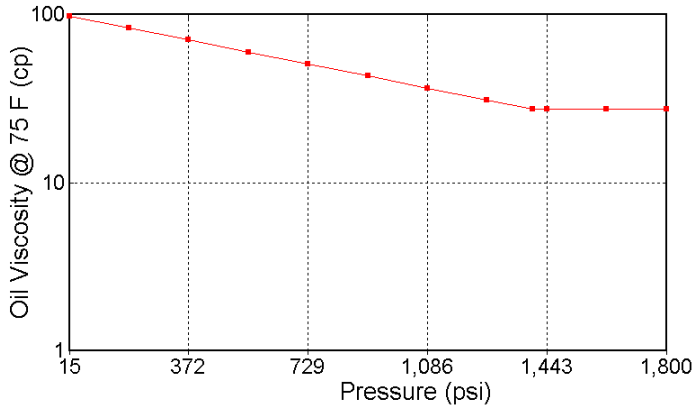

Figure 2-5: Oil viscosity as a function of pressure.

Table 2-3: Base case fluid composition.

	Water	Oil	Gas
Molecular Weight (lb/lbmol)	18.02	385.5	16
Critical Pressure (psi)	3206.2	140	667.2
Critical Temperature (˚F)	705.4	1100	-116.59
Mass Density (lb/ft^3)	62.4	58.706	38
Liquid Compressibility (1/psi)	1.00E-06	1.00E-06	1.00E-06
First Coefficient of the Thermal Expansion Correlation (1/˚F)	1.00E-04	1.00E-04	1.00E-04
First Coefficient in Liquid Phase Heat Capacity (Btu/lbmol-˚F)	100	132.5	100
KV1 (psi)	0	0	7.91E+04
KV4 (˚F)	1	0	-1583.7
KV5 (˚F)	0	0	-446.8
Initial Viscosity (cp)	0.92	27.5	0.02
Molar Fraction of Initial Oil	0	63.20%	36.80%

In order to predict the conditions for optimal recovery using a VRR other than 1, a number of sensitivity studies were conducted using CMG's *S*team *T*hermal *A*dvanced Processes *R*eservoir *S*imulator. STARS was chosen due to its quasi-compositional modeling method that allows simulations to run faster than when using a compositional simulator, such as CMG's *G*eneralized *E*quation-of-State *M*odel Compositional Reservoir Simulator (GEM). We wanted to be able to run both black-oil models and compositional models. Although our base case is essentially a black-oil model, we performed sensitivity studies using other sets of components and K-values at various stages for verification. We used Stone's Model II for three phase model calculations in STARS (Settari and Aziz 1979). All simulations were conducted at essentially isothermal conditions (injected fluid temperature was the same as the initial reservoir temperature).

STARS uses a correlation for the gas-oil equilibrium ratio, *K*, to represent the gas–liquid phase behavior as a function of pressure and temperature:

$$\boldsymbol{K} = \left(\frac{\boldsymbol{KV1}}{\boldsymbol{p}} + \boldsymbol{KV2} \times \boldsymbol{p} + \boldsymbol{KV3}\right) \times \boldsymbol{e}^{\left(\frac{\boldsymbol{KV4}}{\boldsymbol{T}-\boldsymbol{KV5}}\right)} \quad (2\text{-}1)$$

where T is temperature (K) and p is gas phase pressure (kPa), in appropriate units (CMG, 2010). *KV1*, *KV4*, and *KV5* are given in Table 2-3. *KV2* and *KV3* were zero for our set of oil properties.

For all cases, the production rate constraint was 1/10th the pore volume of the system per hour. Thus, the injection rate was determined by the VRR we desired to model. Unless otherwise noted, the base case relative permeability curves and K-values were used.

2.2. Base Case Results

We will now consider the results of our base case for a range of VRR values. We chose to simulate cases for VRR values of 1, 0.9, 0.7, 0.5, 0.2 and 0 and plotted recovery as a function of the VRR at a certain reference point, 0.6 days. We chose to also represent results in this way for all of the cases we will discuss in Chapter 3, unless otherwise noted. Though this VRR spread might be considered coarse, the relationship between VRR and recovery tends to follow a smooth trend due to the dependence of recovery on the pressure gradient at different VRR. Due to the diffusive nature of pressure, there will never be sharp or abrupt changes in recovery values for adjacent VRR. Thus, for our purposes interpolating recovery between these six sets of VRR values is appropriate. Interpolation between VRR recovery values was done using a polynomial curve fit to allow us to plot smooth lines between points, capturing the diffusive nature discussed previously.

The reference point chosen was 0.6 days for our core models, as 0.6 days lies at a point far after water breakthrough, and in the cases of a VRR less than 1, after pressure depletion in the core model. Also, 0.6 days corresponds to about 100% pore volumes injected for the VRR of 1 case. The pressure in our base case core model was allowed to drop to essentially atmospheric pressure. Every simulated case on this particular grid reached atmospheric pressure long before 0.6 days, except for the cases where there was a VRR of 1. For the cases where the VRR was equal to 1 there were only small pressure deviations throughout the life of the models. For further discussion of our choice of a reference point see section 3.4.

The results of recovery as a function of VRR for the base case are shown in Figure 2-6. The inverted S-shaped curve tells us a lot about this specific case. Deviating from a VRR of 1 will cause a large drop in recovery, and injecting no water at all yields a recovery several times smaller than that of the case of a traditional waterflood. The plot tells us little about why a VRR of 1 is so overwhelmingly optimal though.

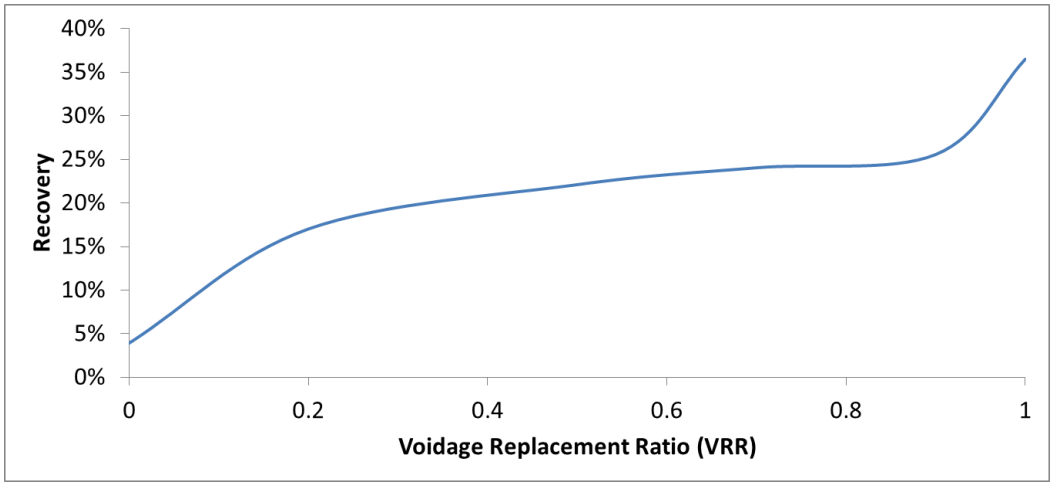

Figure 2-6: Oil recovery as a function of VRR at 0.6 days for the base case.

To determine why a VRR of 1 is so overwhelmingly optimal, we consider how recovery changes in time for each of our simulated VRR cases, shown in Figure 2-7. As seen, each of the cases where water is injected follows a similar trend after a certain point. The cases with curves between a VRR of 1 and 0 all have slight delays between the curves characterized by the VRR constraint and the times the traditional waterflooding recovery profile takes over. It can be seen the delays are longer the smaller the VRR. This effect in the recovery curves is simply an artifact of the wellbore pressure constraints. By some early time, around 0.01 days, the pressure in the core model is completely depleted, and the producer well becomes shut-in until the injector well can inject enough fluid to allow the producer well to start producing again. At this point, the production rate is limited to the injection rate, and we have a VRR of 1 at essentially atmospheric pressure in the model. It takes longer for the producer to start producing again for lower VRR cases due to the associated lower amount of injected fluid volume. This is why the case of a VRR of 0.2 has a longer "plateau" region before picking up production again than the case of a VRR of 0.5. Pressure as a function of early times is shown in Figure 2-8.

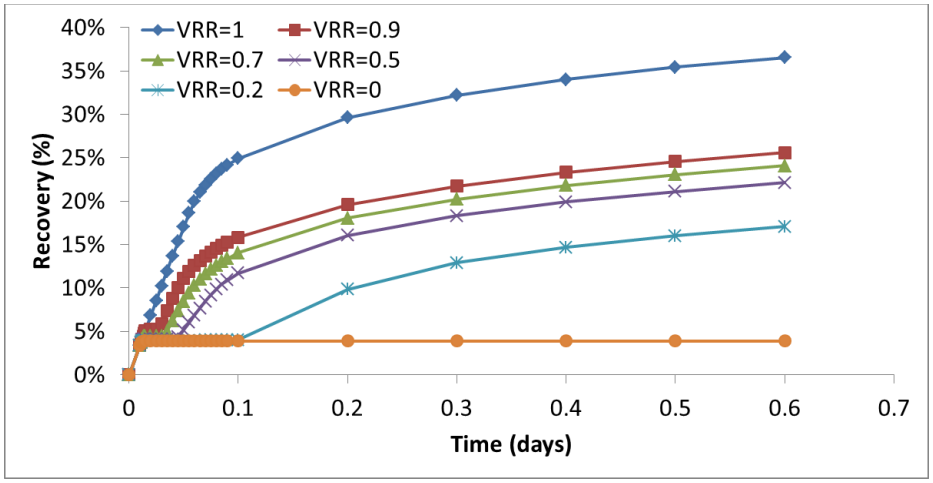

Figure 2-7: Oil recovery over time at various VRR for the base case.

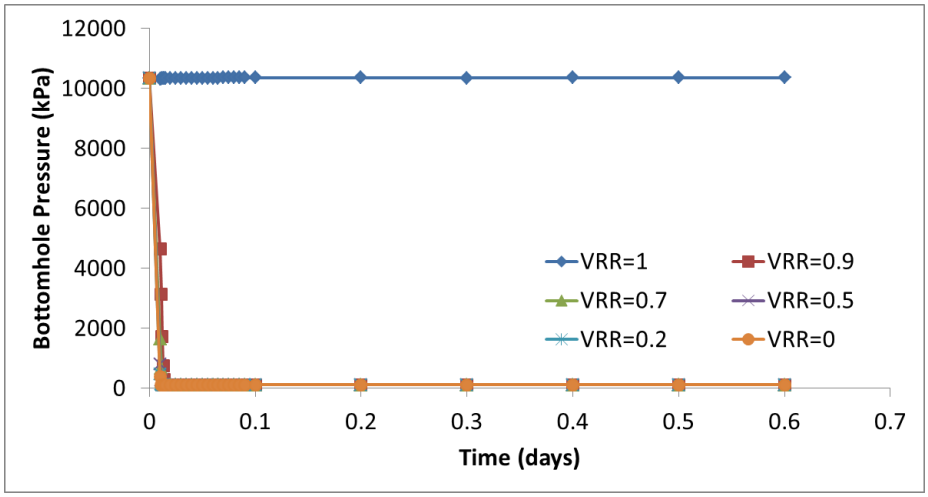

Figure 2-8: Pressure over time at various VRR for the base case.

The pressure depletion in our models is of important consequence. In every case we simulated in this work, the VRR constraint is only maintained until the model is pressure depleted. After pressure depletion, a VRR of 1 takes place for the remainder of the simulation, but the production rate is lower by a factor of the case's VRR when compared to the VRR of 1 case due to the smaller injection rate. Thus, the earlier pressure depletion occurs in a model, the worse results are for a VRR less than 1.

In our base case, the time at which pressure depletion is reached is early relative to the length of the simulation. If we consider the cumulative gas production as shown in Figure 2-9, we see for each case where gas is produced, all the gas is produced at essentially one time; i.e., the gas escapes as rapidly as it evolves from the oil. The fact gas escapes rather quickly should be evident from the relative permeability curves. The curves we have used in our base case have highly mobile gas that does not stay in the model after evolving from the oil. Without gas in the model to maintain pressure, the pressure drops to atmospheric quickly.

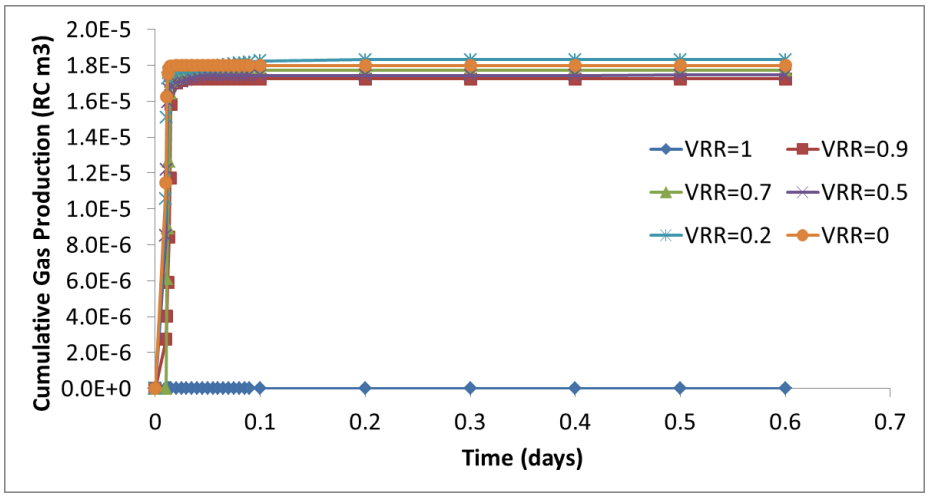

Figure 2-9: Cumulative gas production over time at various VRR for the base case.

We have shown how detrimental a deviation from a VRR of 1 can be to ultimate recovery. In doing so, we have shown how dependent recovery is on pressure maintenance, that in turn is dependent on the mobility of the gas. Both our K-value data and our relative permeability curves imply a medium gravity oil, somewhere between light and heavy. In the literature, foamy oil effects have only been seen in heavy oils that are characterized by different oil compositions, fluid-fluid interactions, and rock-fluid interactions (Tang et al. 2006b, Vittoratos and West 2010). We therefore want to perform sensitivity studies that emulate changes to the oil properties. We will continue this discussion in Chapter 3.

Chapter 3

3.Factors Influencing the Optimal VRR

We have developed and described a base case upon which we performed sensitivity analyses to determine the factors that most influence which VRR is optimal; i.e., the VRR associated with the most oil recovery. We will now illustrate the factors we have seen that have the greatest effect on oil recovery and the optimal VRR.

3.1. Relative Permeability Curves

Our base case used a set of relative permeability curves derived by Honapour-Corey equations; thus, it made sense to vary the Corey exponents we chose and see how this modification altered our results. We modified the oil, water, gas, or liquid Corey exponent and kept all others constant, making it possible to perform an objective comparison between results. Our goal was to see the impact mobility had on the optimal VRR.

Our base case liquid-gas relative permeability curves did not have any critical gas saturation present, but often there is at least a small fraction of gas that cannot be recovered in heavy-oil reservoirs, and this fraction of gas stays in the reservoir (Firoozabadi and Anderson 1994, Treinen et al. 1997, Kumar et al. 2000, Sahni et al. 2004). Given the importance of the role of gas mobility in a depletion drive, it makes sense to perform sensitivity studies to the critical gas saturation in addition to the Corey exponents. We have therefore included three sections where we have performed a sensitivity analysis to the Corey exponents at some specified critical gas saturation.

We chose to vary the Corey water exponent from 1.3 to 8.3 with 5 values and the Corey oil exponent from 1.5 to 9.5 with 5 values as evidenced by Figure 3-1. We varied the Corey gas exponent from 1.5 to 9.5 with 5 values and the Corey liquid exponent from 1.4 to 5.4 with 3 values as evidenced by Figure 3-2. The Corey exponent values chosen were not meant to represent physical systems but rather were used as instruments to convey a wide breadth of scenarios. Relative permeability curves based off physical data are discussed in section 3.2.

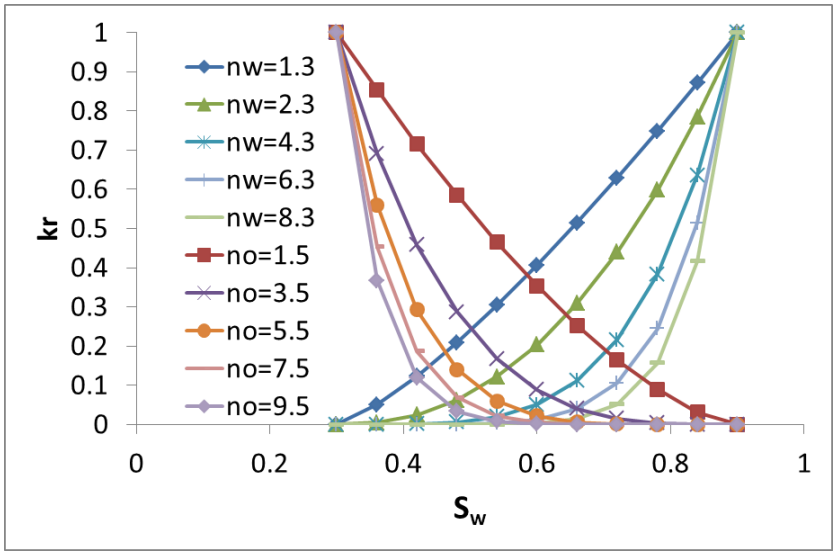

Figure 3-1: Range of Corey oil and water exponents used for relative permeability sensitivity studies.

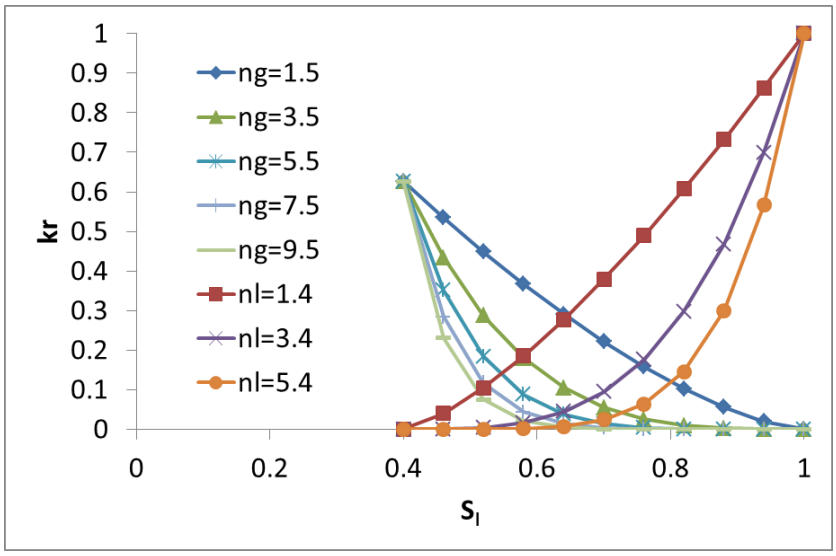

Figure 3-2: Range of Corey liquid and gas exponents used for relative permeability sensitivity studies.

3.1.1. No critical gas saturation

To begin, we will discuss the results that occur when the Corey water exponent is modified as shown in Figure 3-3. The results are entirely expected. We are flooding our model with water while maintaining flow constraints at both the inlet and outlet. In order to maintain a volume balance in the reservoir, oil, water, or gas must leave the system. If we decrease the mobility of water at any given water saturation by increasing its associated Corey exponent, more oil will have to be displaced, yielding greater recoveries. There is no effect on the optimal VRR in these scenarios.

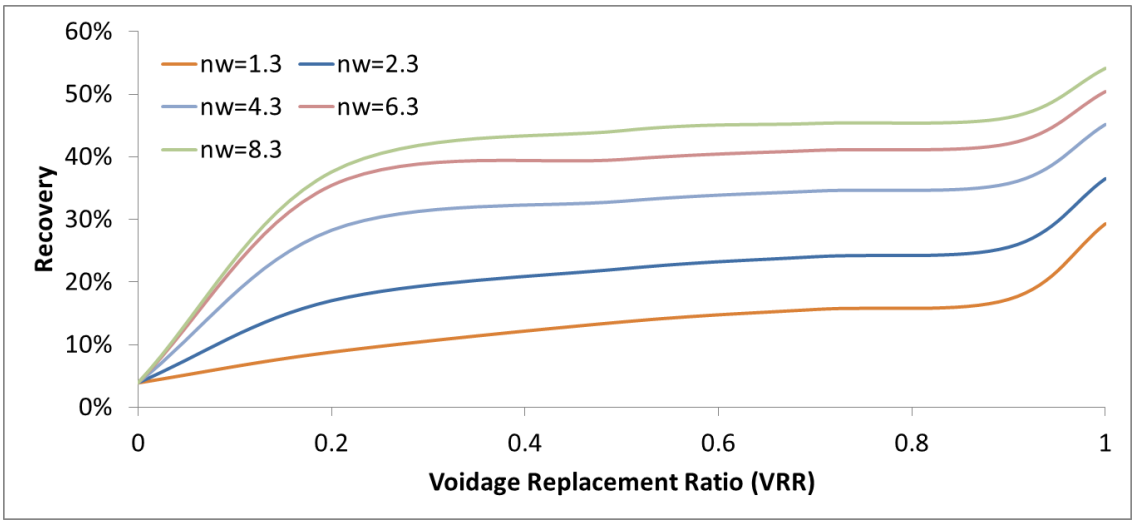

Figure 3-3: Recovery as a function of VRR for different values of the Corey water exponent (ng=1.5; nl=3.4; no=5.5).

Now we consider the case where we modify the Corey oil exponent. Results are shown in Figure 3-4. The behavior is not as intuitive as that of the case where the Corey water exponent is varied. The optimal VRR never alternates, but the superiority of a VRR of 1 over those less than 1 becomes less as the oil becomes less mobile, with an increasing Corey oil exponent. This result makes sense if we think about what is occurring in our model. Even though we keep injecting water into the model, if the oil is not willing to move, larger and larger volumes of water will not have much effect as the water eventually bypasses the oil and flows to the outlet, leaving oil behind.

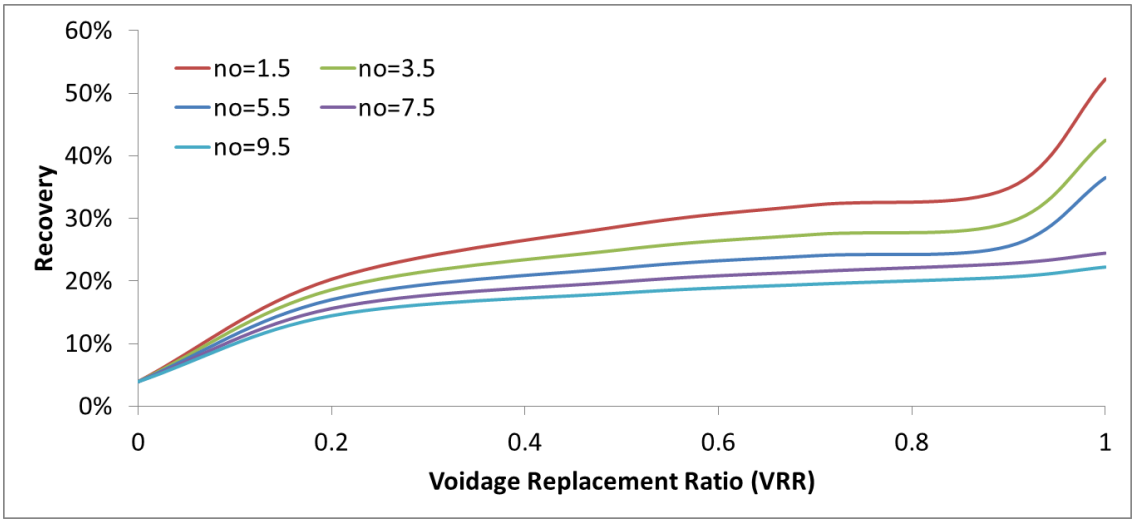

Figure 3-4: Recovery as a function of VRR for different values of the Corey oil exponent (ng=1.5; nl=3.4; nw=2.3).

We now consider the effects of modifications to the liquid-gas relative permeability curves. A change to the relative permeability of liquid alone has no effect on recovery as evidenced by Figure 3-5. The flow of oil and water is governed by the relative permeability of oil and water, respectively, so a change to the relative permeability to liquid has negligible effect.

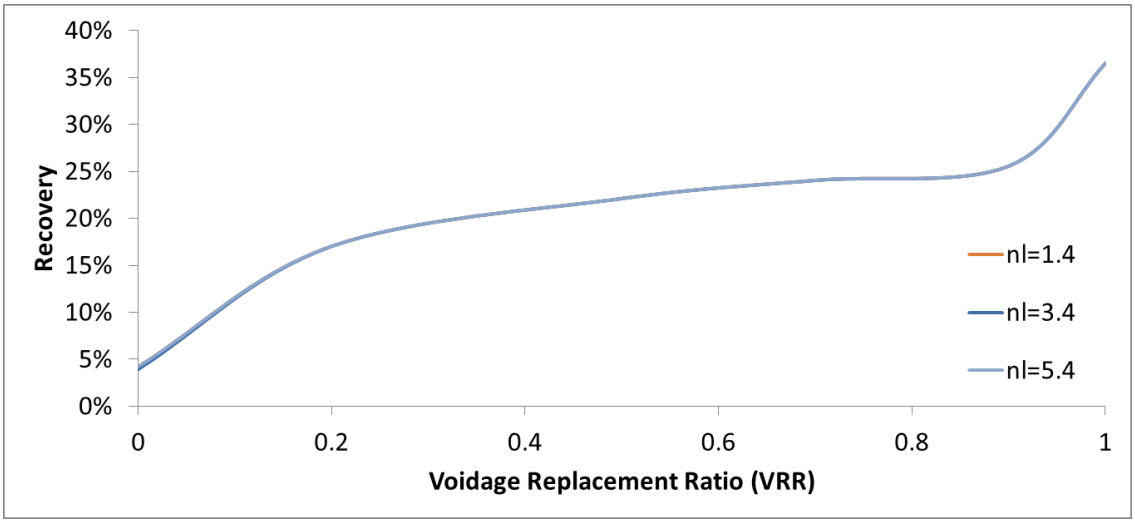

Figure 3-5: Recovery as a function of VRR for different values of the Corey liquid exponent (ng=1.5; no=5.5; nw=2.3); the curves overlay one another as there is virtually no change between the scenarios.

As our previous results show, changes to the relative permeability of oil, water, or liquid do not alter the optimal VRR; however, changing the relative permeability of gas alters the optimal VRR in some cases as evidenced by Figure 3-6. As seen in the figure, the optimal VRR is very sensitive to the mobility of the gas in the model. As gas mobility decreases, the difference between a VRR of 1 and those slightly below 1 become less significant, and a VRR below 1 becomes optimal if the mobility of gas is small enough. This result makes sense if we consider the fact that the gas in our model stabilizes the pressure, so the slower the gas is produced, the longer it takes for the pressure to deplete. Depletion drive, which instills a larger pressure gradient than a waterflood, therefore occurs for much longer periods of time. There is also more time for the oil to navigate through the model during a depletion drive than a waterflood.

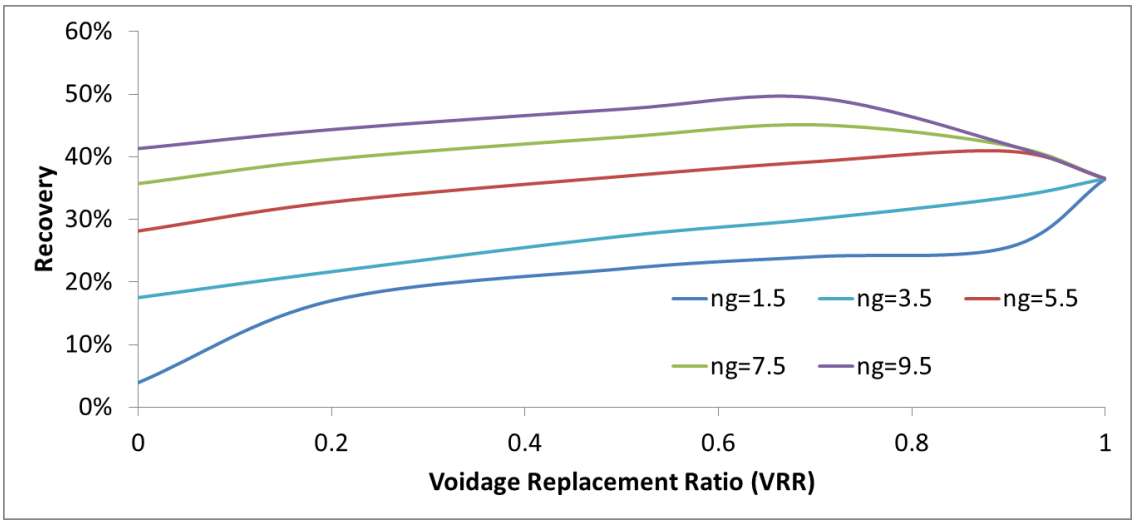

Figure 3-6: Recovery as a function of VRR for different values of the Corey gas exponent (nl=3.4; no=5.5; nw=2.3).

One final observation on the results listed in this section is the connection between the recovery values at a VRR of 1 and 0 over different Corey exponent values. When the liquid-gas relative permeability curves are kept constant, the recovery values as result of only primary depletion, i.e., operating at a VRR of 0, are identical across all Corey oil and water exponents. When the oil-water relative permeability curves are kept constant, the recovery values with a VRR of 1 are identical across all Corey liquid and gas exponents. This result is expected. The oil-water relative permeability curves dominate reservoir performance during water drive, but the liquid-gas curves dominate performance during primary depletion.

3.1.2. Explanation of results

We have shown that modifying the relative permeability to gas alters the optimal VRR, but it may not be obvious as to why in homogeneous core models this is the case. Therefore, we will justify our explanation with results from the simulator. Though our base case model is 3 dimensional, it acts as a 1D core due to the absence of any heterogeneity. Thus, alterations in recovery due to varying gas mobility are simply functions of Buckley-Leverett displacement and phase interference. As gas becomes less mobile within the model, pressure is maintained for a longer duration, water breakthrough is delayed, and more oil is displaced. Our discussion justifies the simulator is indeed processing everything we have shown correctly. We are considering the cases where the Corey gas exponent equals 1.5 and where it is 9.5, the two extremes of our sensitivity analysis in section 3.1.1. We are also considering the results at a VRR of 1, the optimal VRR when the Corey gas exponent equals 1.5, and a VRR of 0.7, the optimal VRR when the Corey gas exponent equals 9.5. We are thus theoretically showing a general set of results that apply to all the other scenarios we discuss in this report.

We first consider the oil mobility in the model at time far after peak production rates. Figure 3-7 and 3-8 confirm that the oil phase mobility in the case where gas is most mobile is greater than in the case where the gas is much less mobile. The fact that the oil saturation is smaller in the case where the gas is less mobile attributes to the smaller mobility. Clearly, if there is less oil, the relative permeability of oil is smaller. The presence of gas also slightly inhibits the flow of oil. When we view Figure 3-9, we see when operating at VRR of 1, the oil mobility is much larger than in the case of a VRR of 0.7 for both scenarios. More oil is recovered with a VRR of 1 than with a VRR of 0.7 for the case with the lower Corey exponent, so the decreased mobility is not attributed to a difference in oil saturations. The difference here is due to the evolution of dissolved gas in the case of a VRR of 0.7 that causes the oil to increase in viscosity. With a VRR of 1, the pressure in the model is never depleted, so the oil maintains all of the dissolved gas, and thus has a lower viscosity in the presence of these lighter components. Even at a time near peak production rates, oil mobility is greatest in the case of a VRR of 1, for the reasons outlined above.

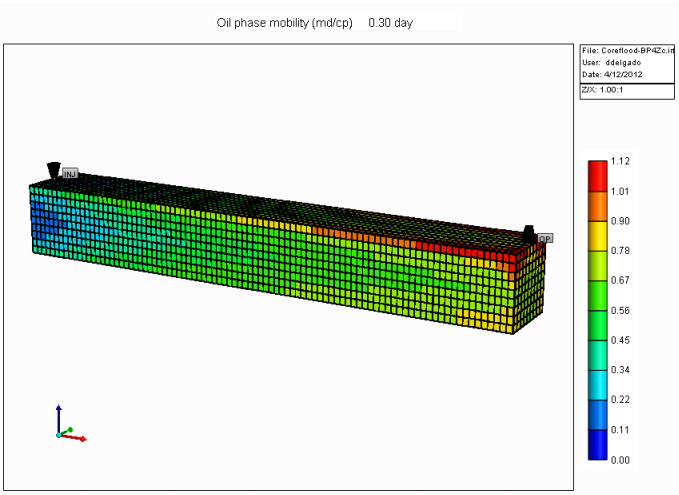

Figure 3-7: Oil mobility at 0.3 days with a VRR of 0.7 and Corey gas exponent of 1.5.

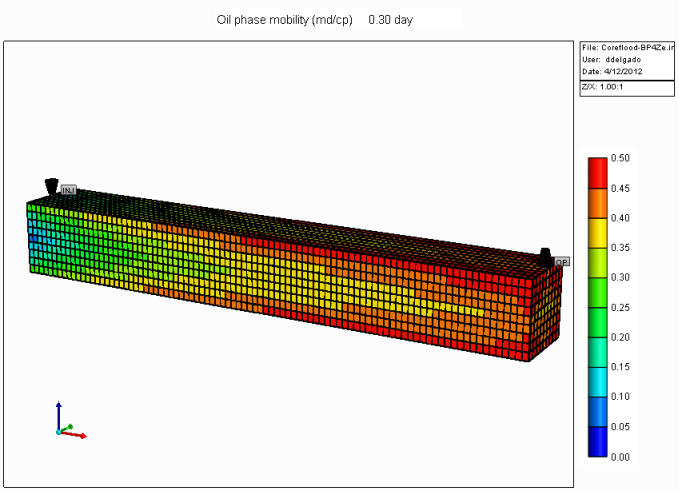

Figure 3-8: Oil mobility at 0.3 days with a VRR of 0.7 and Corey gas exponent of 9.5.

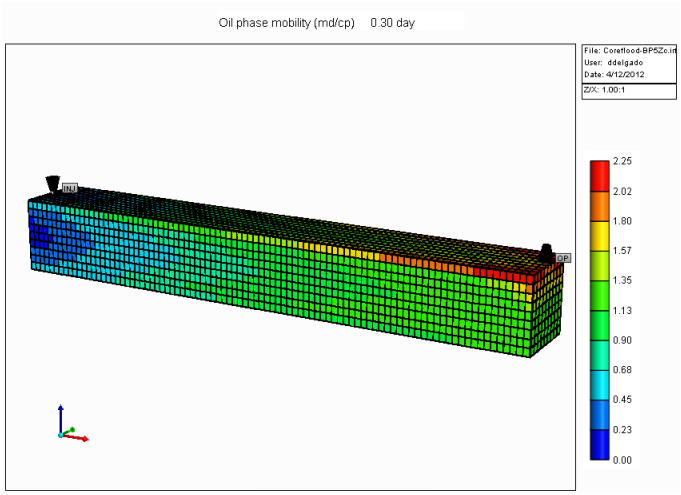

Figure 3-9: Oil mobility at 0.3 days with a VRR of 1 and Corey gas exponent of 1.5/9.5 (results are identical for either exponent).

If the mobility of oil is not governing the increased performance during a VRR of 0.7 with the larger Corey gas exponent, than the oil flow must be governed by the pressure gradient across the model. If we consider the pressure gradient across the model in Figure 3-10, 3-11, and 3-12 at a time sufficiently after peak production rates, the pressure differential in the case of a VRR of 0.7 and large Corey gas exponent is much larger than the case of a VRR of 1 or a VRR of 0.7 with a small Corey gas exponent. Even at times near peak production rates, the pressure differential is still larger in the case of a VRR of 0.7 than in the case of a VRR of 1 for the larger Corey exponent, as evidenced by Figure 3-13 and 3-14.

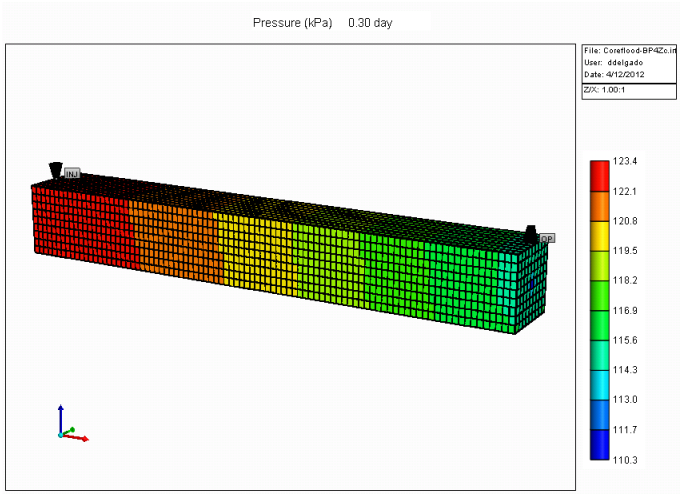

Figure 3-10: Pressure distribution at 0.3 days with a VRR of 0.7 and Corey gas exponent of 1.5.

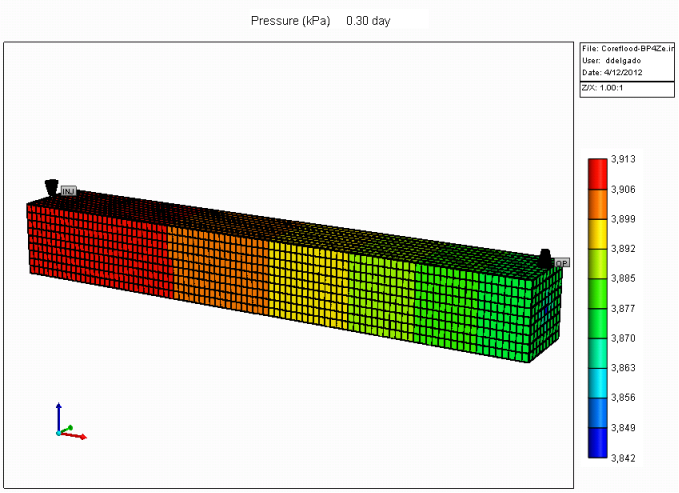

Figure 3-11: Pressure distribution at 0.3 days with a VRR of 0.7 and Corey gas exponent of 9.5.

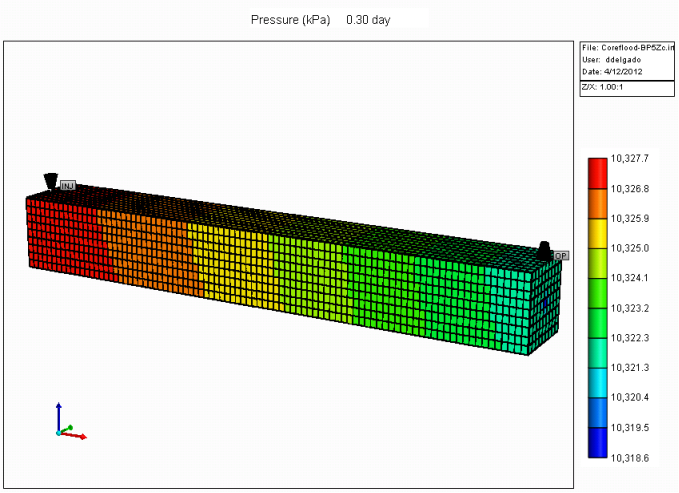

Figure 3-12: Pressure distribution at 0.3 days with a VRR of 1 and Corey gas exponent of 1.5/9.5 (results are similar for both).

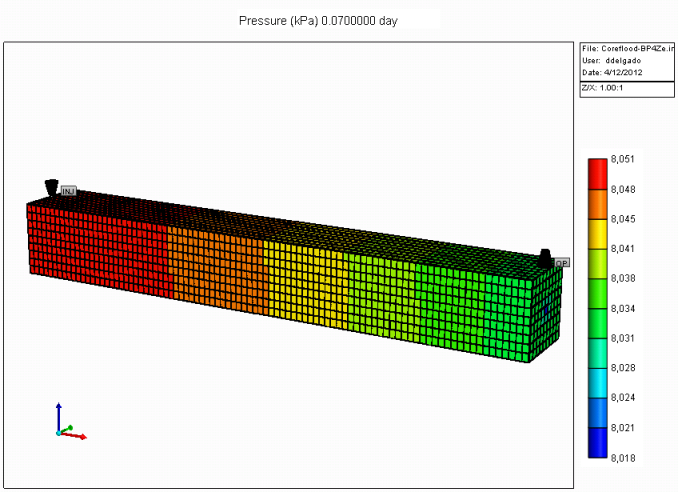

Figure 3-13: Pressure distribution at 0.07 days with a VRR of 0.7 and Corey gas exponent of 9.5.

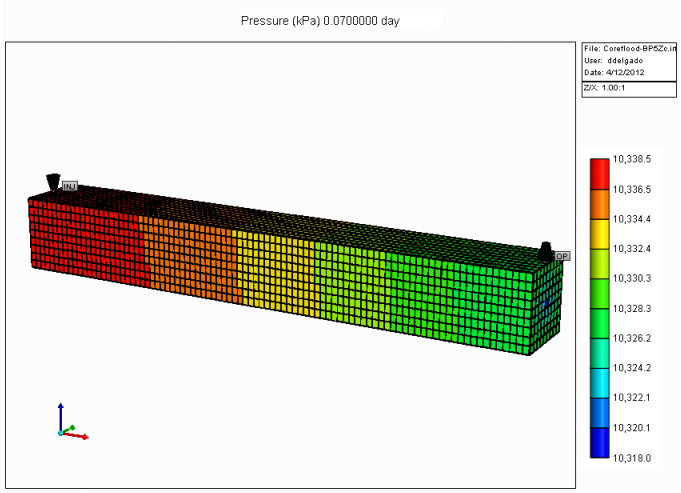

Figure 3-14: Pressure distribution at 0.07 days with a VRR of 1 and Corey gas exponent of 1.5/9.5 (results are similar for both).

3.1.3. 5% critical gas saturation

We now consider the case where the critical gas saturation is 5%. A critical gas saturation near 5% is common in heavy oils and makes for a very reasonable assumption (Firoozabadi and Anderson 1994, Kumar et al. 2000). We performed the exact same sensitivity study as that discussed in section 3.1.1. We first consider the results that occur when the Corey water exponent is modified as shown in Figure 3-15. The results follow a pattern, but note the difference between this case and the one with no critical gas saturation. The difference in recoveries between the cases with a VRR of 1 and 0.9 is much smaller. Again, if we decrease the mobility of water at any given water saturation by increasing its associated Corey exponent, more oil is displaced, yielding greater recoveries. There is a slight effect on the optimal VRR. As the Corey water exponent increases, the optimal VRR switches to 0.9 from 1, though the difference between the recoveries of these two VRR is virtually negligible. We also note the similarity of results of the base case with a critical gas saturation of 5% and that of the base case with no critical gas and a Corey gas exponent of 3.5.

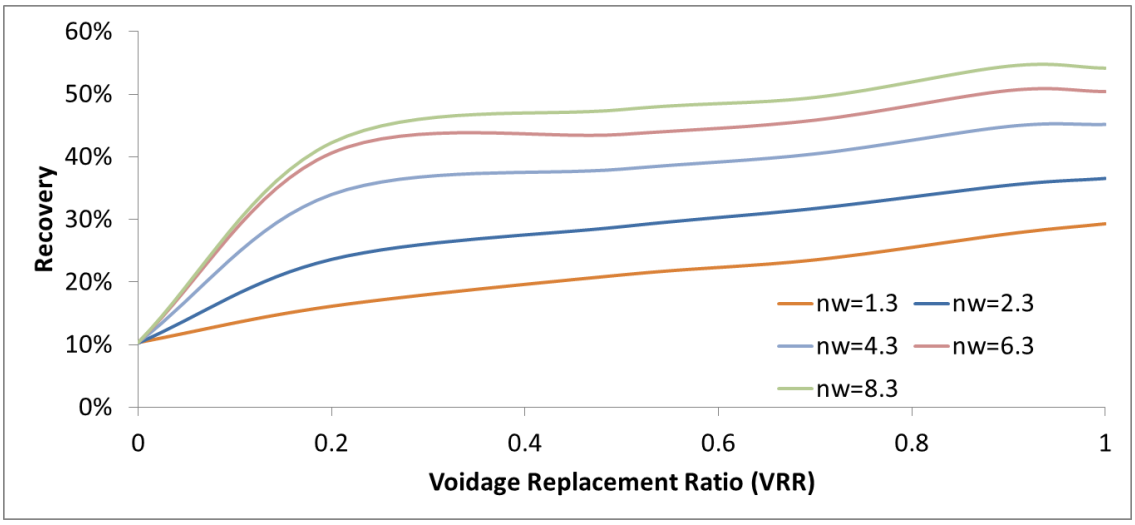

Figure 3-15: Recovery as a function of VRR for different values of the Corey water exponent (ng=1.5; nl=3.4; no=5.5; Sgc=0.05).

Now we consider the case where we modify the Corey oil exponent. Results are shown in Figure 3-16. The behavior represented in the figure is similar to that of the case where there was no critical gas saturation. As in the Corey water exponent sensitivity study, the optimal VRR does alternate between 1 and 0.9. As before, the difference in recovery values between the case of a VRR of 1 and that of a VRR of 0.9 is virtually negligible in the cases where a VRR of 0.9 is optimal. The fact that the optimal VRR switches at all showcases the presence of the critical gas. With a VRR of 1, the critical gas never comes into effect, but with a VRR of 0.9 it does. The effect is small due to the small fraction of critical gas.

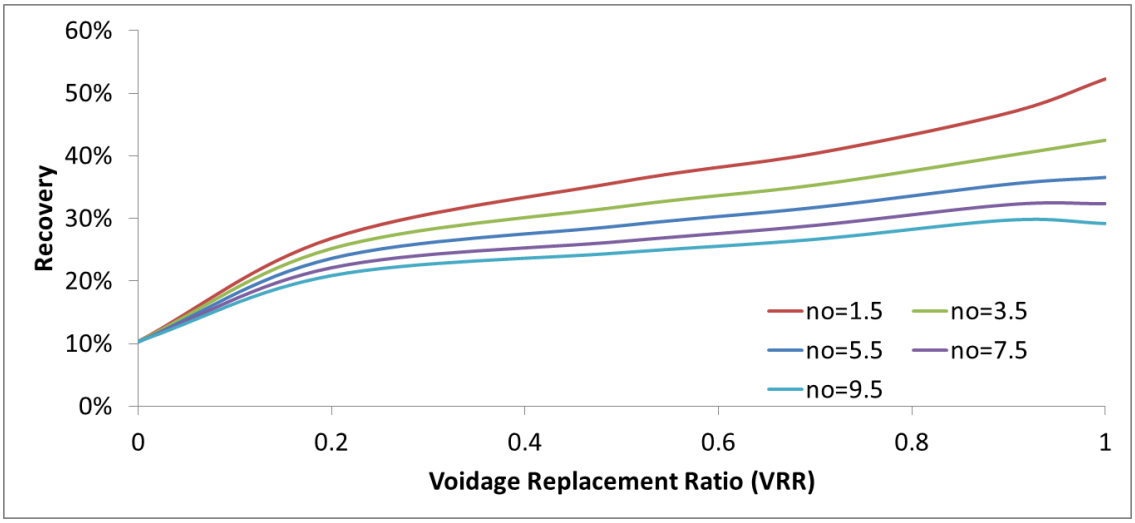

Figure 3-16: Recovery as a function of VRR for different values of the Corey oil exponent (ng=1.5; nl=3.4; nw=2.3; Sgc=0.05).

As Figure 3-17 shows, the relative permeability to liquid curves have no effect. This result is identical to the cases with the no critical gas saturation. Similar to the case of no critical gas, the relative permeability to gas curves strongly affects the optimal VRR as shown in Figure 3-18. These results affirm the observations made in section 3.1.1, however, we notice the addition of critical gas decreases some or all of the advantage of a VRR of 1 over any VRR less than 1 in every case.

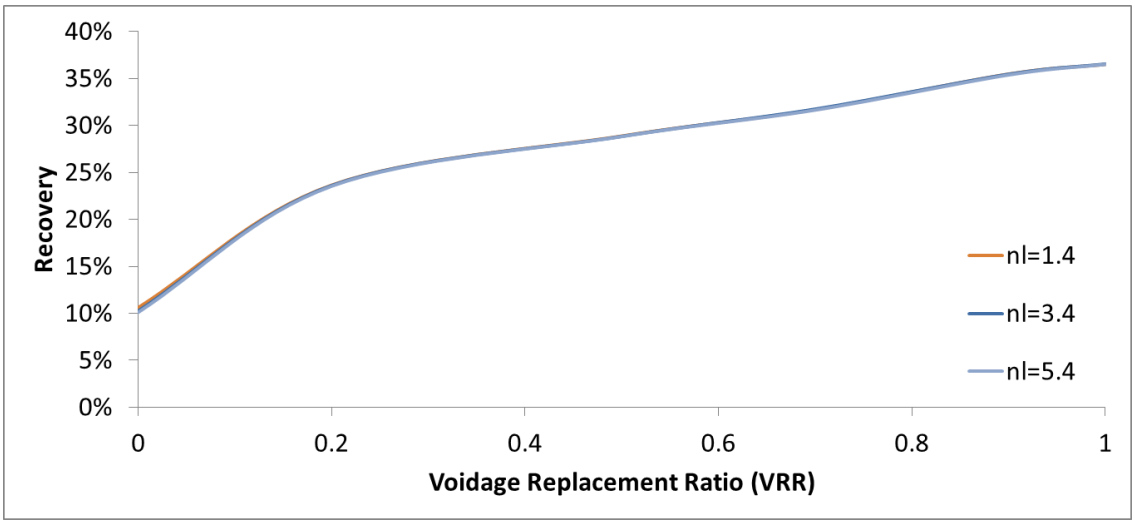

Figure 3-17: Recovery as a function of VRR for different values of the Corey liquid exponent (ng=1.5; no=5.5; nw=2.3; Sgc=0.05); the curves overlay one another as there is virtually no change between the scenarios.

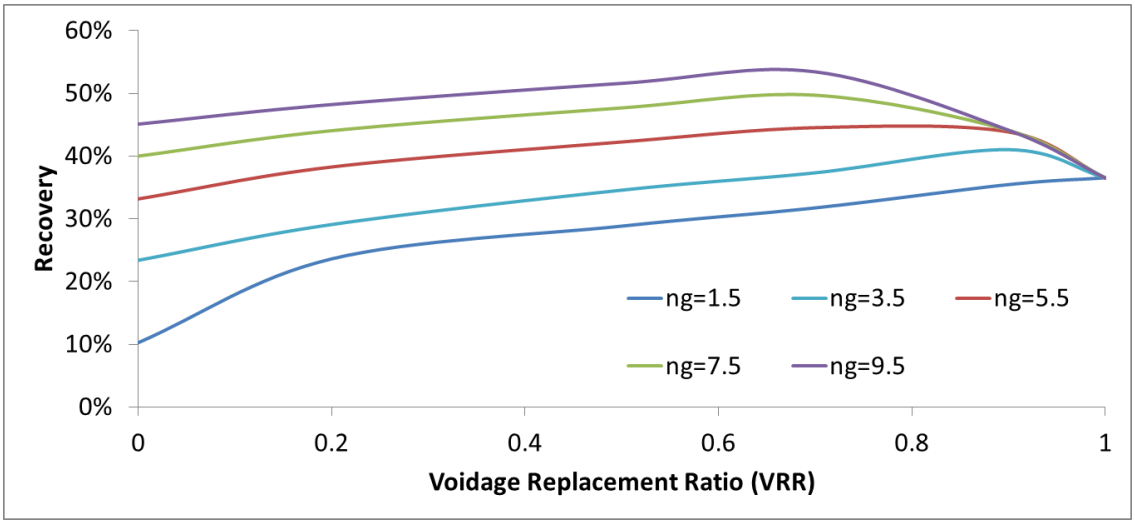

Figure 3-18: Recovery as a function of VRR for different values of the Corey gas exponent (nl=3.4; no=5.5; nw=2.3; Sgc=0.05).

3.1.4. 10% critical gas saturation

Lastly, we consider the case where the critical gas saturation is 10% and apply this property to our base case. A critical gas saturation of 10% has commonly been observed in some experiments on solution gas drive in heavy-oil cores and reservoirs (Sahni et al. 2004, Treinen et al. 1997). We perform the same sensitivity study as discussed in section 3.1.1 and 3.1.3. We consider the results that occur when the Corey water exponent is modified as shown in Figure 3-19. The results follow a similar pattern and the optimal VRR stays constant at 0.9. If we compare to our results in section 3.1.1, we see that the effect of a 10% critical gas saturation on the base case relative permeability curves is as influential as a Corey gas exponent of 5.5 with no critical gas.

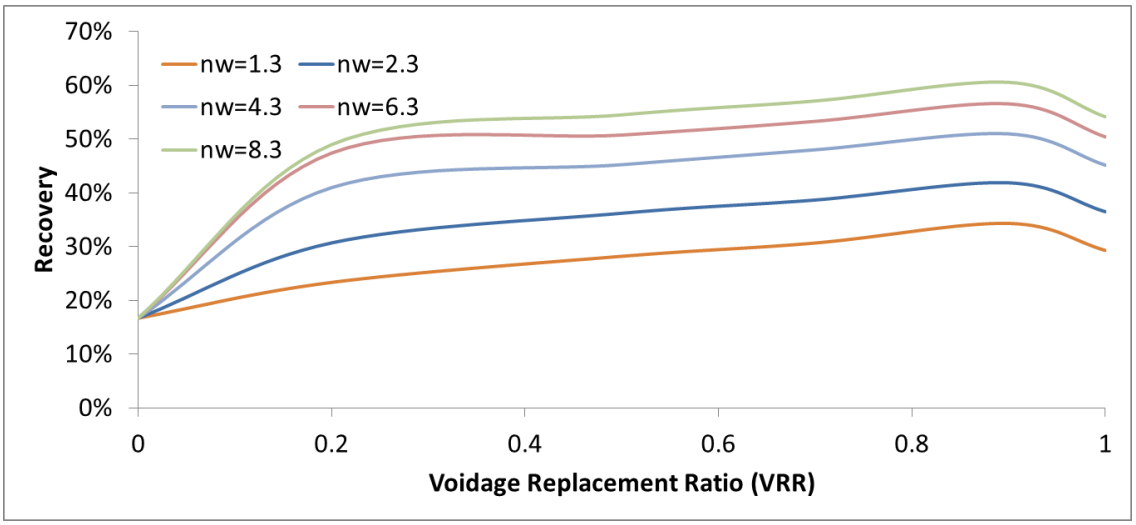

Figure 3-19: Recovery as a function of VRR for different values of the Corey water exponent (ng=1.5; nl=3.4; no=5.5; Sgc=0.1).

Now we consider the case where we modify the Corey oil exponent. Results are shown in Figure 3-30. The results follow a pattern much more closely than the cases with 0% and 5% critical gas saturation. The optimal VRR remains constant at 0.9 as in the case with the Corey water exponents.

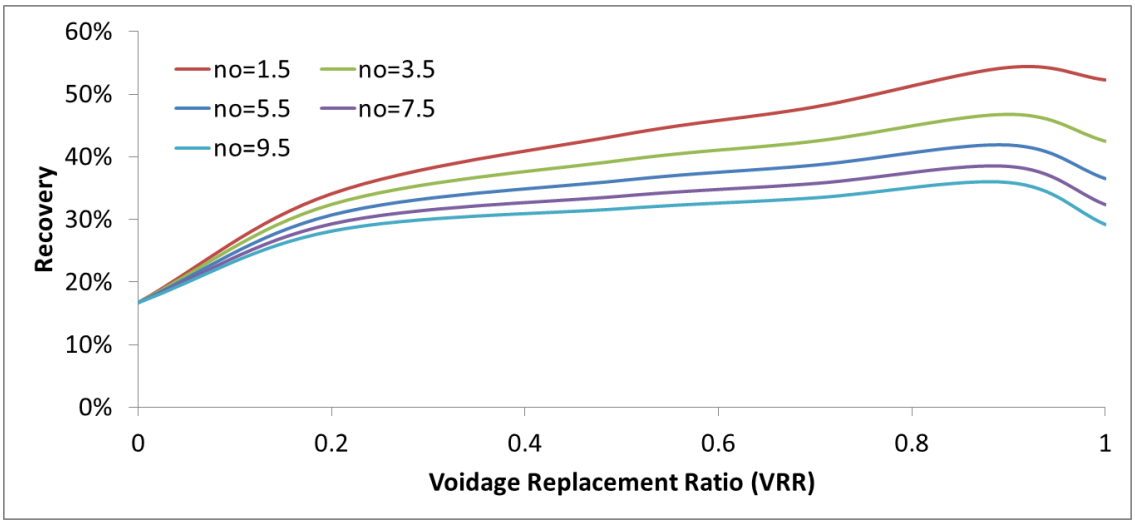

Figure 3-20: Recovery as a function of VRR for different values of the Corey oil exponent (ng=1.5; nl=3.4; nw=2.3; Sgc=0.1).

As Figure 3-21 and 3-22 show, the relative permeability to liquid curves has no effect, and the relative permeability to gas curve dominates the value of the optimal VRR. These results affirm the observations made in sections 3.1.1 and 3.1.3.

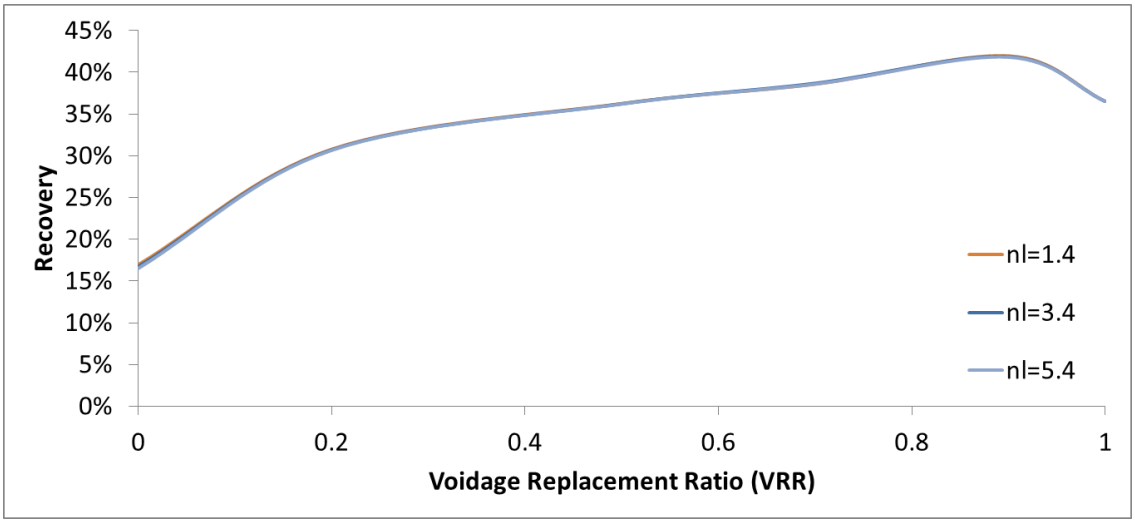

Figure 3-21: Recovery as a function of VRR for different values of the Corey liquid exponent (ng=1.5; no=5.5; nw=2.3; Sgc=0.1); the curves overlay one another as there is virtually no change between the scenarios.

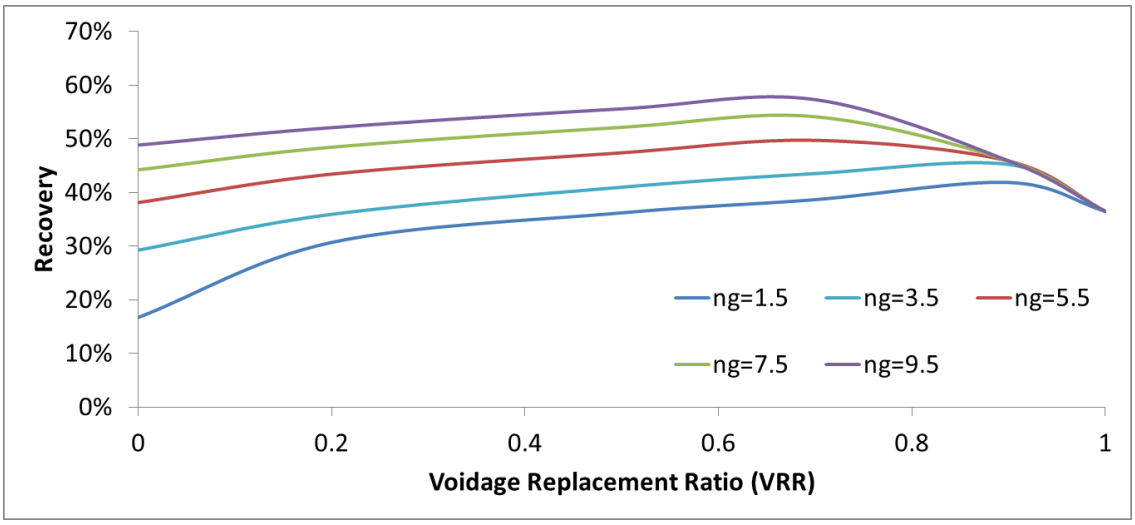

Figure 3-22: Recovery as a function of VRR for different values of the Corey gas exponent (nl=3.4; no=5.5; nw=2.3; Sgc=0.1).

3.1.5. 5% critical gas saturation – role of gas relative permeability

Previously we considered a case with a set of relative permeability curves described in Section 2.1. We modified the critical gas saturation but kept the Corey exponents constant. Now we will consider a case with 5% critical gas where the Corey gas exponent has been modified from the base case and all else is kept constant. Our justification is we have already proven the optimal VRR is most sensitive to the Corey gas exponent. 5% is the mid value for our critical gas saturation sensitivity study and as discussed previously is a reasonable critical gas saturation value for heavy oils (Firoozabadi and Anderson 1994, Kumar et al. 2000). A sensitivity study similar to those performed in sections 3.1.1, 3.1.3, and 3.1.4 was performed with a 5% critical gas saturation and a Corey gas component of 4. All else was kept constant.

First, we consider the results of the Corey water and oil exponent sensitivity studies as shown in Figure 3-23 and 2-24. The results follow patterns similar to those observed in section 3.1.4. Thus, we have proven that when only the relative permeability to water and oil are modified, we can easily replicate results by modifying some combination of critical gas saturation and the Corey gas exponent. This result should not be surprising; we are considering cases with non-unique results that can be achieved by any number of means. Therefore, even though we thus far have only considered abstract sets of relative permeability curves that are not based on any physical reality, our work can easily be extended to other, physical sets of relative permeability curves. More on this topic will be discussed in section 3.2.

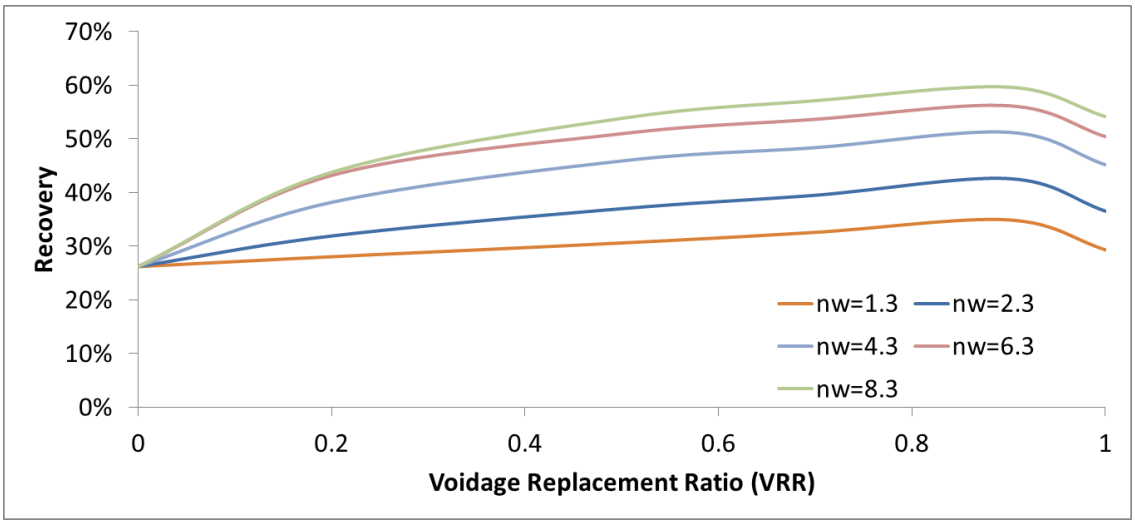

Figure 3-23: Recovery as a function of VRR for different values of the Corey water exponent (ng=1.5; nl=3.4; no=5.5; Sgc=0.05).

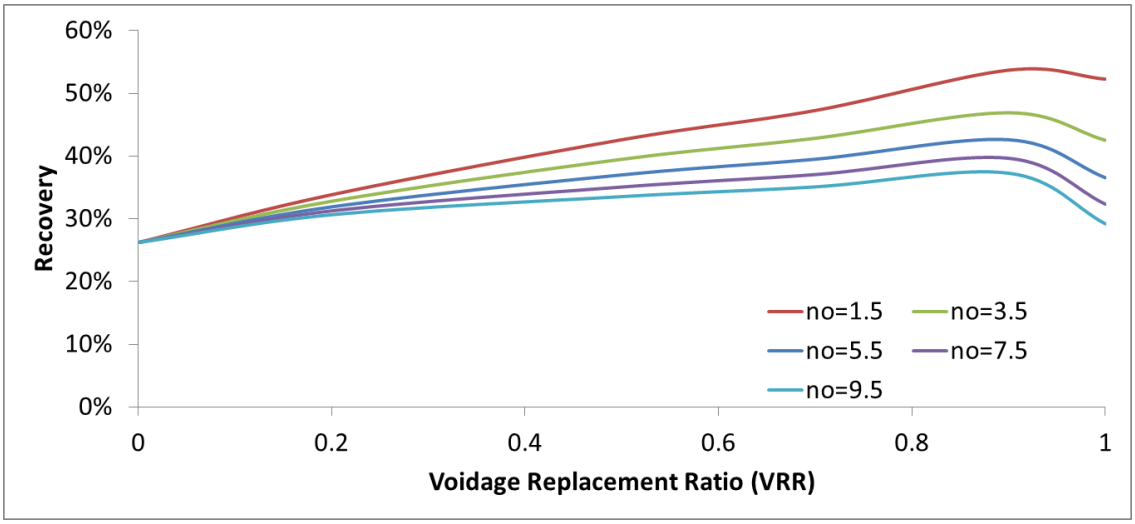

Figure 3-24: Recovery as a function of VRR for different values of the Corey oil exponent (ng=1.5; nl=3.4; nw=2.3; Sgc=0.05).

We now consider the effects of modifications to the liquid-gas relative permeability curves. Modifying the relative permeability of liquid does have an effect on recovery evidenced by Figure 3-25. As the liquid becomes more mobile with a decreasing Corey liquid exponent, more oil is produced. This obvious result was not apparent in sections 3.1.1, 3.1.3, and 3.1.4 due to the negligible values of the gas mobility as a much smaller Corey gas exponent was used in those earlier sections.

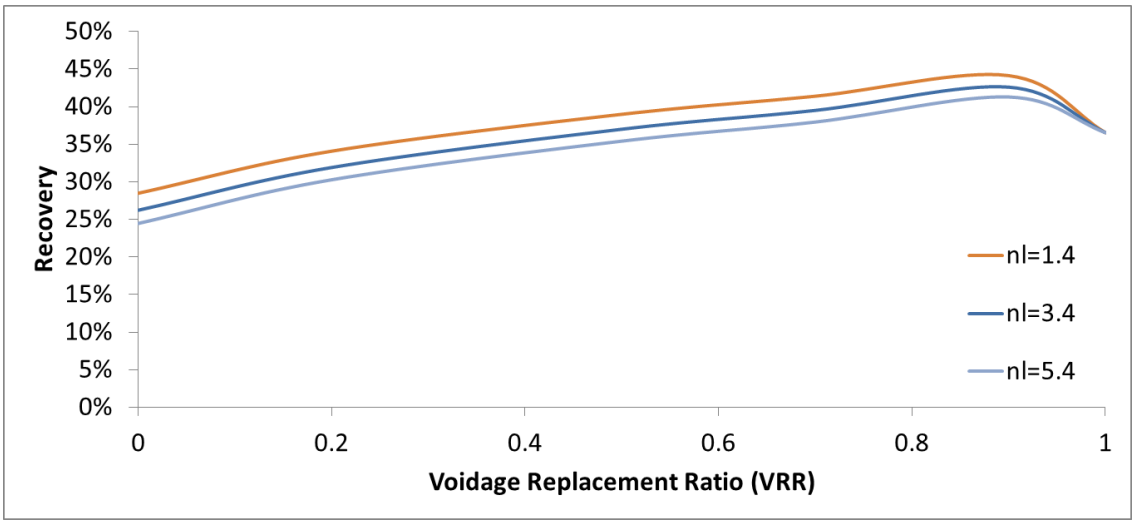

Figure 3-25: Recovery as a function of VRR for different values of the Corey liquid exponent (ng=1.5; no=5.5; nw=2.3; Sgc=0.05); the curves overlay one another as there is virtually no change between the scenarios.

We have shown the recovery at various VRR values varies somewhat predictably with changing oil, water and liquid relative permeability curves but not with the relative permeability to gas. We reaffirm this idea in Figure 3-26, that bears a similar resemblance to the results in section 3.1.4, further showcasing the recovery parallels between this model and the model in 3.1.4, despite their differences.

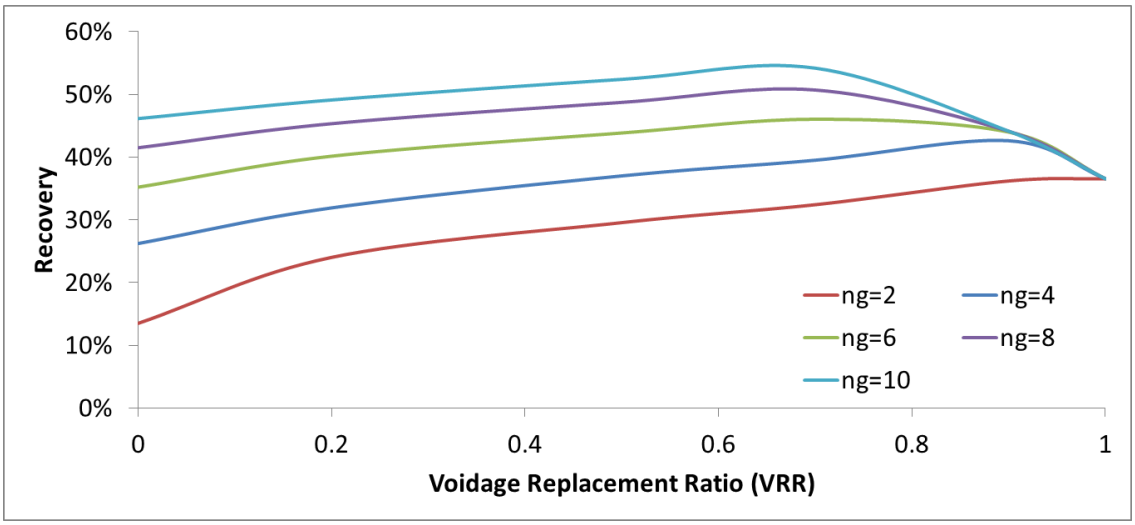

Figure 3-26: Recovery as a function of VRR for different values of the Corey gas exponent (nl=3.4; no=5.5; nw=2.3; Sgc=0.05).

3.1.6. Summary

We have shown in vigorous detail the interplay between the oil, water, liquid, and gas relative permeability curves through the use of modifications to the associated curvatures and the critical gas saturation values. Nonuniqueness of the recovery profiles was also shown. Recovery profiles vary somewhat predictably as a function of the VRR for modifications to the oil, water, and liquid relative permeability curves. We have shown how the advantage of a VRR of 1 reduces as the mobility of oil increases and the mobility of gas decreases. We have also shown how modifications to the relative permeability to gas by either the curvature or the critical gas saturation strongly affect the optimal VRR. We therefore conclude that the relative permeability of the phases, and more specifically, the mobility of gas, strongly affect the optimal VRR.

Our K-values are for a black oil, so the viscosity of only two components matters, that of the oil and that of the gas. By modifying the relative permeability curves of oil, water and gas, we modify the mobility of our phases, and therefore a sensitivity of relative permeability curves will also imply similar results to a modification of the gas and oil phase viscosities. Relative permeability curves are easier to modify and visualize, so we will forego a sensitivity study of the oil and gas viscosities because we have already shown how recovery changes with oil and gas mobility.

3.2. Oil Chemistry

We showed a wide variety of recovery profiles for arbitrarily constructed relative permeability curves. We will now shift our attention to the implementation of physical relative permeability curves. We have already discussed three. We will use our base case set of relative permeability curves, with critical gas saturations of 0%, 5% and 10%, representing medium gravity oils, many heavy oils, and some particular heavy oils, respectively, discussed in the literature (Firoozabadi and Anderson 1994, Treinen et al. 1997, Kumar et al. 2000, Strycker and Wang 2000, Mohanty 2004, Sahni et al. 2004). In addition, to incorporate oil chemistry into our models, we include two other sets of curves, foamy oil and oil emulsion curves, drawn from experimental data in the literature. We will thus have formulated five realistic cases based on observations made in both experiments and in the field by the end of this section.

We will first describe what we mean by oil emulsions. Oil and water are generally immiscible, and an interface forms between the two fluids when in contact with one another. Given certain conditions, oil can emulsify in water; the resulting mixture of oil in water would allow oil to be transported much more quickly than if it were flowing alone, a fact especially true of heavy oils that are hindered significantly by their high viscosities. The conditions at which oil in water emulsions form in heavy oils have been studied in the literature (Schembre et al. 2006).

One possible way oil emulsifies in water, is when the fundamental relationship between the resulting emulsified fluid and the rock is altered. Such a change corresponds with a reduction in wettability between the oil emulsions and the rock matrix when considering fluids in a reservoir. This change in wettability has typically been associated with fines

migration or with some other effect of fines migration (Schembre et al. 2006). Though the wettability change is sometimes attributed to thermal effects, it is notable to say that wettability reductions of similar form have occurred in several field and experimental examples of low salinity waterflooding where thermal effects were not an issue (Lager et al. 2006, Loahardjo et al. 2007). Waterflooding at isothermal conditions with a low salinity fluid has been shown to alter wettability even without the presence of fines migration. The mechanism behind the change in wettability when fines migration does not occur is still in debate though the multicomponent ionic exchange model has been proposed (Lager et al. 2006, Lee et al. 2010). Regardless of whether the effect is a result of fines migration, oil in water emulsions, or multicomponent ionic exchange/the double layer effect, relative permeability curves such as the "emulsion" curves represented in Figure 3-27 do seem adequate to represent physically observed changes in wettability during waterflooding in heavy-oil reservoirs (Jerauld et al. 2006).

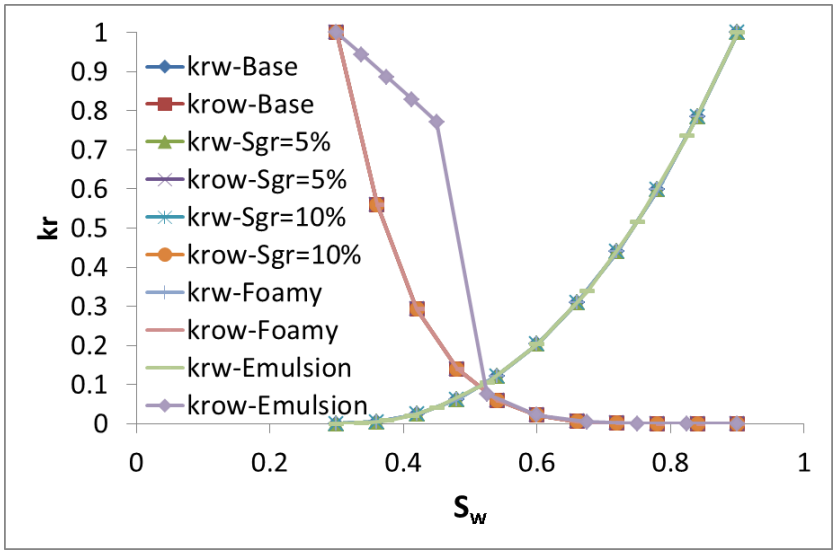

Figure 3-27: Oil-water relative permeability curves for five base cases; all krw and krow curves overlay one another except for krow-Emulsion.

We now consider the concept of a foamy oil. Foamy oils have been observed in the literature for some time (Kumar et al. 2000). The idea of a foamy oil was developed to characterize reservoirs with abnormally high recoveries due to solution gas drive alone (Maini 1995, Bora and Maini 1997). These oils have unusually low gas oil ratios during production below the bubble point. A foamy oil is thought to develop when an oil with particular properties is brought below the bubblepoint and gas is allowed to evolve in the form of bubbles within the oil. These bubbles are thought to be retained within the rock matrix, essentially trapping the evolved gas and allowing the oil to flow uninhibited. Due to the retention of some of the evolved gas in the form of bubbles, the resulting foamy oil maintains a reduced viscosity as well. The foaminess of an oil is thought to be associated with the oil's viscosity, and this phenomena seems to be characteristic of heavy oils only. Vittoratos and West cited foamy oil as an underlying mechanism to improved oil recovery through operating at a VRR less than 1 (2010). Further discussion on foamy oils

is available in the literature (Kumar et al. 2000). Our liquid-gas relative permeability curves for our foamy oil case are based off the experimental data presented in Tang et al. (2006b).

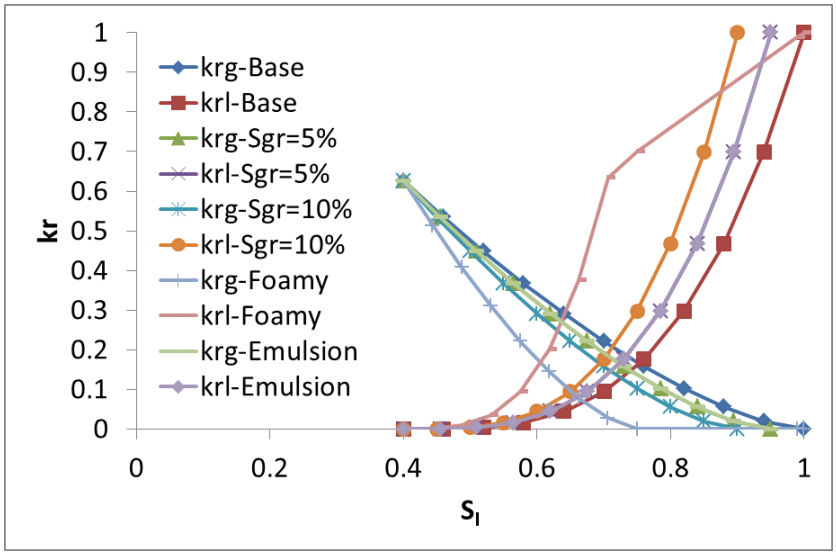

Figure 3-28: Liquid-gas relative permeability curves for five base cases; krl and krg for Sgc=5% and Emulsion overlay one another.

Using the five scenarios we have outlined above, our base case set of relative permeability curves, with critical gas saturations of 0%, 5% and 10%, oil emulsion curves that are identical to the base case with a critical gas saturation of 5% and a modified oil relative permeability curve shown in Figure 3-27, and a foamy oil set of liquid-gas relative permeability curves, we have simulated results for performance in our homogeneous base case model. Recovery is plotted as a function of VRR in Figure 3-29. The recovery values at a VRR of 1 are essentially consistent, with a slight deviation with the oil emulsion curves as expected, but the results are quite dissimilar below a VRR of 1. The oil emulsion case has larger recovery values at every VRR when compared to its counterpart with base case water-oil relative permeability curves, as expected. The difference in recovery between the two cases is largest at a VRR between 1 and 0, and the difference peaks at 0.5 VRR. This somewhat unintuitive result is interesting if we consider our results in section 3.1 where an increased oil mobility seemed to lessen the advantage of a VRR of 1. We see this observation take full effect here, but most significantly between a VRR of 0.5 and 0.7 rather than at that of 0.9.

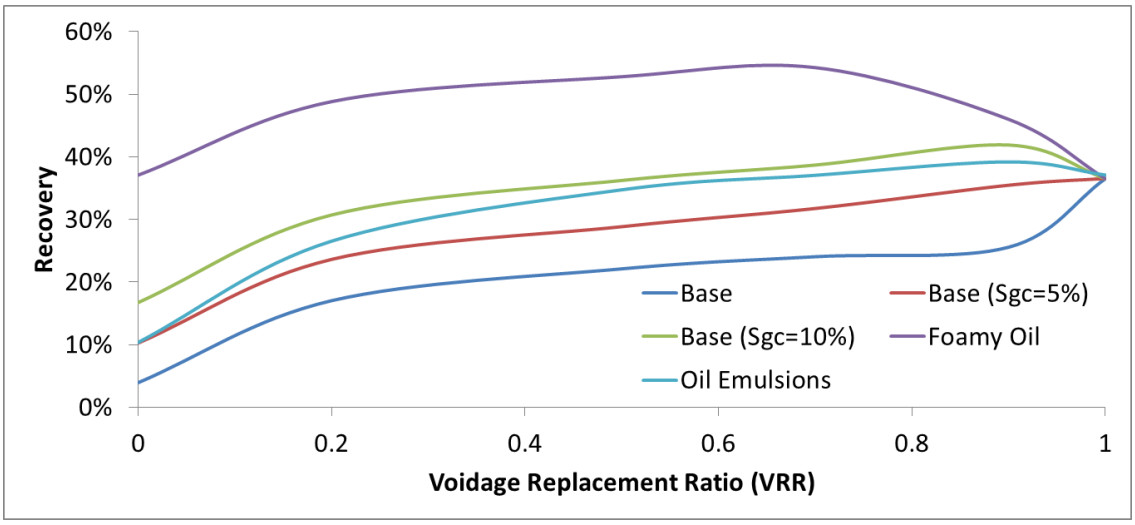

Figure 3-29: Recovery as a function of VRR at 0.6 days for five cases developed from real data.

The results of the foamy oil case are by far the most interesting. They are in almost complete contrast to our base case. For one, a VRR of 1 yields the least recovery of all other scenarios involving the foamy oil relative permeability curves. The optimal VRR of 0.7 grants almost 18% more incremental oil recovery than performing a standard waterflood at a VRR of 1. It may seem shocking that primary recovery yields almost 40% recovery of the original oil in place in the foamy oil case, but this recovery value for a VRR of 0 matches experimental data observed in the literature (Tang et al. 2006b). Thus, the recovery profile displayed in Figure 3-29 is not unrealistic for a core-scale experiment.

It is important to consider the implications of our results. If water is a source of concern, than even in the case where there is a 5% critical gas, a reasonable assumption for many heavy-oil reservoirs, one can achieve virtually the same recovery by using a VRR of 0.9, while thus using less water. If oil emulsions are present in the reservoir, one would be missing out on a little over 2% incremental recovery by not operating at a VRR of 0.9 when compared to that of 1. At 10% critical gas, one would be missing out over 5% incremental recovery. In the case of a foamy oil, it is far more beneficial to operate at a VRR below 1, and operating as low as a VRR of 0.7 is optimal by a significant margin which coincides with observations made in the literature for other types of heavy-oil reservoirs (Vittoratos and West 2010). The primary recovery value for the foamy oil case coincides with observations in the literature (Tang et al. 2006b).

3.3. Reservoir Heterogeneity

We will next discuss the role of reservoir heterogeneity in influencing the optimal VRR. We have thus far only considered performance in a homogeneous core model, but given the widespread heterogeneity existing in hydrocarbon reservoirs, it is important to consider the effect of perturbations to our base case model. We will consider a heterogeneous permeability distribution, high permeability streaks, impermeable streaks,

and cul-de-sacs that are analogues to heterogeneous features in real-life reservoirs such a fractures, faults, and areas of weak connectivity.

Heterogeneity plays an important role in our particular study for a number of reasons. When we consider the mechanisms behind how a traditional waterflood operates, this fact becomes obvious. During a field-scale waterflood, water pierces its way through the reservoir from an injector well associated with a high pressure to a producer well associated with a lower pressure. The water is driven by this pressure gradient but flows according to the path of least resistance. Oil in the large pores within the reservoir along the path of the injected water is swept out. If we consider times far into the future, we see that water travels along this "backbone" path for the remainder of the waterflood. Any "dangling ends" are bypassed, that along with capillary pressure, contributes to residual oil in our reservoir. It has been theorized that combining a solution gas drive with this water drive leads to oil recovery from these dangling ends (Vittoratos and West 2010). If we wish to consider the full potential of improved recovery from a VRR less than 1, we must consider heterogeneity and these dangling ends.

3.3.1. Heterogeneous permeability distribution

We begin our study of reservoir heterogeneity with a heterogeneous permeability distribution. We created a log normal permeability distribution based off simple Gaussian simulation in SGEMS. The distribution was constructed such that the mean was the permeability in our base case homogeneous model. A histogram of permeability values generated by SGEMS is shown in Figure 3-30. The result of running our set of five base cases on this model is shown in Figure 3-31. Results are expected. Recovery as a function of VRR is essentially exactly the same as it was in a model with a homogeneous permeability distribution. Perturbations to the permeability are averaged out over the model and act as if there is one single value, the effective permeability, as is used in our homogeneous case.

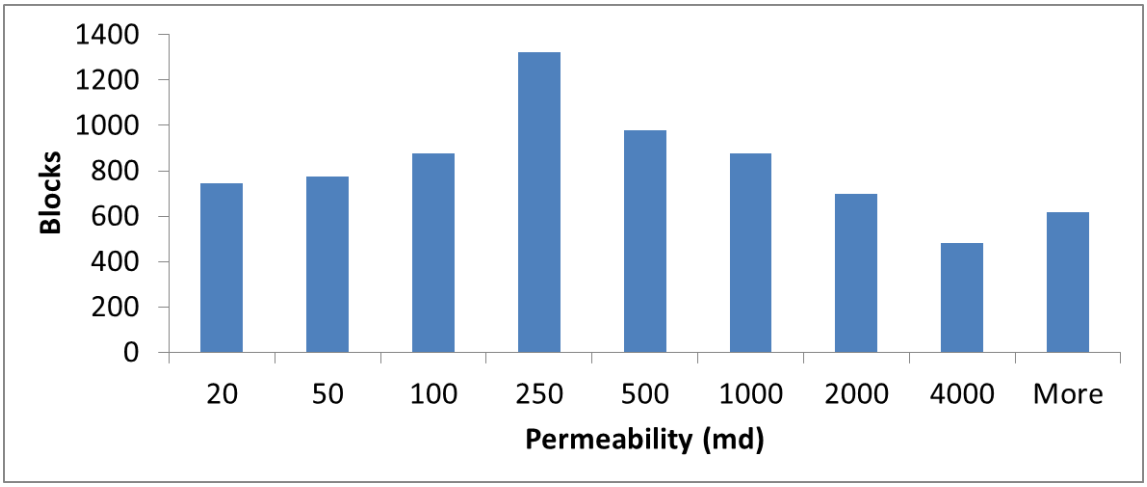

Figure 3-30: Histogram of permeability distribution generated by SGems in model with a heterogeneous permeability distribution.

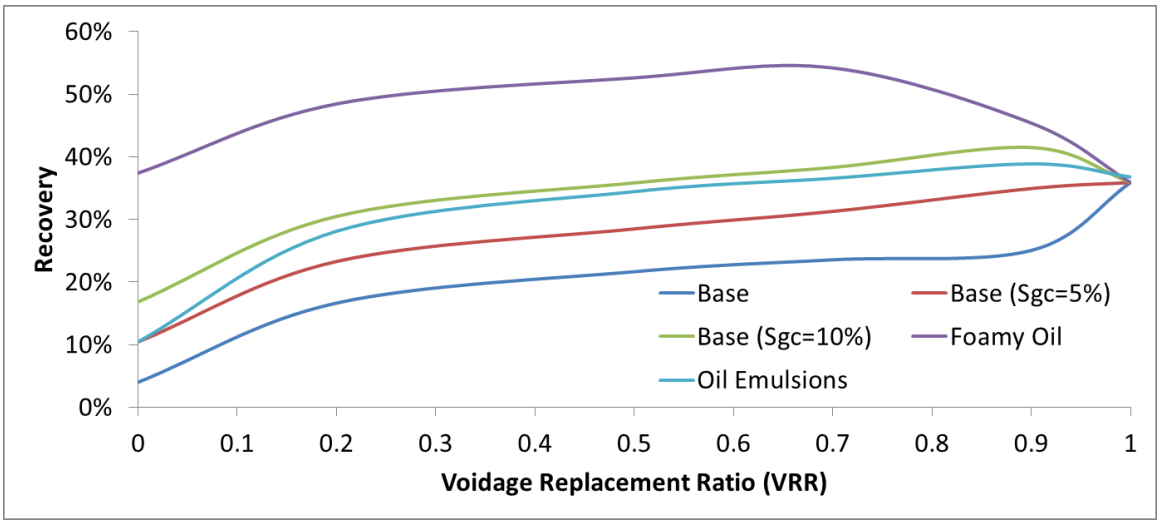

Figure 3-31: Recovery as a function of VRR at 0.6 days for five cases in a model with a heterogeneous permeability distribution.

3.3.2. Fracture parallel to flow

We will next consider the case where a streak of high permeability cells runs directly through the middle of the model, in the i-direction. Thus, the streak runs directly through both the producer and injector wells. The permeability of this streak was chosen to be 100 times larger than that of the base permeability in all directions. In total, there were 91 cells with this increased permeability, all in the i-direction. This modification was done to see the effect of creating a preferred path between injector and producer.

Results of our adjustments are shown in Figure 3-32. In this case, a VRR of 1 is suboptimal for all of our five cases. This result makes physical sense if we consider water is flushed out of the model almost as quickly as it is injected. The fluid travels mainly along the preferred path located between the injector and producer. In the cases where the VRR is dropped below 1, solution gas drive is allowed to take effect and oil from outside the "fracture" is allowed to be produced. The recovery values almost never deviate from the value obtained at primary depletion for any of the five cases due to the fact the water injected is never allowed to assist in sweeping the oil out in regions outside the high permeability region. The oil emulsion case has no added benefit to its counterpart due to the fact recovery is dependent exclusively on the liquid-gas relative permeability curves for VRR values below 1, as discussed in section 3.1.1.

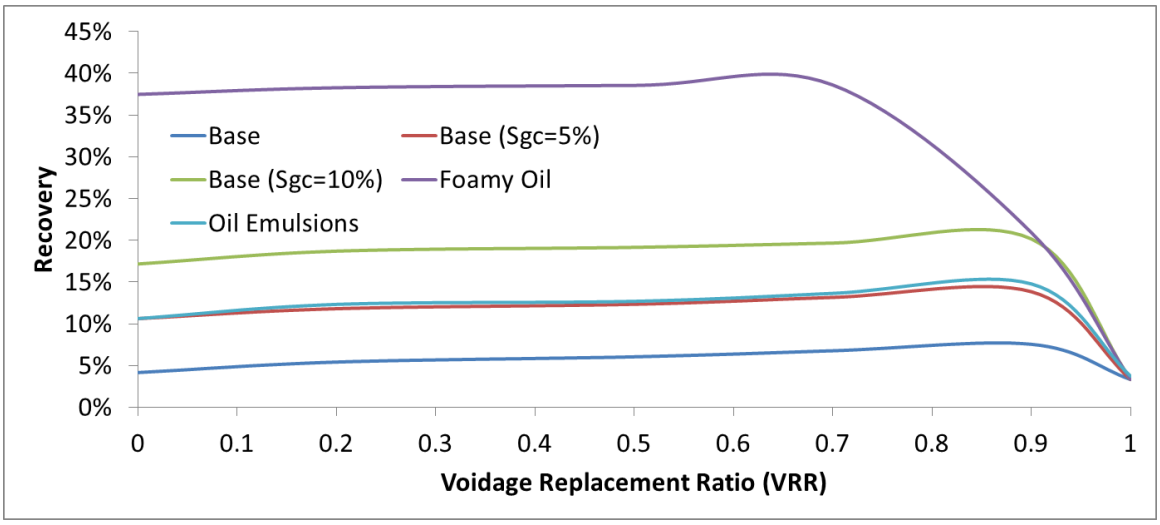

Figure 3-32: Recovery as a function of VRR at 0.6 days for five cases in a model with a horizontal fracture parallel to flow.

It is worth noting the recovery values are not exactly flat for every VRR less than 1. All but the foamy oil case, that has an optimal VRR of 0.7, have an optimal VRR of 0.9.

3.3.3. A fracture parallel and a fracture perpendicular to flow

Next we consider the case where we modify the model described in 3.3.2, and increase the permeability of 9 cells spanning the k-direction by a 100 in all directions. The cells were modified such that the center of the modified cells lied exactly in the center of the cells previously modified in the i-direction. This change was done to see the effects of preferential vertical flow in the center of the model.

The results of this new alteration are shown in Figure 3-33. The recovery values are visually identical to those with the model with only the fracture parallel to flow. The pressure gradient is driving fluids across the fracture parallel to flow, so a fracture perpendicular to flow instills no added benefit in terms of sweep efficiency.

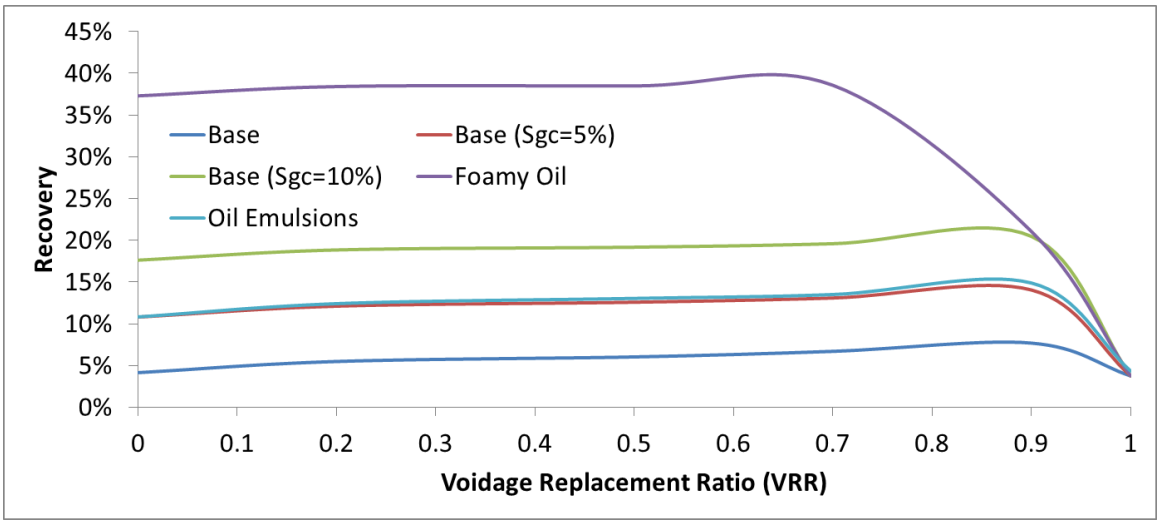

Figure 3-33: Recovery as a function of VRR at 0.6 days for five cases in a model with a horizontal fracture parallel to flow and a vertical fracture perpendicular to flow.

3.3.4. Walls parallel to flow

Next we consider anisotropy in a scenario where impermeable "walls" run along the i-direction, parallel to flow, across all cells in the k-direction as shown in Figure 3-34. We define "walls" as cells impermeable in one or more directions. In this case, only the permeability in the j-direction is null; i.e., flow can only run in the i or k directions. Analogues to such scenarios are faults that run parallel to flow between the injector and producer wells.

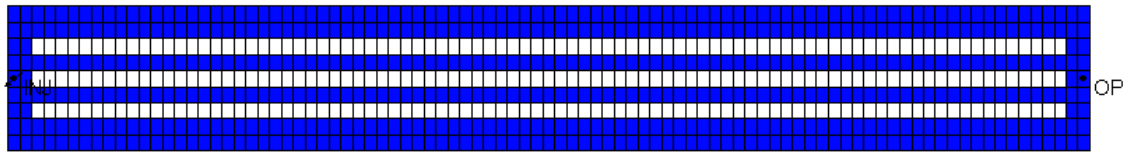

Figure 3-34: I-J slice of model with impermeable walls parallel to flow; white cells are impermeable in the j-direction (in the direction of top to bottom in the picture above).

Results for this previously described scenario are shown in Figure 3-35. They are identical to the results shown in the absence of anisotropy in the base case model. The result is merely a reality check. We would expect in such a small-scale model of a core for flow to be completely in the i-direction with little cross-flow. We saw a similar result in section 3.3.3 where virtually no flow deviated from the i-direction into the k-direction, even with favorable permeability.

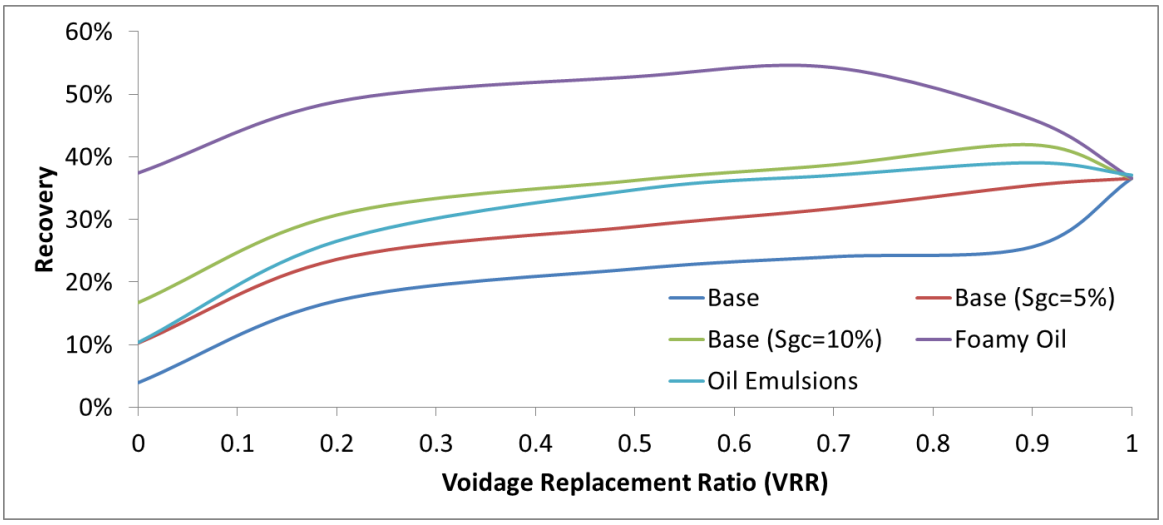

Figure 3-35: Recovery as a function of VRR at 0.6 days for five cases in a model with impermeable walls parallel to flow.

3.3.5. Walls perpendicular to flow

Now we consider the case where there are impermeable walls perpendicular to flow; i.e., we create cells along the j-direction that are impermeable in the i-direction across all cells in the k-direction. A top-down view of this model is shown in Figure 3-36. An analogue to this model is a scenario in which small faults run across the path of producer and injector wells.

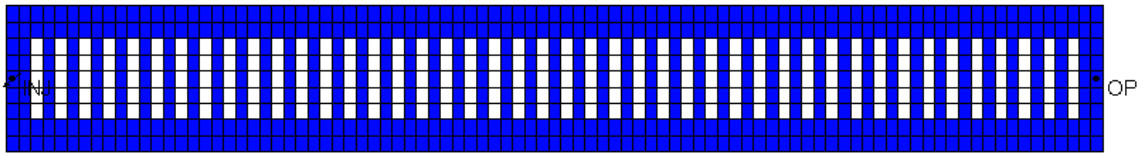

Figure 3-36: I-J slice of model with impermeable walls perpendicular to flow; white cells are impermeable in the i-direction (in the direction of right to left in the picture above).

Recovery as a function of VRR is plotted in Figure 3-37 for the case of impermeable walls perpendicular to flow. It may at first seem like there is little difference in the curvature of the results when compared to the homogeneous base case, though recovery values are far different. The difference in recovery is easy enough to explain. Fluids prefer to flow along the i-direction, so when there are boundaries preventing flow in this direction, the oil remains trapped for the most part between these walls, and only a small amount of oil that manages to flow in the j-direction makes it into the "backbone" channels where it is produced.

If we look closely enough, we see that the curvature of the recovery curves is slightly different from those in pertaining to the homogeneous base case. The recovery values associated with a VRR of 1 are not as advantageous as they are in the homogeneous base case. The optimal VRR for the case where S_{gc}=5% becomes 0.9 as a result of this change. The effect is not large, but we can imagine how this effect would be compounded if connectivity varied throughout our model.

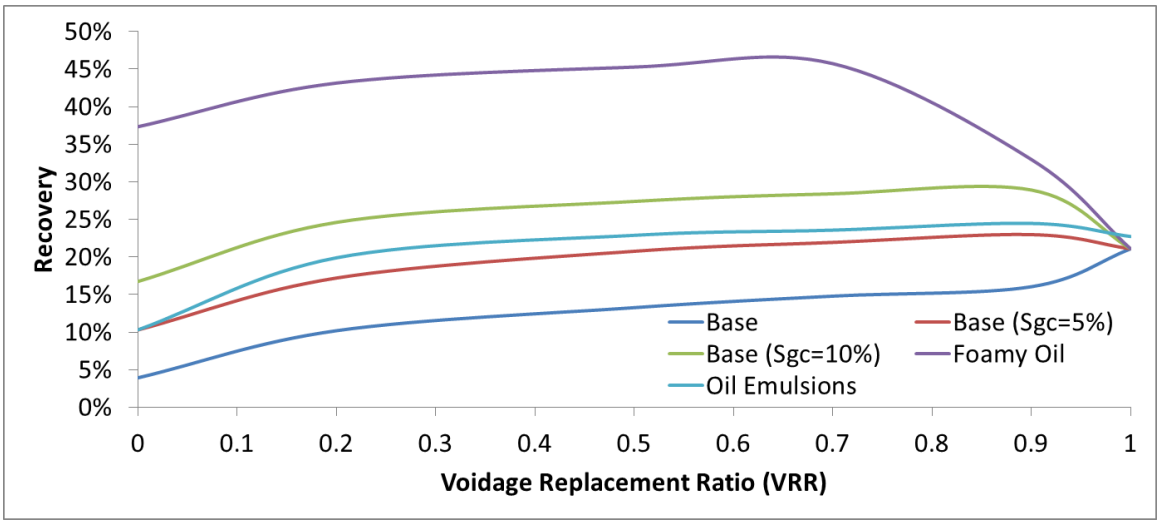

Figure 3-37: Recovery as a function of VRR at 0.6 days for five cases in a model with impermeable walls parallel to flow.

3.3.6. Cul-de-sacs

Lastly, we consider the case where there are cul-de-sacs in our model, the direct analogue to the dangling ends in a reservoir, or small pockets of poor connectivity. To construct this kind of model we merely add cells impermeable in the j-direction at every depth in between the cells that are impermeable in the i-direction running along the center of the model, as shown in Figure 3-38. This model is identical to the one used in section 3.3.5, except for the inclusion of the cells that are impermeable in the j-direction in between the walls.

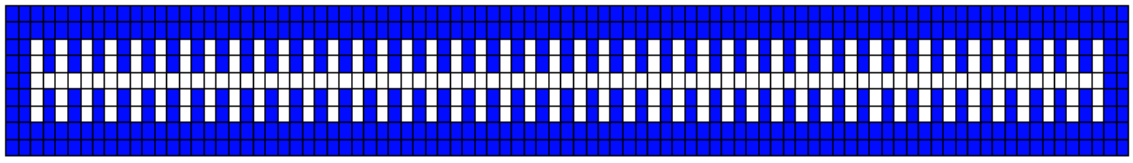

Figure 3-38: I-J slice of model with cul-de-sacs; the model is identical to the case with that of the one with impermeable walls perpendicular to flow except for the inclusion of cells that are impermeable in the j-direction.

The consequence of this new model is shown in Figure 3-39. The results are essentially the same as those in the case of walls perpendicular to flow which makes sense due to the fact barriers to i-directional flow are the biggest inhibiters to fluid movement and flow across the j-direction is minor, as has been shown. Recovery is slightly smaller for the cul-de-sac case when compared to the case with impermeable walls perpendicular to flow because the oil in the center blocks between walls in the cul-de-sac case is essentially immobilized because no flow is allowed in the j-direction in those cells, and the surrounding cells are impermeable in the i-direction. This reduction in recovery is minor in most cases.

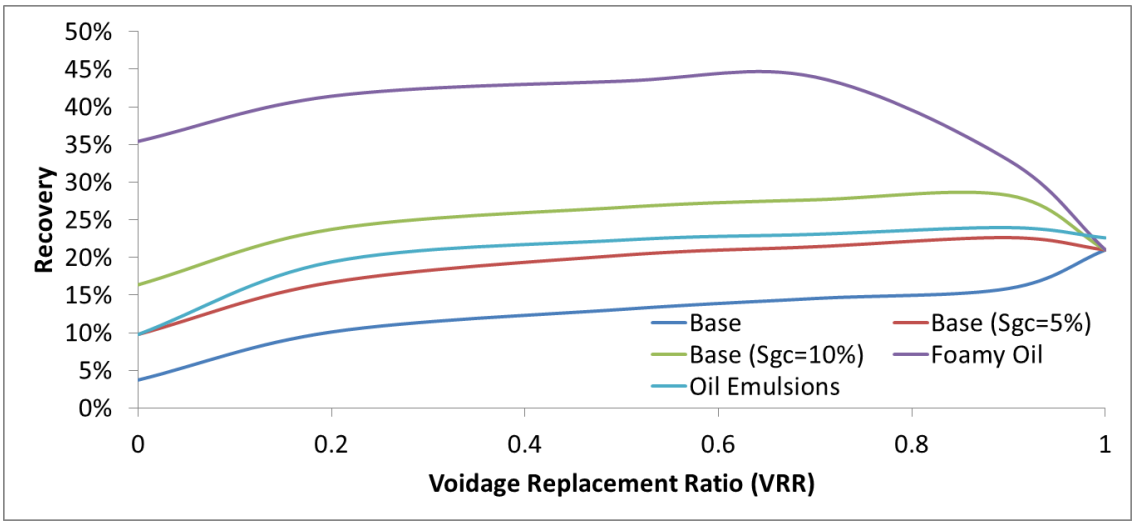

Figure 3-39: Recovery as a function of VRR at 0.6 days for five cases in a model with cul-de-sacs.

We want to focus on how the performance of scenarios with a VRR of 1 compares with the performance of those with a VRR of less than 1. Considering the homogeneous base case model, a VRR of 1 gets 12.5% and 4.8% more incremental oil recovery than a VRR of 0.7 for the base case with 0% and 5% critical gas saturation, respectively, as shown in Figure 3-40. With the 10% critical gas saturation base case and the foamy oil case, incremental recovery is actually 2.2% and 17.7%, respectively, lower with a VRR of 1 than a VRR of 0.7, as shown in Figures 3-40 and 3-41. Recovery for the oil emulsions case is essentially the same with a VRR of 1 and 0.7. If we consider the cul-de-sac model, there is only 6.4% more incremental recovery when performing at a VRR of 1 as opposed to that of 0.7 with the base case and no critical gas. For the 5% critical gas case and the oil emulsions case, there is slightly negative incremental recovery, and for the 10% critical gas and foamy oil cases, 6.7% and 23% incremental recovery, respectively, are missed. The trend is similar for other VRR values when compared to a VRR of 1. Thus, even if it is not overly apparent from the recovery curves in Figure 3-39, the recovery with a VRR of 1 is far less advantageous in the cul-de-sac model than the homogeneous cores, as seen in Figures 3-40 and 3-41. We can see that for the case of 5% critical gas saturation, the optimal VRR has actually switched to 0.9 from 1 in the homogeneous model, and even a VRR of 0.7 performs better than a VRR of 1 in the cul-de-sac case. It

is also worth noting that given the smaller recoveries in the cul-de-sac model, such changes in incremental recovery are more significant than similar values resulting from the homogeneous core.

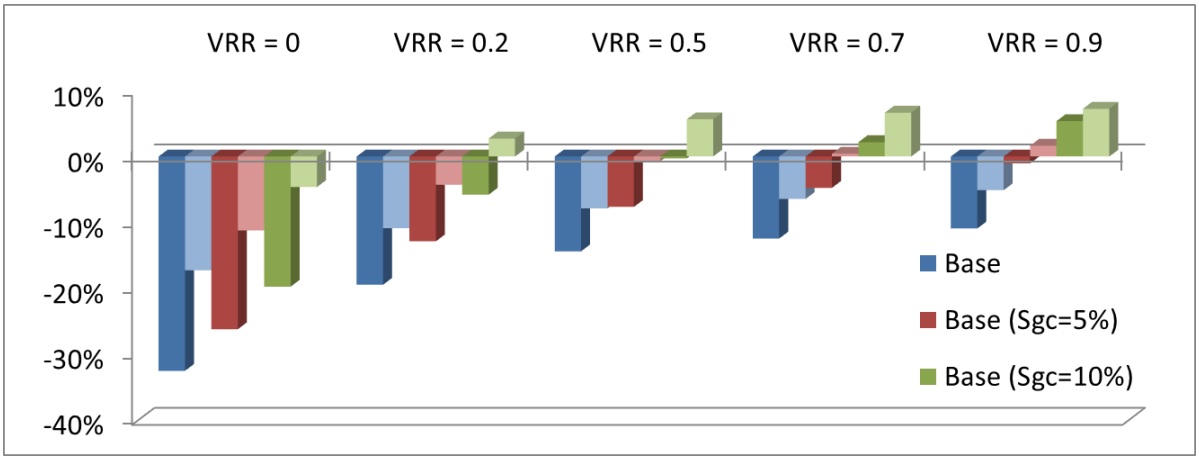

Figure 3-40: Difference between the recovery at a specified VRR and the recovery at a VRR of 1 for three cases. The darker colors correspond to results using the homogeneous core-model, while the lighter colors correspond to results using the cul-de-sac model.

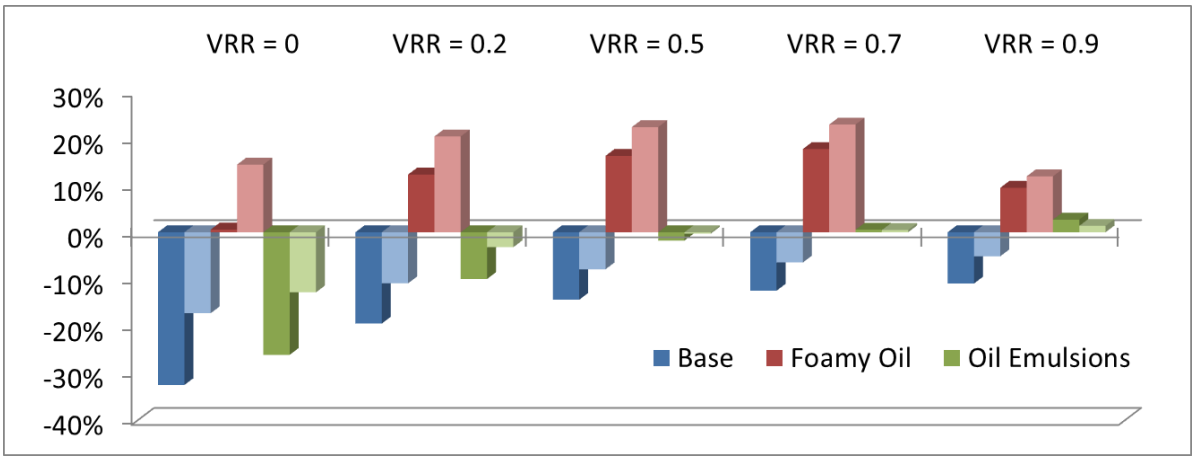

Figure 3-41: Difference between the recovery at a specified VRR and the recovery at a VRR of 1 for two other cases. The darker colors correspond to results using the homogeneous core-model, while the lighter colors correspond to results using the cul-de-sac model.

3.3.7. 3D Cul-de-sac Models

We have described three models each characterized by some heterogeneity in the form of impermeable walls perpendicular or parallel to flow, or both, in the form of cul-de-sacs. While technically 3-dimensional, our models are effectively only 2 dimensional in some sense, given the walls extend along the entire length of the k-direction. It is important to note the models depicted in Figures 3-34, 3-36, and 3-38 do have 3 dimensional characteristics to them. At end time, there is always some degree of difference in the oil saturation in the blocks in the top layers when compared to those in the bottom layers, even in the case of no or negligible gas saturation as in the base case. Ruling out the

presence of gas, whose saturation is naturally greater in the upper layers for the cases with critical gas saturations, the difference between the oil saturations at the top and bottom layers is around 1-3% in all the cases.

To make our results more representative of what would occur in the natural world, we decided to include 3-dimensionality to our models by removing any heterogeneity in the top 2 and bottom 2 layers of the models presented in Figures 3-34, 3-36, and 3-38. Before analyzing the results, we note it is obvious this change will lead to much higher observed recoveries due to the lack of barriers to flow in four out of the nine layers. Thus, we will not present the results of the simulations on the model with impermeable walls parallel to flow, because they are identical to those shown in Figure 3-29 or 3-35. The results of simulations on the model with walls perpendicular to flow are virtually identical to those on the model with cul-de-sacs, so we will only discuss the results of the cul-de-sac simulations. A plot of recovery is shown in Figure 3-42. Not only is recovery greater in all cases when compared to the results depicted in our effectively 2-dimensional model in Figure 3-39, a comparison of recoveries shows those recoveries associated with a VRR less than 1 are less favorable relative to those with a VRR of 1 in this modified 3-dimensional model when compared to the results using the effectively 2-dimensional model, as shown in Figures 3-43 and 3-44. As we decrease the heterogeneity in our model, a traditional waterflood, with a VRR of 1, becomes more favorable as expected. More oil is allowed to escape in the vertical direction when we remove any anisotropy in the top and bottom layers.

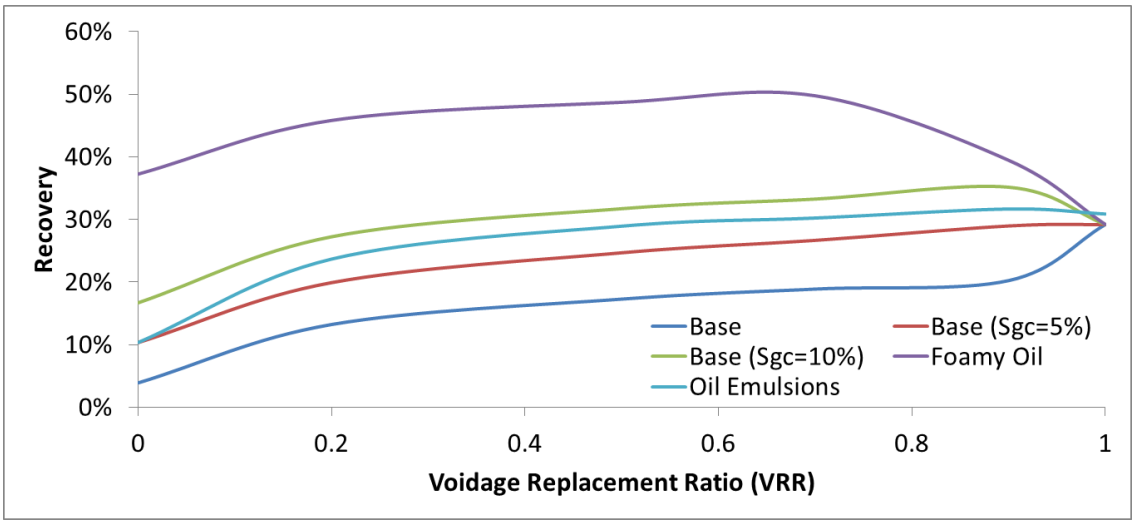

Figure 3-42: Recovery as a function of VRR at 0.6 days for five base cases in a modified 3D model with cul-de-sacs.

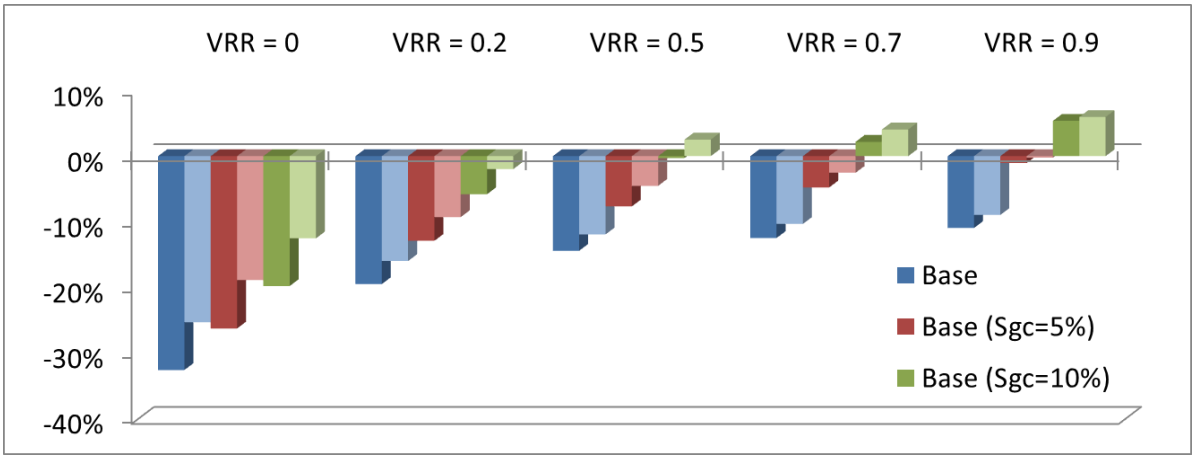

Figure 3-43: Difference between the recovery at a specified VRR and the recovery at a VRR of 1 for three cases. The darker colors correspond to results using the homogeneous core-model, while the lighter colors correspond to results using the modified cul-de-sac model.

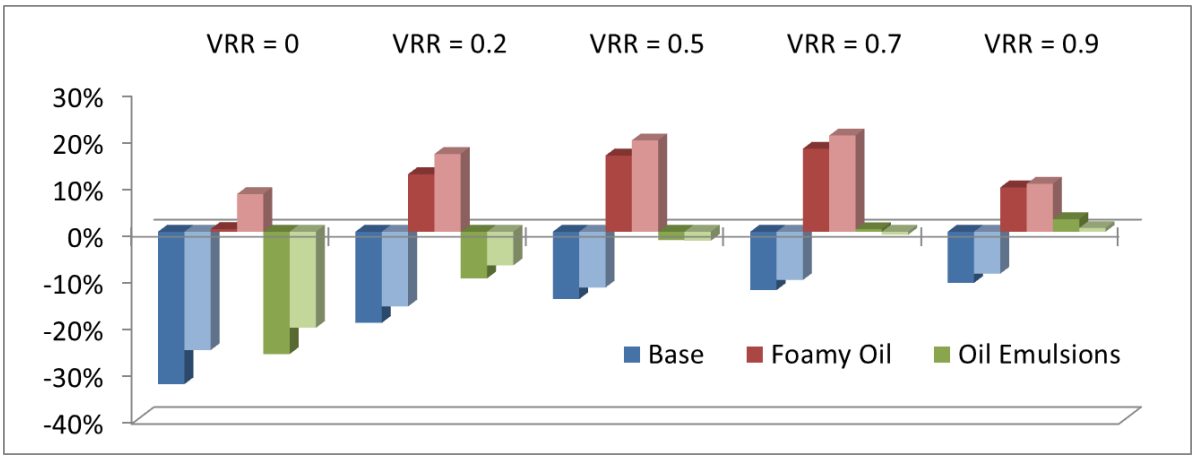

Figure 3-44: Difference between the recovery at a specified VRR and the recovery at a VRR of 1 for two other cases. The darker colors correspond to results using the homogeneous core-model, while the lighter colors correspond to results using the modified cul-de-sac model.

3.3.8. Summary

We have shown that idealized heterogeneity affects the effectiveness of a VRR of 1 and even causes a change in the optimal VRR for our cases. By heterogeneity we mean differences in connectivity across our model, not randomness. Randomness associated with the permeability distribution is of no impact, emphasizing that our assumption of an effective permeability is valid. However, large heterogeneous features in the model or anisotropy can affect the optimal VRR. The presence of fractures, or any highly permeable conduits, vastly reduces the effectiveness of a traditional waterflood. Impermeable barriers perpendicular to flow cause not only reduced recovery, but also

decrease the effectiveness of waterfloods operating at VRR of 1 compared to those less than 1. The presence of cul-de-sacs or physical oil-trapping regions in a model can also have this effect.

3.4. Reference Scale

Thus far we have represented our results at particular time periods. We chose a time sufficiently far after peak production rates to avoid bias toward waterfloods performed at a VRR less than 1, as explained in section 2.1. Using other times or dimensionless times as reference points for reporting results affects the optimal VRR- a somewhat intuitive fact. In this section we will justify our use of a reference scale and show the results of the optimal VRR given the use of other reference scales.

3.4.1. Time

We have used a particular time, 0.6 days, as a reference scale for all the studies performed in this chapter. At 0.6 days, every model's cumulative oil production is asymptotically approaching its theoretical maximum production, even cases involving the foamy oil relative permeability curves, where non-negligible oil production occurs up until later times. The time of 0.6 days is long past peak production rates and pressure depletion in the model, for cases of a VRR less than 1. For this reason, we believe it provides a much fairer comparison across every scenario we have studied. It is important to note, however, due to the fact the pressure in the core is already depleted in the cases of a VRR less than 1, the VRR constraint is not maintained for the vast majority of time before 0.6 days.

We have already shown the results at 0.6 days for our five scenarios in the homogeneous cores in section 3.2. Now we will consider the results at 0.3 days and 0.07 days as shown in Figures 3-45 and 3-46. The recovery values are different in both cases when compared to those at time 0.6 days, for obvious reasons. At 0.3 days, the recovery profiles are similar to those at 0.6 days; however, the optimal VRR for the base case with S_{gc}=5% is 0.9 at 0.3 days as opposed to 1 at 0.6 days. The difference is marginal at both times, so we do not consider this a significant effect. At 0.07 days, the recovery profiles are in stark contrast to those at 0.3 and 0.6 days. 0.07 days represent a time almost immediately after peak production rates in all five cases. Thus, the VRR constraint has been maintained throughout all the time before 0.07 days. The problem with using such an early time to compare results is apparent in Figure 3-46. There is a large bias to VRR's below 1 in all but the base case. Using such early times does not take into consideration the long-term impact of a depletion drive; i.e., complete pressure depletion of the model. At 0.7 days, the pressure drops to atmospheric, the BHP constraint, in all but the cases where VRR is 1, implying production after this point is marginal for those cases.

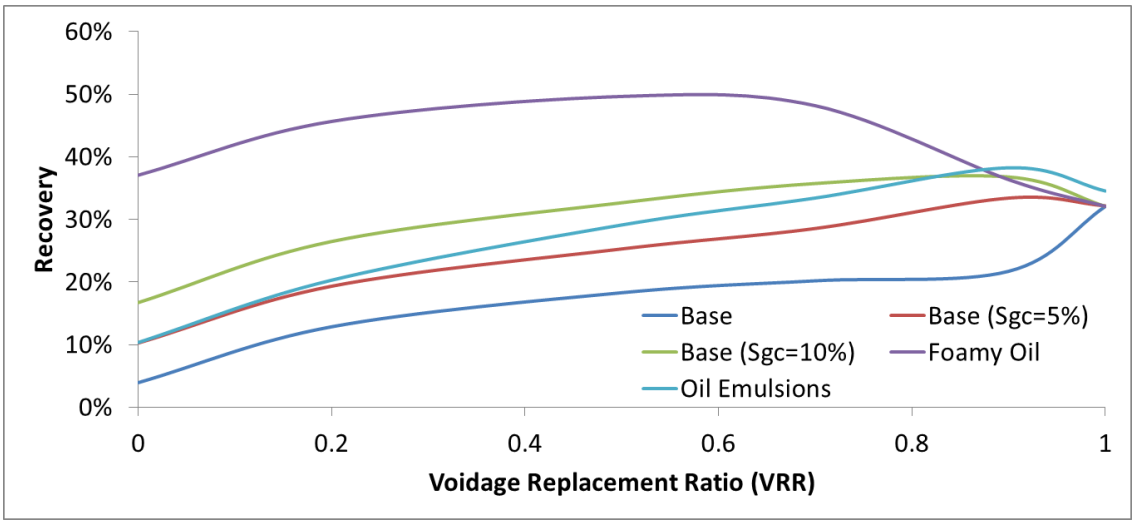

Figure 3-45: Recovery as a function of VRR at 0.3 days for five cases.

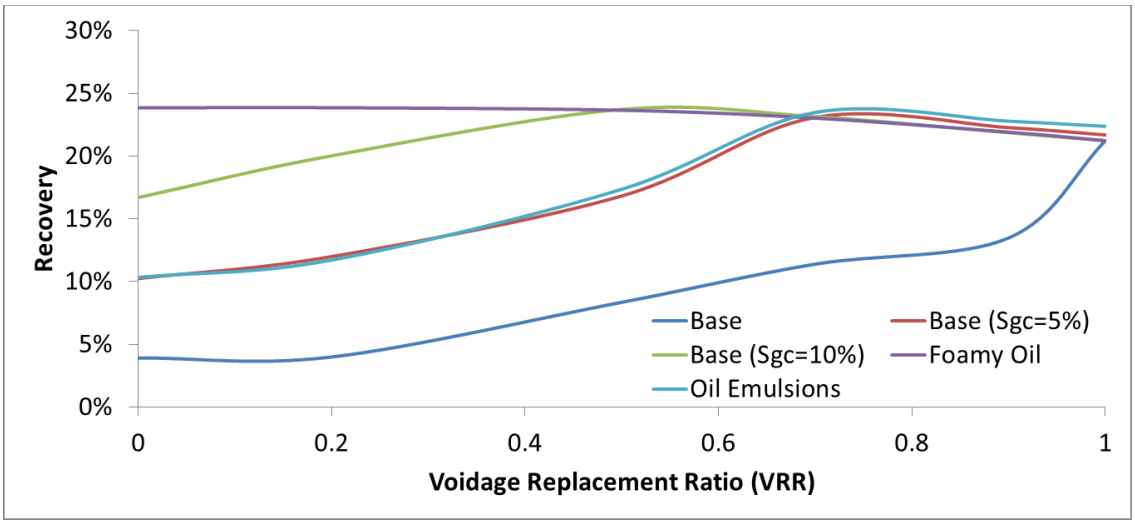

Figure 3-46: Recovery as a function of VRR at 0.07 days for five cases.

In these homogeneous, small-scale models, where connectivity does not come into play, it can be argued that considering the time only pre-pressure depletion gives an unfair bias to scenarios involving a VRR less than 1. For larger scale reservoir models, where connectivity is more of an issue and the pressure transient is much less uniform, it would be fair to consider production before the reservoir pressure has fallen sufficiently low, but for the case of small-scale homogeneous models, it appears better to consider times long after pressure depletion. This assumption is justified later with our results in section 4.2.

3.4.2. Dimensionless time

Typically, recovery is represented in terms of dimensionless time, most commonly in terms of pore volumes injected, in order to place all scenarios on a level playing field.

Viewing results that are unconstrained by time allows for more universal comparisons. In most cases, representing recovery in terms of dimensionless time is optimal for this reason, but this fact is not generally true. We must consider when a reservoir is operated at a VRR below 1 there is a both a water drive and depletion drive. Thus even at a VRR close to 0, a small fraction of water injected will appear to be associated with large volumes of fluids produced, when in fact the production is associated with the depletion drive and not the water drive. As evidence of some of the flaws of using pore volumes injected as our reference scale, we present Figure 3-47 that depicts recovery as a function of pore volumes injected for different VRR for our base case. Note the contrast with Figure 2-7. Unless a very small pore volumes injected value is chosen, all models using a VRR between a VRR of 1 and 0 merge onto one another, due to the issue discussed in section 2.2 in which pressure depletion causes late times to act as waterfloods with a VRR of 1, at reduced production rates. Because no water is injected during primary depletion, a straight line representing the final recovery for a VRR of 0 is plotted for reference.

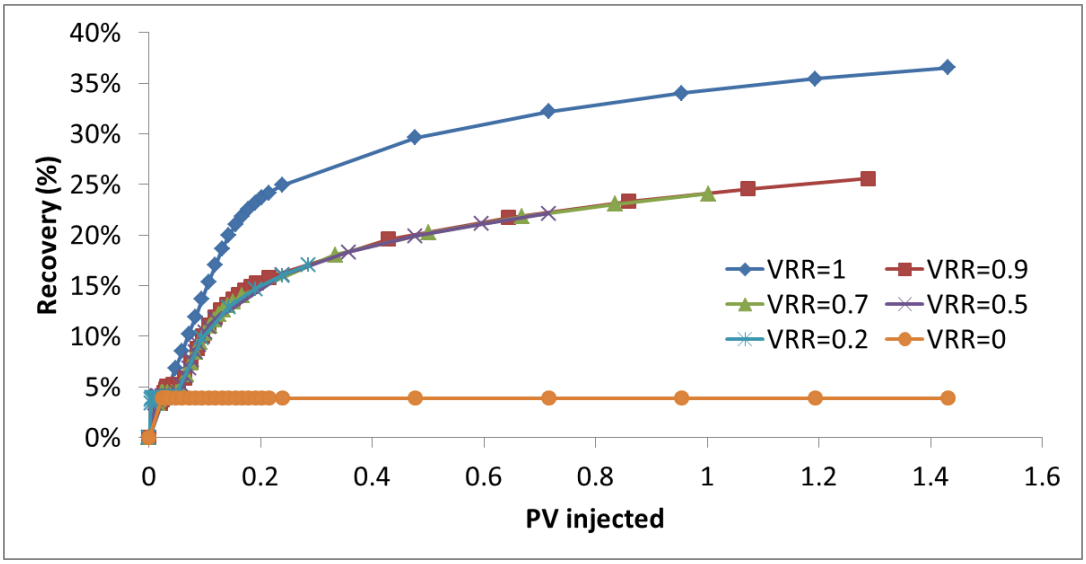

Figure 3-47: Recovery as a function of pore volumes injected for the base case.

Figure 3-48 shows how pore volumes injected can bias models with a VRR less than 1. If we try to determine the optimal VRR at some point like 0.2 PV_{inj} for the case where S_{gc} is 5%, we get that a VRR of 0.9, 0.7, and 0.5 are all better than a VRR of 1, even though when we use time as a reference, a VRR of 1 is optimal (see Figure 3-29). We thus run into some problems in determining the optimal VRR. If water use is our main concern, than clearly a VRR of 0.5 is optimal, in terms of the oil produced to water injected ratio, when we have a small amount of critical gas present in our system, but if overall oil recovery is our main concern, than a VRR of 1 is optimal.

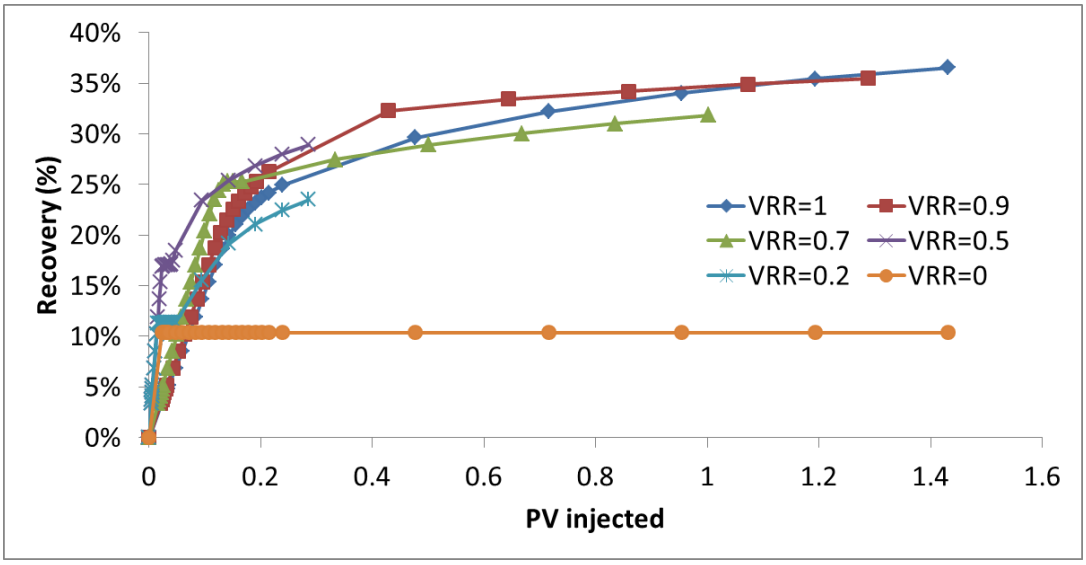

Figure 3-48: Recovery as a function of pore volumes injected for the base case with S_{gc} = 5%.

It is impossible without an analytical derivation for each simulated case to determine what fraction of oil was produced by depletion drive and what fraction was produced by a water drive in the case where the VRR is between 1 and 0. Assumptions based on differentiating the two can also lead to bias. For this reason, among others, we have chosen not to represent our results in terms of a dimensionless time. Using a time-based reference scale also makes post processing of results substantially easier, as only one flow rate needs to be monitored and not two.

To combat the problems with using pore volumes injected as our reference scale, we tried to develop another dimensionless reference scale. We considered using a reference scale based on the sum of pore volumes injected and produced. Thus we are accounting for both injected water and produced hydrocarbons. When we used this metric as a comparison, we found that the recovery profiles bear a surprising resemblance to that of our time metric, both in terms of recovery and the optimal VRR. Because of the lack of clear superiority, we therefore decided to stick with using time as our reference scale.

If we consider the base case, we can see in Figure 3-49 the merging of recovery profiles for cases where the VRR is less than 1 still occurs at large $PV_{inj+prod}$ values. Note the contrast of Figure 2-7 with Figure 3-49. If we consider 0.5 or 1 $PV_{inj+prod}$ as our reference point, we see the same trend in optimal VRR values as seen in Figure 3-29, although this method of comparison makes a VRR of 1 appear much more optimal. Now we will consider Figure 3-50. If we add some critical gas into our system and consider 0.5 or 1 $PV_{inj+prod}$ as our reference point, we get a delineation of the optimal VRR values that matches the trend observed in Figure 3-29, with appropriate spacing. This trend was observed for the remaining 3 base case relative permeability curve sets we modeled.

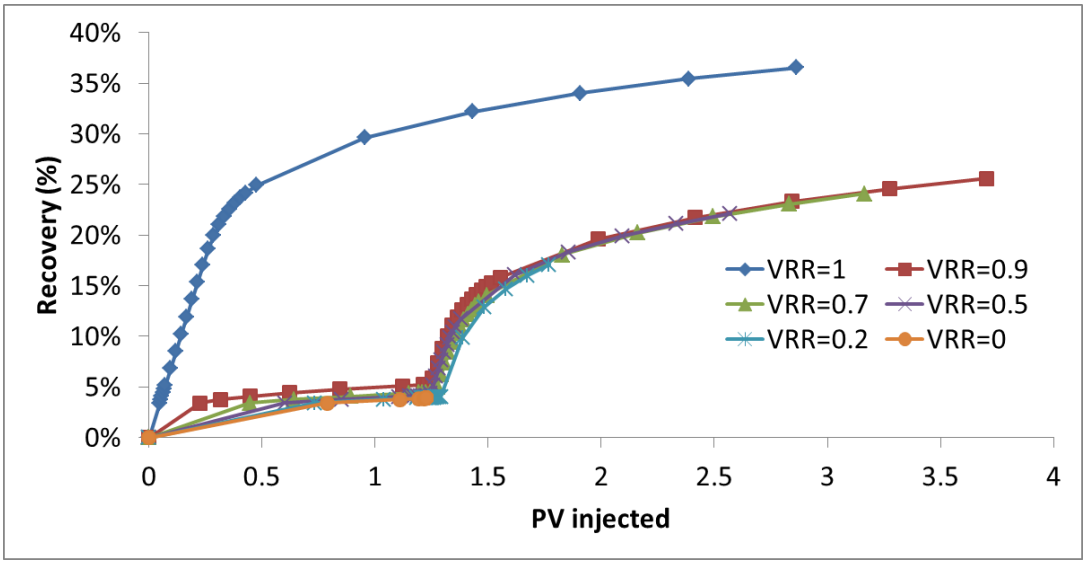

Figure 3-49: Recovery as a function of pore volumes injected for the base case.

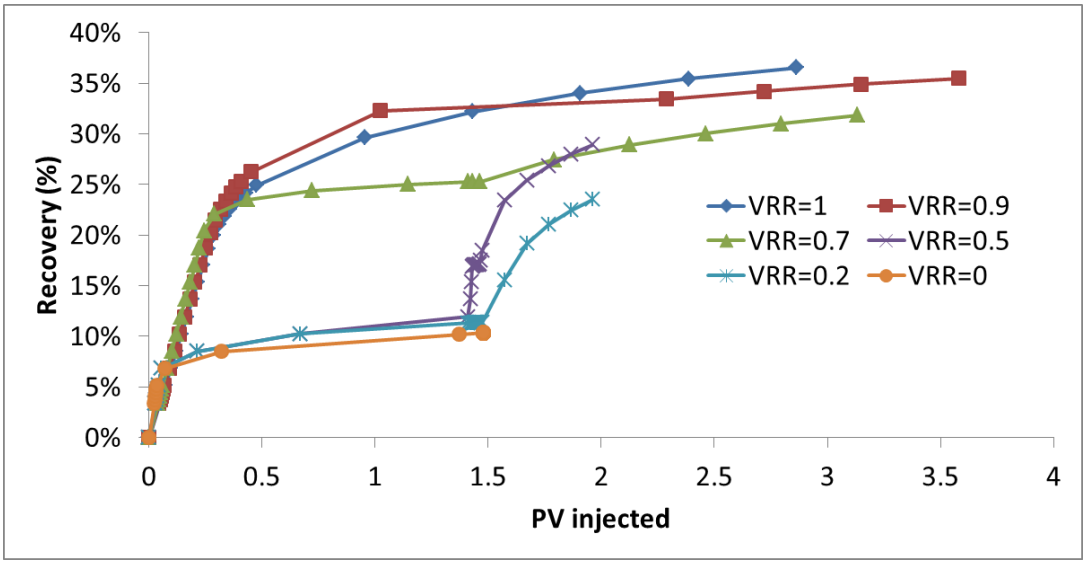

Figure 3-50: Recovery as a function of pore volumes injected for the base case with S_{gc} = 5%.

3.5. Timing

In all the cases thus far considered, we have operated at a single VRR until the pressure in our model has been depleted, at which time the production rate drops to the injection rate for that particular VRR. In practice, it might be infeasible to operate at the same VRR throughout the life of a project. In fact, it might actually be optimal to switch between VRR operating constraints depending on what stage of production is occurring. In this work, we have not looked extensively into the issue of optimizing recovery based

off VRR switch-off times, but we have made some observations based on our core-scale model.

For the purposes of the present study, we only considered switch-offs between 1 and 0.7, the optimal VRR for the base case and foamy oil case, respectively. For the cases where the VRR changed, we chose the transition time to occur after 0.09 days. This choice of time was arbitrary and used only as a means of generating results that were easily interpretable by eye alone. We will first consider the base case that has an optimal VRR of 1 in our homogeneous model. Figure 3-51 shows the recovery profiles of cases where the VRR is constant at 1 and 0.7, and for cases where the VRR transitions from one to the other. As can be seen from the figure, dropping to a VRR of 0.7 from 1 results in about a 7% reduction in recovery. We have already shown how a VRR of 0.7 is less advantageous than a VRR of 1 for our base case, so this result is expected.

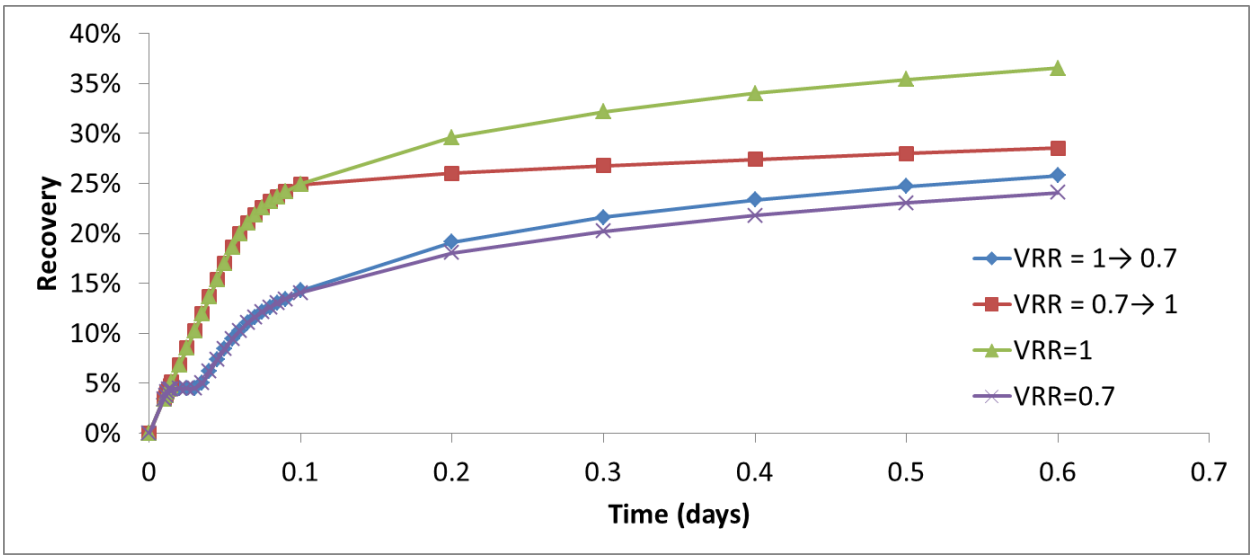

Figure 3-51: Recovery profiles using the base case relative permeability curves for a VRR of 1 and 0.7 as well as for scenarios where the VRR switches between one value to another (indicated by arrows) after 0.09 days.

When we increase the VRR from 0.7 to 1, there is a slight increase in recovery. It was mentioned in section 2.2 that upon pressure depletion in the scenarios where our models are operating at a VRR less than 1, the production rate drops to whatever the injection rate was specified at based on the VRR. This reduction in production rate effectively implies that the model is acting at a modified VRR of 1 with respect to the base case model that is under a constant operational constraint of a VRR of 1. When we say the VRR was "increased from 0.7 to 1", we mean to say both the injection and production rates are increased at the transition time after 0.09 days to correspond to the case where there was a VRR constraint of 1 from the beginning. If we imagine a scenario where we were injecting 0.7 bbl/d of water at a VRR of 0.7, when we alter the VRR to 1, we are injecting and producing at a rate of 1 bbl/d.

After 0.09 days, the curvature of the case where there is a transition from a VRR of 0.7 to a VRR of 1 matches the curvature of the case of a VRR of 1. The former case never catches up to the latter case as is evidenced by Figure 3-47 due to the lost time spent operating at the suboptimal VRR of 0.7.

We now turn our attention to a case where a VRR of 0.7 yields greater recoveries than a VRR of 1. Figure 3-52 displays the results of simulations on the foamy oil case, having executed the same procedure we tested on the base case to generate Figure 3-47. For the foamy oil case, a VRR of 0.7 is optimal, so switching to a VRR of 1 causes the recovery curve to climb less steeply than if the entire operation was conducted at a VRR of 0.7. Notice the rate of increase in recovery is identical for a VRR of 1 and for the case where a VRR of 1 begins after a VRR of 0.7 at 0.09 days.

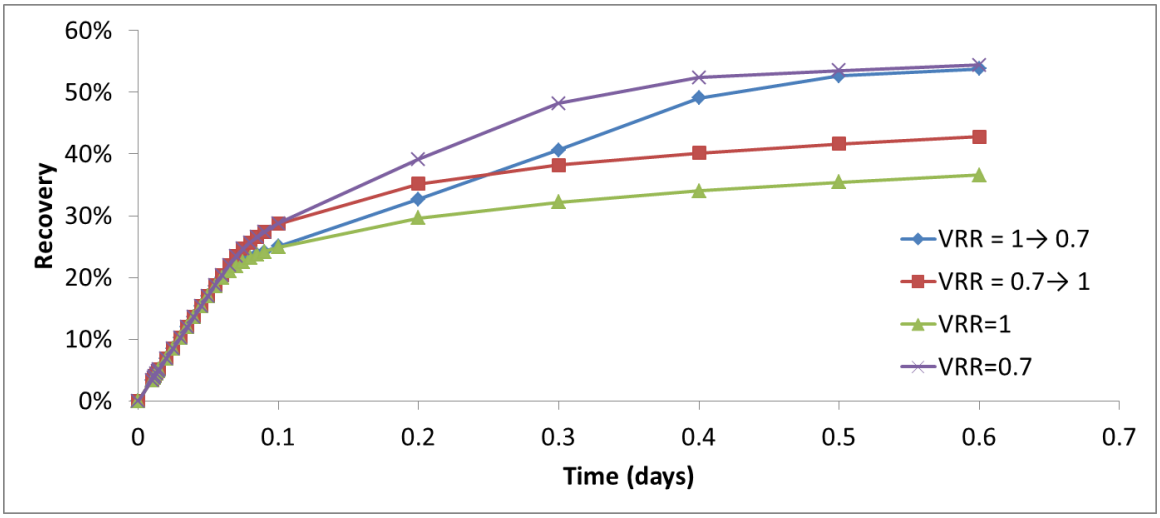

Figure 3-52: Recovery profiles using the foamy oil case relative permeability curves for a VRR of 1 and 0.7 as well as for scenarios where the VRR switches between one value to another (indicated by arrows) after 0.09 days.

The recovery profile characterizing the case where a VRR of 1 is switched to a VRR of 0.7 shows the absence of any sort of hysteresis effect for our homogeneous base case model. As can be seen in Figure 3-48, the recovery at 0.6 days is essentially equal for the case where we begin operating at a VRR of 1 and switch to a VRR of 0.7 and the case where we operated at a VRR of 0.7 all along.

In our study of the influence of timing on the optimal VRR, we have seen the absence of hysteresis effects in our homogeneous base case model. We have illustrated how switching from one VRR to another gives intuitive results. It is not clear how altering the operational VRR influences results in the presence of significant heterogeneity. Reservoir-scale models that model channels or incorporate dual porosity models might have unexpected responses to VRR switch-offs. These kinds of effects need to be analyzed on a case by case basis and require optimization tools involving numerous simulations or proxy-fitting, so we leave this topic as an area of future work.

3.6. Summary

We have shown how a number of factors influence the optimal VRR when using a numerical simulator. Oil and gas relative permeability, the critical gas saturation of the evolved gas, the chemistry of the oil, reservoir heterogeneity in the form of fractures, faults, or cul-de-sacs, and the reference scale used to analyze results all affect the optimal VRR. The most dominant factor affecting the optimal VRR is the mobility of the gas. Using reasonable sets of relative permeability curves based off data from the literature, we have shown how the optimal VRR can vary based off the gas mobility of the system. It is therefore quite obvious that proper characterization of the liquid-gas interactions in a system is imperative before any analysis of the optimal VRR is conducted. The effect of heterogeneity also has been shown to have some impact, typically causing a VRR less than 1 to become more favorable relative to the homogeneous case. It is thus also important to properly understand the connectivity of a system before attempting to analyze the optimal VRR.

Chapter 4

4. Application to a Realistic Reservoir Model

4.1. Model Description

In our sensitivity studies of the optimal VRR, we tested our five base case relative permeability curves introduced in section 3.3 on a large-scale reservoir model. The model was developed by Hongmei Li under supervision of Jef Caers testing the sensitivity to shale drapes to channelized reservoirs (Li 2008). We used the reference model for our purposes. The reservoir is based off industry-provided data on a channelized deep-water reservoir. It represents a turbidite reservoir with areas of varying connectivity. Permeability values are 2 Darcy when not zero in a particular, or all, directions, except in the vertical direction. Vertical permeability is $1/10^{th}$ the horizontal permeability in all blocks. Other reservoir parameters are constant across all blocks as well. There are three producers and two injectors along with 28207 active cells in the grid. A detailed description of the model is available elsewhere (Li 2008).

We simulated the full-scale reservoir model using CMG's *Im*plicit-*Ex*plicit Black Oil Simulator, IMEX, and used the base case fluid data with parameters described in section 2.1. Rock properties are consistent with Li's model. Li's model has a sufficiently small rock compressibility so pore volume reduction is negligible, indicating negligible subsidence or compaction drive. Our initial pressure was chosen to be 1800 psi at the top of the reservoir. Figure 4-1 shows the initial pressure distribution in the grid. Notice each layer is made up of sinusoidal channels of varying dimensions. A detailed view of each layer shows large gaps in connectivity within the layer as well as between many of the other layers. A bottom-hole pressure constraint of 300 psi was enforced at the producers and one and half times the initial reservoir pressure at the injectors.

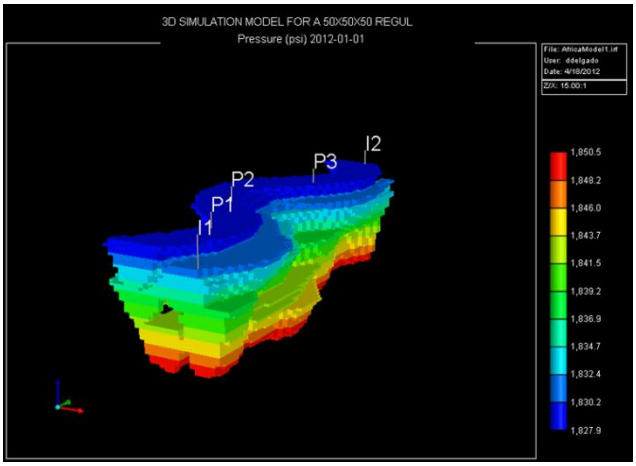

Figure 4-1: Pressure distribution in modified Li model.

4.2. Results

We took each of our sets of relative permeability curves for the five cases developed in section 3.2 and applied them to Li's modified geological model. Figure 4-2 shows recovery as a function of the VRR for all five cases. It is obvious from the results that the foamy oil case yields an overly optimistic outcome given the unrealistically high primary recovery (VRR of 0) performance. It is unclear whether to assume an entire reservoir can be maintained under such foamy conditions. We show the results of the foamy oil case purely for comprehensiveness in our recovery sensitivity study. Due to the infeasibility of the foamy oil case results, we disregard the foamy oil case for now and consider the other four cases as shown in Figure 4-3. Sensitivity studies done with our foamy oil relative permeability curves to make a more realistic model were conducted in Section 4.3.

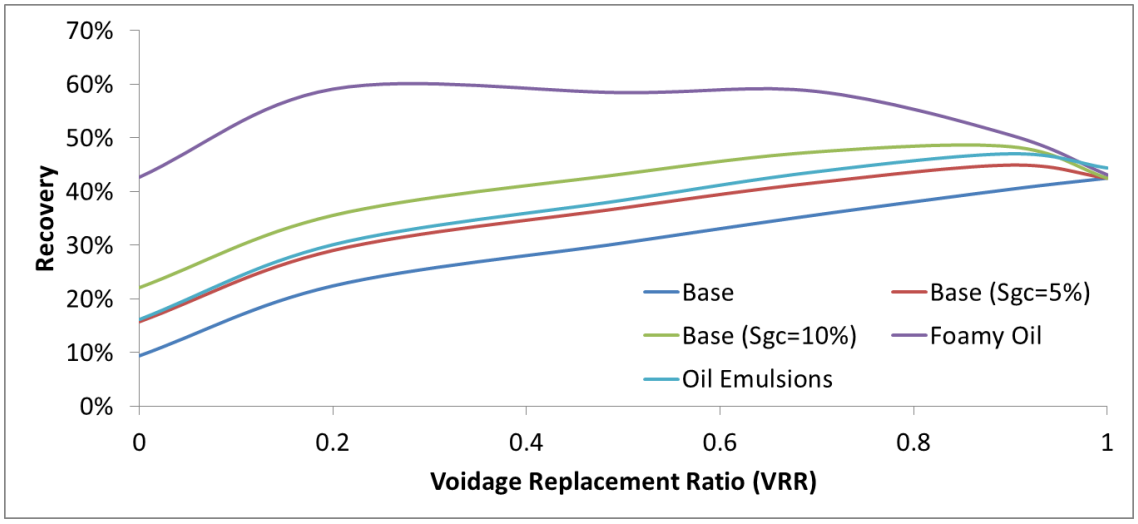

Figure 4-2: Recovery as a function of the VRR for our five base cases in the modified Li model.

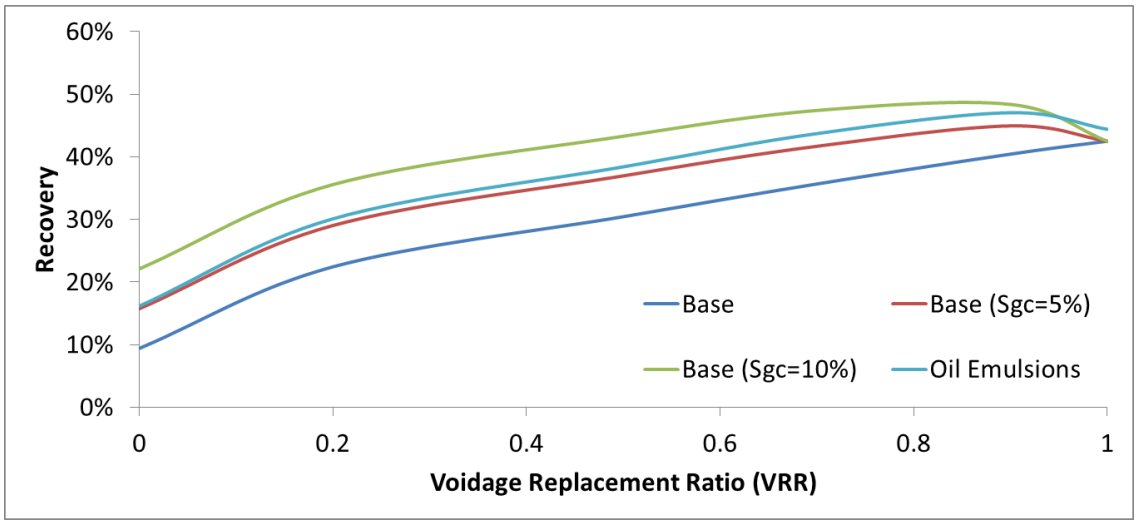

Figure 4-3: Recovery as a function of the VRR excluding the foamy oil case in the modified Li model.

It is interesting to note how strongly the connectivity of the reservoir has affected the shape of the recovery profiles when compared to our results in Figure 3-29. There is no longer a sharp decline in recovery when reducing the VRR below 1 for the base case. For the oil emulsions case and the base case with 5% critical gas, a VRR of 0.9 is noticeably better than a VRR of 1, and the oil emulsions case no longer adds as significant a benefit. When there is 10% critical gas, a VRR of 0.7 is now less disadvantageous when compared to a VRR of 1 or 0.9 than was the case in our homogeneous base case model.

The contrast between Figure 3-29 and 4-3 is explained when considering the differences in how each model operates. This comparison is most easily done when viewing the pressure profile. To avoid cluttering in our figures, we are only considering the base case with 5%, 10% and no critical gas. The oil emulsions case has similar enough results to the base case with 5% critical gas that we can exclude it from our analysis for now, and we have already explained the errors that might be associated with considering the results of the foamy oil case.

Before we consider any specific case, we emphasize that there are three producers and two injectors in our model, so the pressure distribution is not uniform near each well, as evidenced by Figure 4-4. The connectivity of at each depth varies significantly. The producers and injectors in the model can only influence one another through particular channels. Notice the bottomhole pressure is highest at producer 1, or P1, for every VRR except 0.2 and 0.5, where producer 2, P2, is marginally higher. For large VRR, the water injected at the injectors, I1 and I2, causes the pressure to rise in the nearest adjacent producer wells, P1 and P3, respectively. When there are a sufficient amount of liquids available in the reservoir to drive flow, cross-flow becomes negligible given the difference between the horizontal and vertical permeability, and the bottomhole pressures vary for each well even at late times.

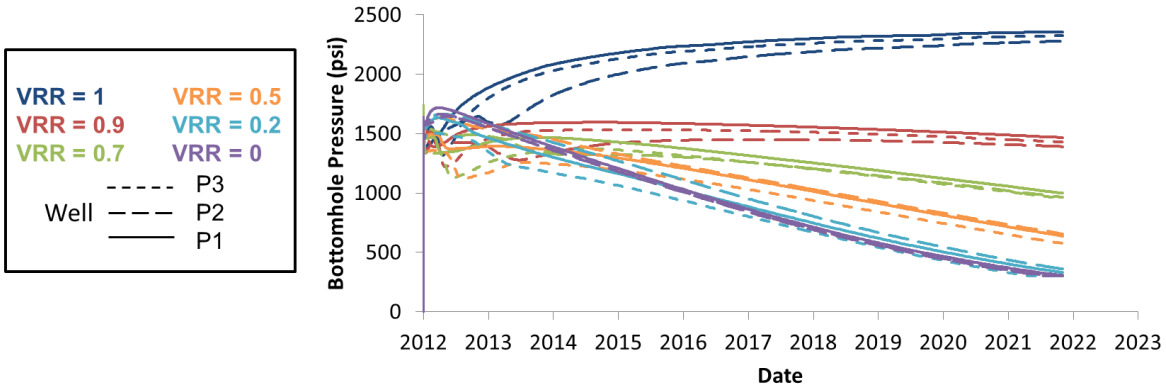

Figure 4-4: Bottomhole pressure for various VRR for each producer in the base case in the modified Li model.

As the VRR approaches 0, the injectors cannot elevate the pressure quickly enough in the channels containing P1 and P3 that quickly deplete the fluids surrounding them. Thus P2, which is less influenced by either the injectors or producers, has a bottomhole pressure slightly above its counterpart producers. At a VRR of 0, both the pressures at P2 and P3 decline somewhat faster than the pressure at P1, initially. Because the mobility of gas is high in our base case, the vertical permeability is around 200 milliDarcy, and there are no liquids dominating flow in the horizontal direction, much of the evolved gas flows to the producer in the top depths, P1. With less impedance to maintain the operational bottomhole fluid rate constraint, P1 can therefore take a slightly larger pressure initially. All three producers stabilize to the same pressure because cross-flow between depths becomes non-negligible over time. These occurrences showcase the degree of heterogeneity in the model.

The connectivity in the model also causes the recovery profiles shown in Figure 4-5. Notice producer 2, P2, produced the majority of oil in all cases except for the case where the VRR is 0.2. The performance of P1 and P3 is virtually consistent for every VRR except 0, the case of primary depletion. P2 lies in the middle of the model, between P1 and P3 that are near the injectors I1 and I2, respectively. P1, P3, I1, and I2 interchangeably are perforated at identical depths at one point or another. P2 is only perforated at the same depth as one well, I2, and only at some depths. P2 is the only producer perforated at some depths that contain no injector. P2 is also the perforated at the greatest depths. The difference in performance between the producers increases as the VRR increases; at a VRR of 1, P2 produces about 25% of the recoverable oil in the model, while P1 and P3 only produce about 5%. As the VRR increases, P2 benefits from an increased pressure drive in the reservoir. P2 is the least connected to any other well, so not only is it able to produce more oil because of a lack of interference with any other producers, as evidenced by its dominance in the case where the VRR is 0, but it also produces less water than the other producers because of its dampened connectivity with the injector wells. As is shown in Figure 4-6, the water oil ratio is consistently lower for P2.

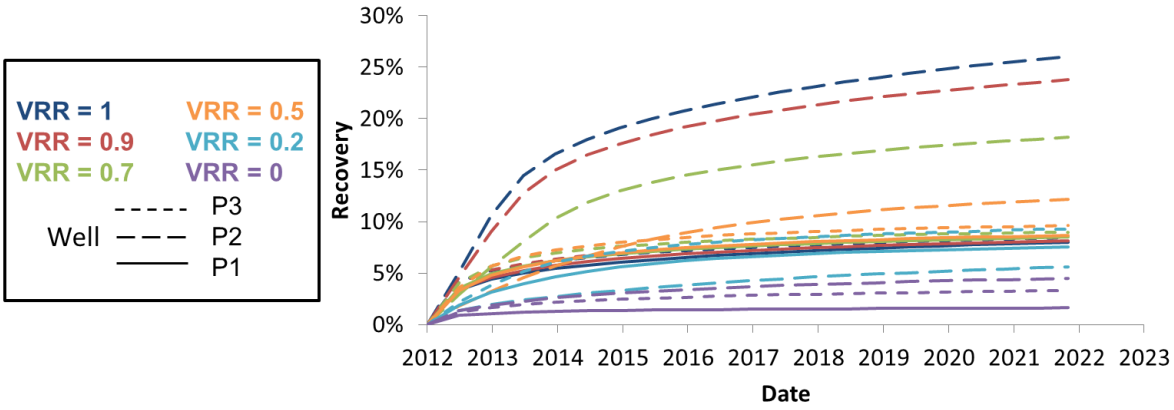

Figure 4-5: Recovery for various VRR for each producer in the base case in the modified Li model.

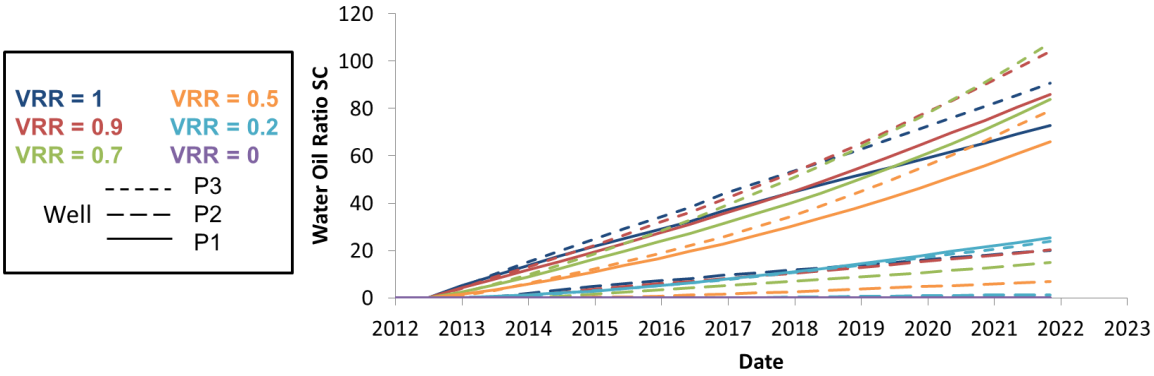

Figure 4-6: Water oil ratio at surface conditions for various VRR for each producer in the base case in the modified Li model.

P2 falls out of favor in the case where the VRR is 0.2 for similar reasons as those previously outlines. P2 is poorly connected to the injectors, so hardly any volume is swept by the water injected at the depths P2 is perforated. Since a VRR of 0.2 implies little pressure maintenance due to the injected fluids, P2 does not receive any of the benefit it receives at other operational VRR's.

Now that we have considered the heterogeneity of the model and its impact on each well, we will look holistically at our results for each case. If we consider how the average pressure in our model changes with the inclusion of critical gas, as Figure 4-7 shows, we see a critical gas saturation hardly modifies the overall pressure response. This observation of the average pressure might be surprising given how different the recovery profiles look, as shown in Figure 4-8. Though the differences in recovery are most stark for small VRR values such as 0 and 0.2, there is a noticeable difference in recoveries at every VRR besides 1, as expected from our study of core models in Chapter 3.

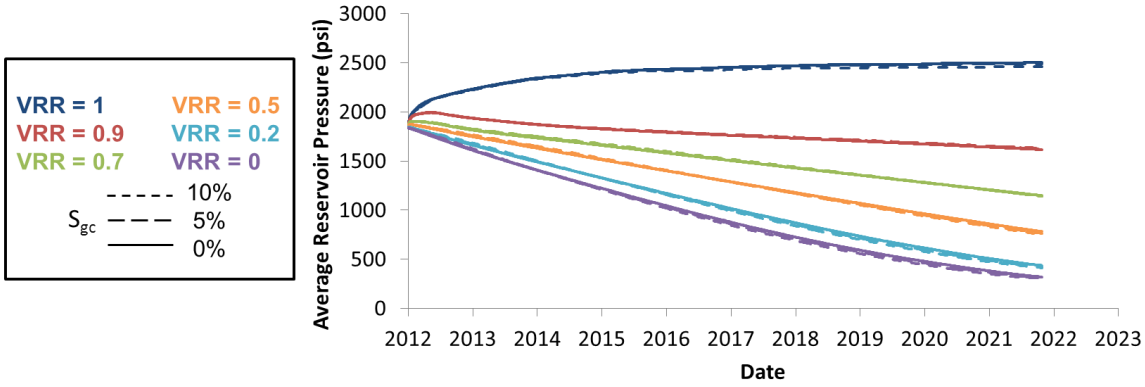

Figure 4-7: Average reservoir pressure as a function of time for the base case with critical gas saturation values of 0, 5, and 10%.

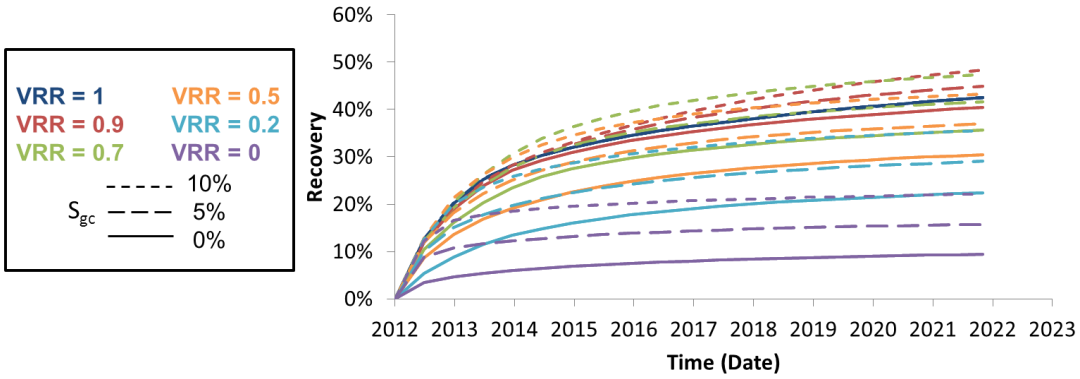

Figure 4-8: Recovery as a function of time for the base case with a critical gas saturation of 0, 5 and 10%.

Considering the average pressure profiles in our models, notice for larger VRR values below 1, the rate of pressure decline is relatively constant, but for smaller VRR values, like 0.2 or 0 or the tail-end of 0.5, the rate of decline decreases making the BHP curves look slightly concave. Also notice in the case of a VRR of 1, the pressure in the reservoir actually increases. There is also a slight increase in pressure initially when a VRR of 0.9 or 0.7 is used. This result should be intuitive. If a waterflood was conducted in a reservoir before any primary recovery had taken place, the pressure in the reservoir increases initially. As more water floods in, the water saturation near the injectors increases and the oil relative permeability decreases significantly creating a much greater resistance to flow that causes the pressure to rise throughout the reservoir. It is only logical the pressure rises. Note the pressure in the reservoir does not exceed the bottomhole pressure constraint of the injector, one and a half times the initial reservoir pressure. Note also none of the average reservoir pressures in any of the scenarios fall below the bottomhole pressure constraint of the producer, even in the case of primary depletion. As a reminder, the rock compressibility of our model is small, and it has been confirmed that at most only negligible compaction occurs in each scenario.

Though the average pressure deviation is small for each of the three critical gas saturation cases, we note the change in recovery with the critical gas saturation by viewing the gas oil ratio and water oil ratio as shown in Figures 4-9, 4-10, and 4-11. Notice the water oil ratio decreases as the critical gas saturation in our model increases. We expect the WOR to be smaller in the presence of a larger critical gas saturation due to interference of the three phases. When gas is kept in our system, it inhibits the flow of water, allowing more oil to migrate to the producers. This interference is of greatest benefit for larger VRR values below 1, between 0.5 and 1, where there is an optimal ratio of water invading to the oil in place. The water creates drive and the gas keeps the oil at the forefront of the flow path.

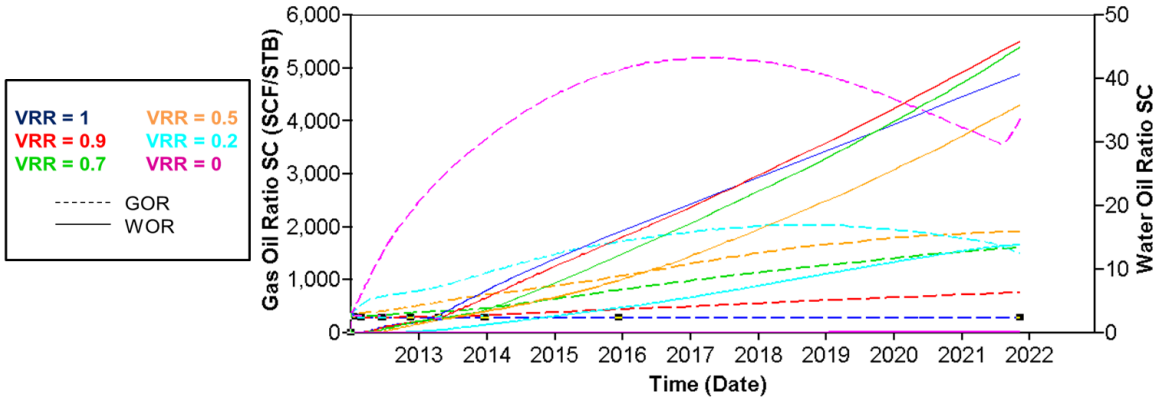

Figure 4-9: WOR and GOR as a function of time for the base case with no critical gas saturation.

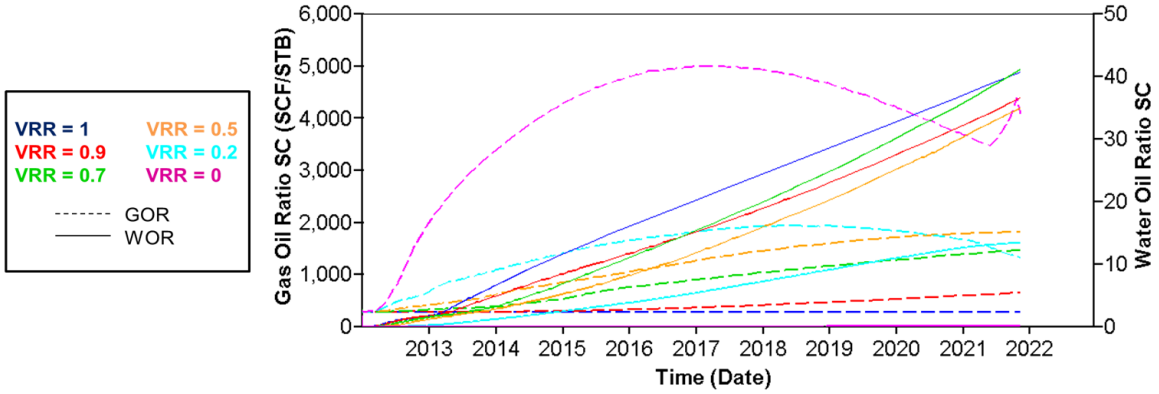

Figure 4-10: WOR and GOR as a function of time for the base case with a critical gas saturation of 5%.

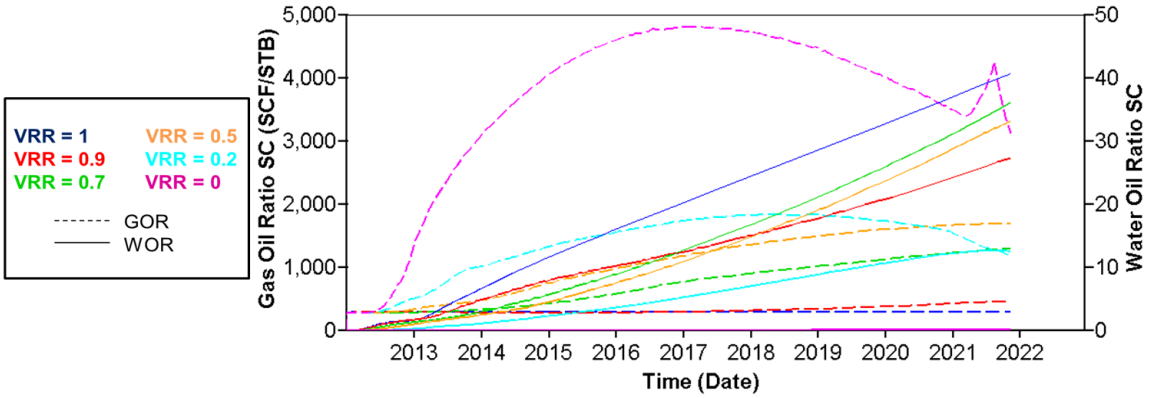

Figure 4-11: WOR and GOR as a function of time for the base case with a critical gas saturation of 10%.

The gas oil ratio decreases with an increase in the critical gas saturation, as expected. With a critical gas saturation of 10%, a VRR of 0.9 and 1 produce similar GOR profiles, and are only beginning to deviate significantly near the model's end-life. With no critical gas saturation, a VRR of 0.9 and VRR of 1 produce GOR profiles that start differing markedly after only 2 years. Similar observations can be made of GOR profiles at other VRR. The rate of increase is noticeably smaller in the models with gas kept in the system. These results are testament to the fact we are producing more oil at every VRR below 1 when the critical gas saturation increases, as evidenced by Figure 4-8.

It is important to state the GOR values decrease with an increased critical gas saturation due to the increased recovery oil, not because there is a reduction in gas production at surface conditions. If we view gas production at the surface for each of our three base case scenarios as shown in Figure 4-12, we see gas production actually increases as critical gas saturation increases. This result is purely a function of the increased production of oil. As more oil is produced in the reservoir, more gas evolves from the oil at the surface, so more gas is recovered. If we consider only gas production bottom-hole, as in Figure 4-13, we are affirmed that indeed gas production goes down as the critical gas saturation increases, as more gas is trapped within the system.

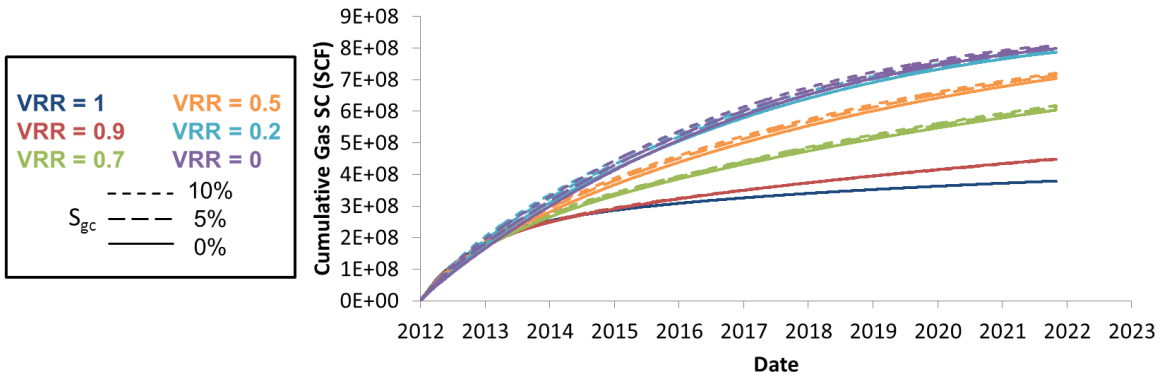

Figure 4-12: Cumulative gas production at the surface for three base cases.

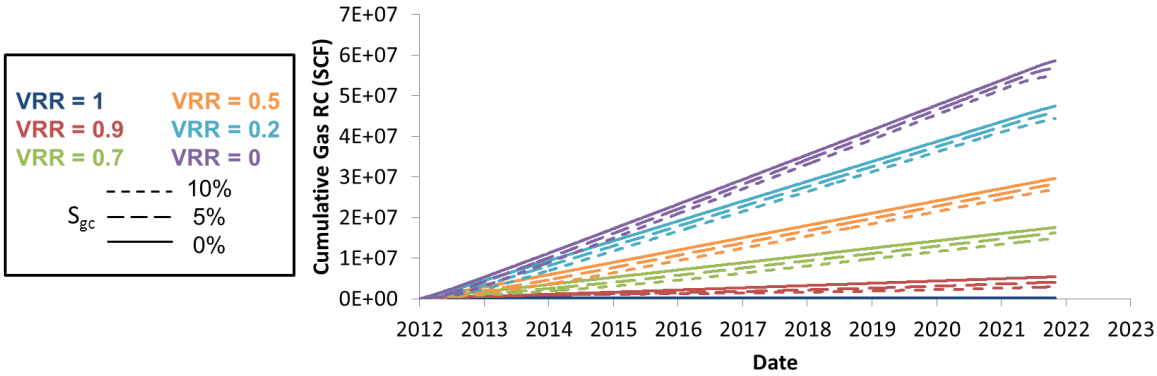

Figure 4-13: Cumulative gas production in the reservoir for three base cases.

As a last note, we want to comment our bottom hole fluid constraint of 3000 bbl/d, or 1000 bbl/d per producer, was upheld throughout every case for every VRR. The bottom hole liquid flow rates did deviate, however, as shown in Figure 4-14. It should be intuitive that if our production rates far exceed our injection rates, as they do for low VRR values, less liquid is capable of being produced within a given timeframe. The gap between the liquid we produce and the fluid we are required to produce by our operational constraint bottom hole is made up by gas. For a VRR below 1, the pressure in our reservoir will drop as shown in Figure 4-7. When the pressure drops below the bubblepoint, gas in our model evolves out of the oil and start being produced. As less liquid is produced, more gas is produced and more expansion of the gas in the reservoir occurs. When we increase the critical gas saturation, more gas is trapped within the reservoir, so our liquid rate declines less quickly as the retained gas drives out more liquid. Thus, by viewing the bottom hole liquid rate profiles, we have affirmed our conclusions made previously with our cumulative oil, GOR, and average reservoir pressure plots.

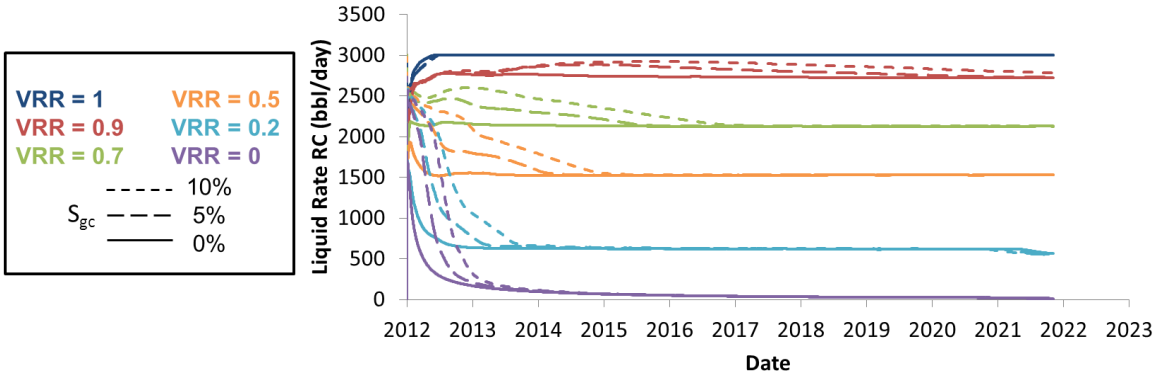

Figure 4-14: Liquid rate in the reservoir for three base cases.

4.3. Adaption to Foamy Oil Model

We have explained why our foamy oil set of relative permeability curves should not be directly applied universally in our reservoir model. Flow will almost always be fastest near the wellbore, so it might be reasonable to assume foamy oil effects near the wellbores in our model, if we hypothetically assume our operational flow rate constraints and the reservoir oil properties allowed foamy oil effects to occur. In practice, an operator could enduce foam in the oil around the producers by forcing a certain production rate after which they could continue operating at their desired VRR.

For now, we will only consider foamy oil effects near the producer wells. Though the flow rate can be fast near the injector wells, the pressure is decreasing much less rapidly near the injectors so less gas evolves and it should be rarer for foamy oil effects to occur. We will consider a case where only the blocks in which our producers were perforated have characteristic foamy oil behavior, and a case where the foamy oil effect extends outward to two blocks adjacent to each perforated block in each direction.

Figure 4-15 shows the effect of instilling foamy oil behavior in only some of the blocks in our model. We can see the difference between our base case and the case where only the perforated producer blocks are modified to have foamy oil characteristics is slight. There is a noticeable difference between the base case and the case where we have modified a few of the blocks surrounding the producers, though the difference is still relatively small. The optimal VRR does change for this latter case as can be seen in the plot. Our results indicate the foamy oil effect will only be significant if a large quantity of blocks in our model have oil and rock properties characterized by foamy oil behavior. A block with foamy oil behavior will not necessarily modify the surrounding blocks in a significantly influential way.

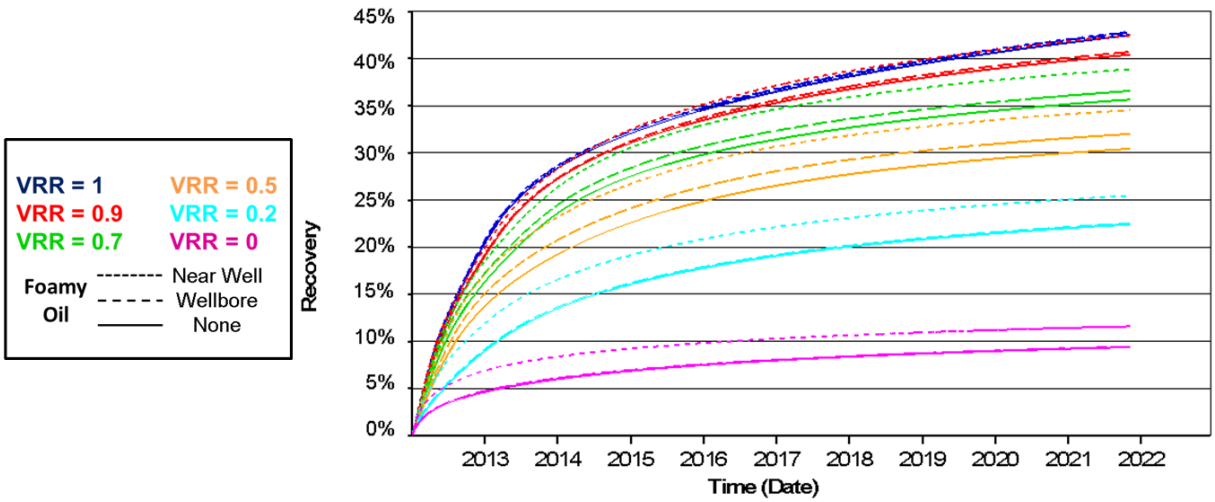

Figure 4-15: Recovery sensitivity to blocks with foamy oil characteristics.

Chapter 5

5. Conclusions

From our analysis, we conclude the key factors that make operating at a VRR below 1 optimal are the gas mobility and geological heterogeneity. In general, the less mobile the gas and more compartmentalized the system, the more favorable a VRR below 1 becomes. We have shown through both core-scale and reservoir-scale models using numerical simulation that various factors influence the optimal VRR. The mobility of gas is by far the most important parameter influencing the optimal VRR. Therefore, proper characterization of the liquid-gas interactions through relative permeability curves, the critical gas saturation, and the oil composition are essential when modeling. Our results have shown the non-uniqueness of a particular set of relative permeability curves to recovery at various operational VRR. Various fluid and rock combinations lead to similar results in recovery. We have shown the role of chemistry on the optimal VRR through the consideration of both oil emulsion and foamy oil relative permeability curves arising from the literature. Thus, we have shown a physical basis by which the optimal VRR varies substantially.

We note that the optimal VRR is a relative term. If water is a source of concern then different reference metrics are useful to quantify the optimal VRR. We have discussed the role of time and nondimensionallized time in determining the optimal VRR. The metrics we have discussed are applicable on a case by case basis depending on the economics of a situation.

Through the use of core-scale and reservoir-scale models, we have shown the role of heterogeneity in influencing the optimal VRR. While the randomness associated with the permeability and porosity distribution is not believed to influence the optimal VRR, analogues to faults and fractures have been shown to impact results. Permeability cul-de-sacs, or regions of poor connectivity with limited access to the water swept area, are shown to influence the optimal VRR. In general, large heterogeneous features were shown to make a VRR less than 1 more favorable. The role of heterogeneity was shown to tie to connectivity. The results of our simulations on a heavily channelized reservoir model feature the large degree of influence connectivity has on the optimal VRR.

Chapter 6

6. Future Work

We have left a number of topics for future work. While we have investigated most of what we discuss in this chapter, our data was not substantial enough for full analysis here, and so we leave it for future study.

One of the more commercially attractive areas of study is the timing of VRR "switch-offs." While we investigated the response of the core-scale model to alternating between two different VRR's, we were handicapped by the homogeneous nature of our model. Heterogeneity undoubtedly influences any hysteresis effects that occur when switching between one or more VRR's. Any hysteresis that takes place likely is unique to the reservoir model, so such a study can only be conducted on a case-by-case basis. Optimization tools that deal in finding optimal recovery paths would greatly benefit such a pursuit.

We have also considered the role of ternary diagrams that display how oil relative permeability changes with changes to the oil, water, and gas saturations, as a screening tool for deducing whether or not reducing the VRR below 1 is effective. Given how heavily influenced the optimal VRR is to the gas mobility, there is potentially a correlation between the ternary diagram describing a system and the effectiveness of a reduction in the VRR below 1. Such analysis appears to require either an analytical solution or some sort of optimization tool.

A sensitivity analysis to the oil composition and the oil-gas equilibrium ratios we have chosen would also be of great benefit to understanding the factors influencing the optimal VRR. We used a black-oil model with solution gas, but real-world crude-oil compositions are often much more diverse, especially heavy and viscous oils, where a reduced VRR was shown to be of most benefit. The impact of the oil composition on viscosity might not be the only effect, and something new could be revealed about the role of oil composition and the optimal VRR.

We have considered oil chemistry in our study, but only through the use of static relative permeability curves. Considering static relative permeability effects oversimplifies the role of oil chemistry. Chemical effects occur in response to some stimulus, so having foamy oil or oil emulsion behavior initially present in the relative permeability curves is a poor approximation. A better approach may be rate dependent relative permeability curves that take into account the conditions observed. For example, a combination of flow rate conditions and oil composition could instill foamy effects in particular portions of a model. By developing a mechanistic model, reservoir geology and pressure conditions could trigger oil emulsions. In order to incorporate rate dependent relative

permeability curves, a better core-scale and field-scale of understanding of how such oil chemistry effects evolve is required.

We have thus far not discussed the three-phase model to determine the relative permeability to oil, water, and gas as the saturation of each phase changes with time. We have proven the importance of the relative permeability to gas in all of our models shown in Chapter 3. The three-phase relative permeability model is of great importance. We compare two of the most popular three-phase models in commercial reservoir simulation in Appendix A. It has been shown in the literature, however, that models based off real data and real rock properties often require modified three-phase models, if gas or oil trapping was significant for example (Blunt 2000). A study of the influence of the three-phase model on measured data where other parameters are known with relative certainty would be useful. A full analysis of hysteresis in the three-phase relative permeability relationships is also warranted.

Nomenclature

B_o = Oil formation volume factor
GOR = Gas oil ratio
k_r = Relative permeability
k_{rg} = Relative permeability to gas
k_{rl} = Relative permeability to liquid
k_{row} = Relative permeability to oil with respect to water
k_{rw} = Relative permeability to water
n_g = Corey gas exponent
n_l = Corey liquid exponent
n_o = Corey oil exponent
n_w = Corey water exponent
p = Pressure
K = Gas-oil equilibrium ratio
KV1 = First constant used in the gas-oil equilibrium ratio equation (2-1)
KV2 = Second constant used in the gas-oil equilibrium ratio equation (2-1)
KV3 = Third constant used in the gas-oil equilibrium ratio equation (2-1)
KV4 = Fourth constant used in the gas-oil equilibrium ratio equation (2-1)
KV5 = Fifth constant used in the gas-oil equilibrium ratio equation (2-1)
S_{gc} = Critical gas saturation
S_l = Liquid saturation
S_w = Water saturation
SC = Standard conditions
SCF = Standard cubic foot
STB = Standard barrel
T = Temperature
RC = Reservoir conditions
WOR = Water oil ratio
VRR = Voidage replacement ratio

References

Aziz, K., and Settari A., 1979. “Petroleum Reservoir Simulation," Applied Science Publishers Ltd., London.

Bora, R. and Maini B. B., Flow Visualization Studies of Solution Gas Drive Process in Heavy Oil Reservoirs Using a Glass Micromodel; SPE 37519 Presented at the SPE International Thermal Operations and Heavy Oil Symposium, Bakersfield, CA, Feb. 10-12, 1997.

Blunt, M.J., An Empirical Model for Three-phase Relative Permeability; SPE J., 5 (2000), pp. 435–445.

Brice, B. W. and Renouf, G., 2008. Increasing Oil Recovery from Heavy Oil Waterfloods, SPE 117327.

Li, H. “Hierarchic Modeling and History Matching of Multi-scale Flow Barriers in Channelized Reservoirs”. Ph.D. dissertation, Stanford University, 2008.

Computer Modeling Group, LTD, 2010. STARS Version 2010 User’s Guide. CMG Calgary, Alberta, Canada.

Corey, A.T., Rathjens, C.H., Henderson, J.H. and Wyllie, M.R.J., 1956. Three-phase Relative Permeability, SPE 737-G-P.

Dyes, A. B., 1954. Production of Water-driven Reservoirs below their Bubble Point, SPE 417-G.

Firoozabadi, A. and Anderson, A..: “Visualization and Measurements of Gas Evolution and Flow of Heavy and Light Oil in Porous Media,” paper SPE 28930 presented at the 1994 SPE annual Technical Conference and Exhibition, New Orleans, LA.

Jerauld, G.R., Lin C.Y., Webb, K.J., and Seccombe, J.C., “Modeling Low-Salinity Waterflooding” SPE 102239, presented at the Annual Meeting of SPE 2006.

Kumar, R., Pooladi-Darvish, M., and Okazawa T.: “An Investigation into Enhanced Recovery under Solution Gas Drive in Heavy Oil Reservoirs,” SPE 59336 presented at the SPE Improved Recovery Symposium, Tulsa, OK, April 2-5, 2000.

Loahardjo, N., Xie, X., Yin, P., and Morrow, N.R., 2007. Low salinity waterflooding of reservoir rock. SCA2007-29.

Lager, A., Webb, K.J., Black, C.J.J., Singleton, M. and Sorbie, K.S.: “Low Salinity Oil Recovery – An Experimental Investigation” Proceedings of International Symposium of the Society of Core Analysts, Trondheim, Norway, Sept. 2006.

Lee, S.Y., Webb, K.J., Collins, I.R., Lager, A., Clarke, S.M., O’Sullivan, M., Routh, A.F., and Wang, X. 2010. Low Salinity Oil Recovery—Increasing Understanding of the Underlying Mechanisms. Paper SPE 129722 presented at the SPE Improved Oil Recovery Symposium, Tulsa, 24–28 April. doi: 10.2118/129722-MS.

Maini, B.B., Is it Futile to Measure Relative Permeability for Heavy Oil Reservoirs; Presented at the 46th Annual Technical Meeting of the Petroleum Society of CIM, Banff, AB, Canada, May 14-17, 1995.

Mohanty, K.K., 2004. Development of Shallow Viscous Oil Reserves in North Slope, Final Report to the U.S. Department of Energy, ID Number: DE-FC26-01BC15186.

Rangel-German, E.R., Schembre, J., Sandberg, C., and Kovscek, A.R., 2004. Electrical-heating-assisted Recovery for Heavy Oil, Soc. Pet. Eng. J., 45 213–231.

Sahni, A. Gadelle, F., Kumar, M., Tomutsa, L., and Kovscek, A.R. 2004. Experiments and Analysis of Heavy Oil Solution Gas Drive. SPEREE 7 (3): 217-229. SPE-88442-PA.

Schembre, J.M., Tang, G.-Q., and Kovscek, A.R., 2006. Interrelationship of Temperature and Wettability on the Relative Permeability of Heavy Oil in Diatomaceous Rocks, Soc. Pet. Eng. J., 93831-PA-P.

Strycker, A. and Wang, S., 2000. Recovery Processes for Schrader Bluff, Alaska. TRW Petroleum Technologies.

Strycker, A., Sarathi, P., and Wang, S., 1999. Evaluation of In Situ Combustion for Schrader Bluff, Fossile Energy.

Tang, G.-Q., Y. Leung, L. M. Castanier, A. Sahni, F. Gadelle, M. Kumar, and A. R. Kovscek, 2006a. An Investigation of the Effect of Oil Composition on Heavy Oil Solution Gas Drive, Soc. Pet. Eng. J., 11(1) 58-70.

Tang, G.-Q., Y. Leung, L. M. Castanier, A. Sahni, F. Gadelle, M. Kumar, and A. R. Kovscek, 2006b. Heavy-Oil Solution Gas Drive in Consolidated and Unconsolidated Rock, Soc. Pet. Eng. J., 11(2) 259-268.

Tang. G.-Q. and A. R. Kovscek, 2011. High-Resolution Imaging of Unstable, Forced Imbibition in Berea Sandstone, Transport in Porous Media 86: 647-664. DOI 10.1007/s11242-010-9643-3.

Treinen, R.J., Ring, W.W., Spence, A..P., Mirabal, M. de. And Hueurta, M.: "Hamaca: Solution Gas Drive Recovery in a Heavy Oil Reservoir, Experimental Results", SPE 39031 presented at the Fifth Latin America and Caribbean Petroleum Engineering Conference and Exhibition held in Rio de Janeiro, Brazil, 30 August – 3 September 1997.

Vittoratos, E., Brice, B.W., West, C.C., Digert, S.A., Chambers, B.C., 2006. Optimizing Heavy Oil Waterflooding: Are the Light Oil Paradigms Applicable?, First World Heavy Oil Conference, Beijing, China, Nov. 12 – 15.

Vittoratos, E., West, C.C., Black, C.J., 2007. Flow Regimes of Heavy Oils Under Water Displacement, EAGE 14th European IOR, April 22 -24, Cairo, Egypt.

Vittoratos, S. E. and C.C. West, 2010. Optimal Heavy Oil Waterood Management May Differ from that of Light Oils, SPE 129545.

Appendix A

A. Three-Phase Models

For all of the studies discussed in this work, we have chosen to use the Stone II three-phase model to determine the relative permeability to oil, water, and gas as the saturation of each phase changes with time (Aziz and Settari 1979). Given the large importance of the relative permeability to gas in all of our models shown in Chapter 3, it can be argued that the three-phase model is of great importance. This would be a valid argument if the relative permeability curves used are based off physical data and it was theoretically possible to better match observed data in a reservoir. For our purposes, our relative permeability curves are constructs, loosely based off real data, but in no way used to match some particular fluid and rock properties. It can be argued then, that the relative permeability curves can take into account any inaccuracies in the three-phase model. If an accurate three-phase model was desired, there are possible options in the literature that could be applied (Blunt 2000).

For most commercial applications, either The Stone II or Baker's Linear Interpolation Model would be used to model three-phase flow, due to their widespread availability in numerical simulators. A summary of these models is available in the CMG STARS manual (2010). To test the sensitivity of our results to the three-phase model we chose, we conducted simulations of identical models to those discussed in Chapter 3 and 4, only altering the three-phase model. Our base case simulations were conducted using the Stone II three-phase model, so we will now consider the results found using Baker's Linear Interpolation Model.

Figure A-1 shows the recovery simulated for each of the five sets of relative permeability curves developed in section 3.3, applied on our base case core model and using Baker's Linear Interpolation three-phase model. There is an obvious similarity with the results of our base case results shown in Figure 3-29. Taking the difference between recovery values between the results found using Stone's II Model and Baker's Linear Interpolation three phase model at various VRR shows how trivial the difference is in most cases. Figure A-2 shows that in all but the foamy oil case, the difference between the results using either three-phase model is negligible. For the foamy oil case, the difference is above 1% in the cases between VRR of 0 and 1.

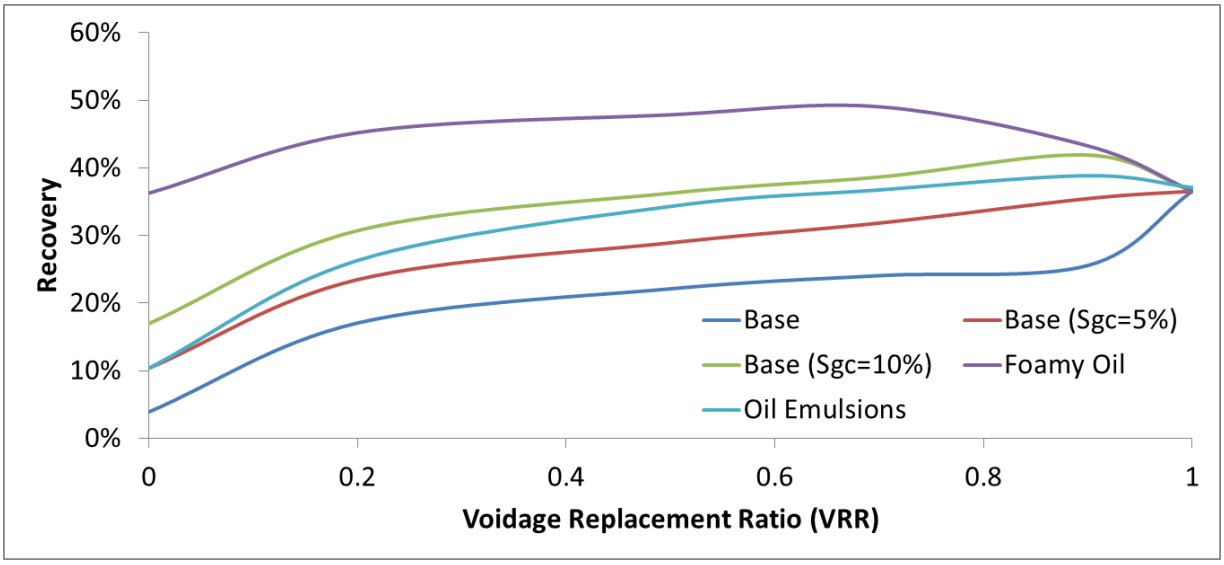

Figure A-1: Recovery as a function of VRR at 0.6 days for five base cases in base case core model using Baker's Linear Interpolation three-phase model.

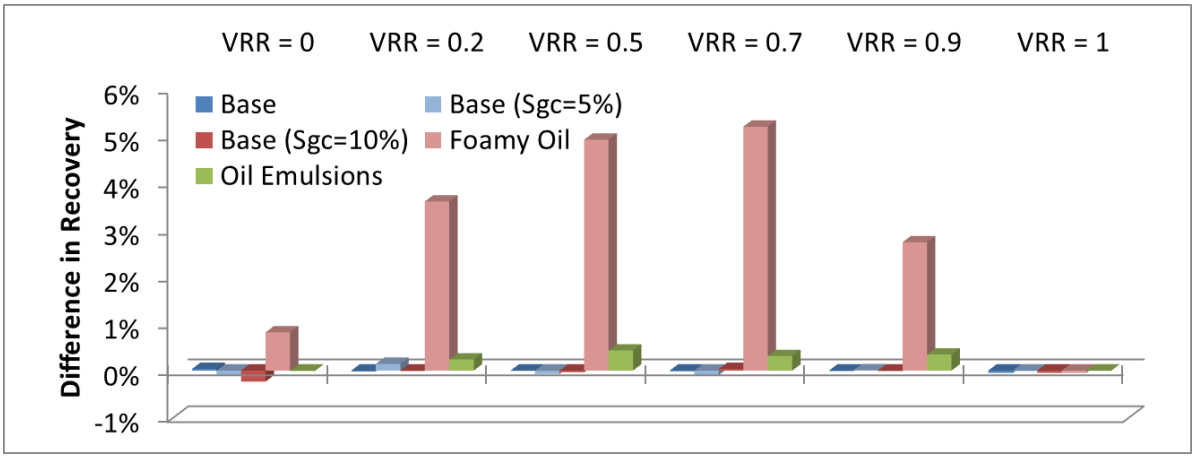

Figure A-2: Difference between the recovery found using the Stone II three-phase model and the recovery found using Baker's Linear Interpolation three-phase model for various VRR for the base case core model.

If we consider the ternary diagrams generated using both Stone's II Model and the Baker Linear Interpolation Model given the foamy oil relative permeability curves in Figure 3-28, we might consider a somewhat different result. Figure A-3 shows the ternary diagram pertaining to Stone's II Model, and Figure A-4 to Baker's model, with the color representing the relative size of the relative permeability to oil. As can be seen, even though there is a much larger area encompassing the highest relative permeability to oil values for the Baker model, because the Baker has much shallower gradients relative to Stone's model, the area of interest lies in a more favorable position with Stone's model than with Baker's. We define the area of interest as the point at which the majority of the

simulation occurs, i.e., the point at which the saturations remain relatively stable at after pressure depletion in the model.

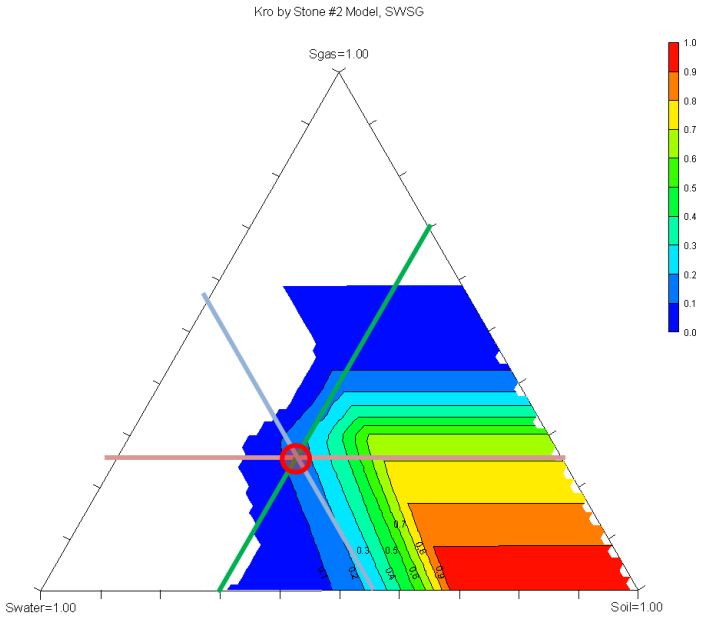

Figure A-3: Ternary diagram for the foamy oil case's relative permeability to oil generated using the Stone II three-phase model. The intersection point highlighted with the red circle indicates the average saturations of each phase after pressure depletion.

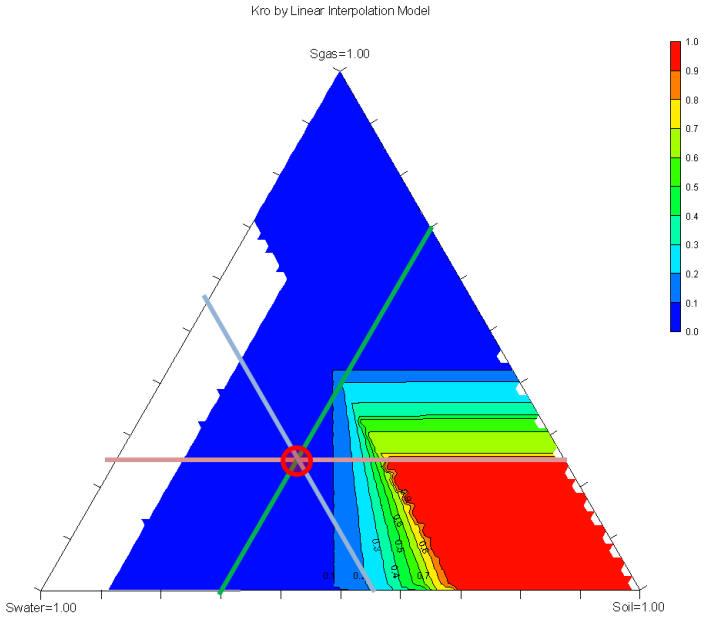

Figure A-4: Ternary diagram for the foamy oil case's relative permeability to oil generated using Baker's Linear Interpolation Model. The intersection point highlighted with the red circle indicates the average saturations of each phase after pressure depletion.

The foamy oil case is an idealized case based upon core-level observations, as discussed in section 4.3. Our main concern is how valid the choice of our three-phase model is for a commercial application. Thus, we consider the sensitivity to our three-phase model in the large model discussed in Chapter 4. Figure A-5 shows the recovery profiles as we vary the critical gas saturation in Li's modified model. Figure A-6 shows the magnitude of the difference between the results observed with the Stone II and Baker's Linear Interpolation three-phase models. As can be seen, the differences are highest for the cases between a VRR of 1 or 0, and only become significant when the critical gas saturation is highest. A 4% difference might be considered significant in some cases, but given the large uncertainty already present in reservoir simulation, such a discrepancy might be considered negligible.

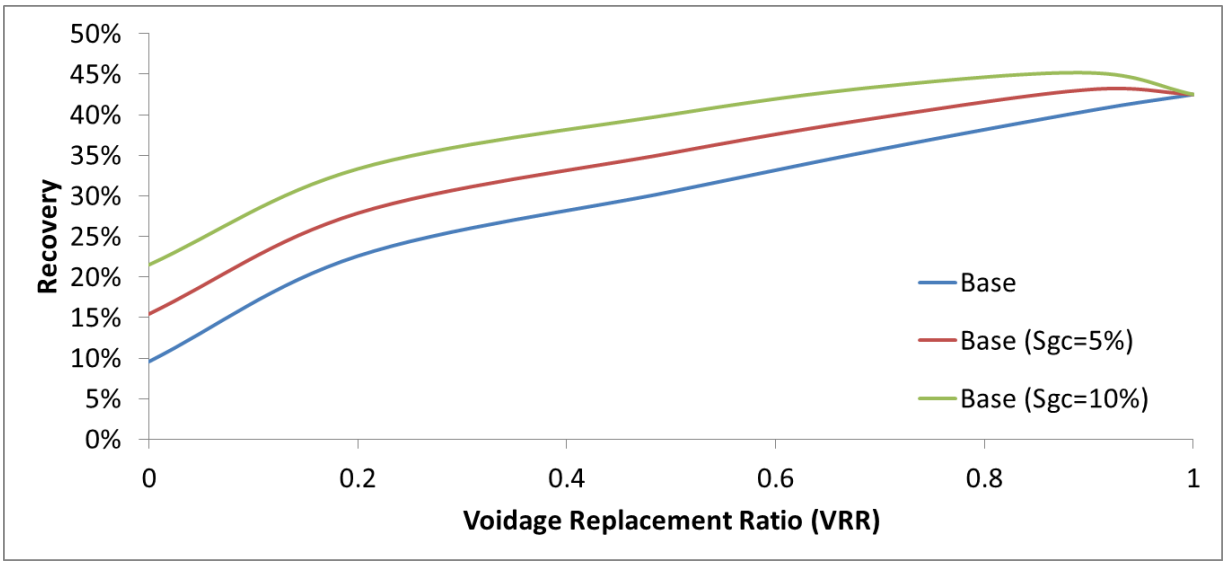

Figure A-5: Recovery as a function of VRR at 0.6 days for five base cases in the reservoir-scale model using Baker's Linear Interpolation three-phase model.

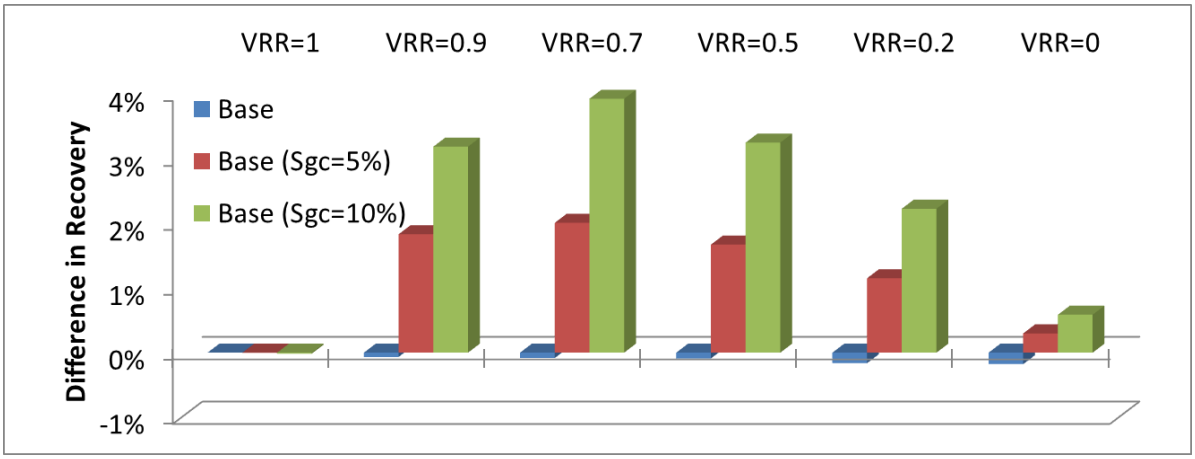

Figure A-6: Difference between the recovery found using the Stone II three-phase model and the recovery found using Baker's Linear Interpolation three-phase model for various VRR for a reservoir-scale model.

Again, we can visualize the discrepancies by viewing the ternary diagrams of each 3 phase model. We will consider only the case where the critical saturation is 10%, because this case has the largest differences in end-point recoveries using each three-phase model. The ternary diagrams for each three-phase model are shown in Figure A-7 and A-8. The diagram generated from Stone's model has deeper gradients between each oil relative permeability value when compared to the diagram generated by Baker's model. Because our reservoir-scale models never achieve complete reservoir pressure depletion as with our core-scale models, various cells in our model are being depleted over time. Thus, the full spectrum of our ternary diagrams must be considered below 20% gas saturation, the highest gas saturation achieved the top layers of each channel. As we view the ternary diagrams from right to left along our area of interest, we can immediately see that because of the deeper gradients existing in the ternary diagram produced from Stone's model, there will be longer intervals when the oil relative permeability will be favorable, relative to the scenario in which Baker's model is used. The differences are slight, which is why we see only small differences in results using the two different three-phase models.

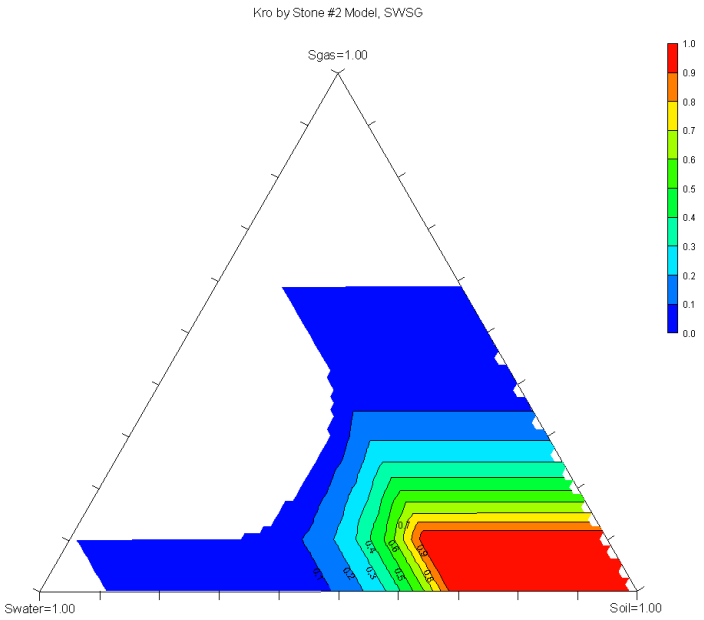

Figure A-7: Ternary diagram for the S_{gc} = 10% case's relative permeability to oil generated using the Stone II three-phase model.

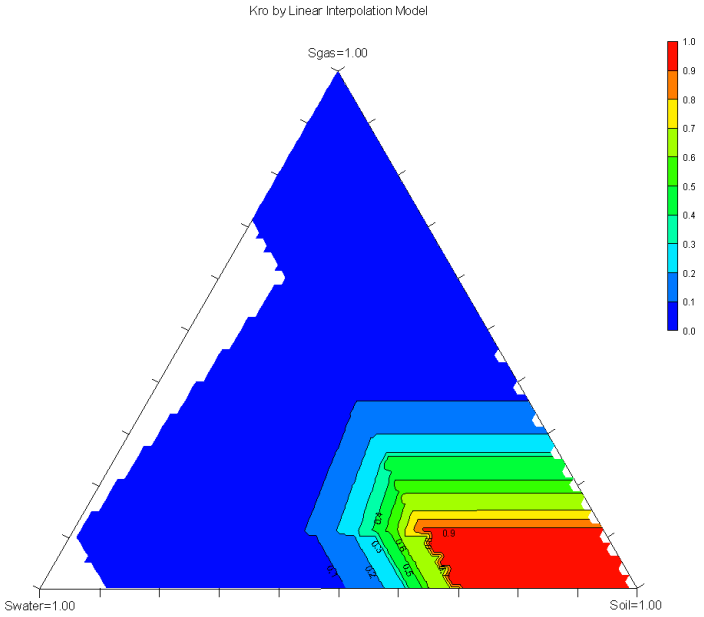

Figure A-8: Ternary diagram for the S_{gc} = 10% case's relative permeability to oil generated using Baker's Linear Interpolation Model.

We would like to make clear, our results do not imply the three-phase model is unimportant; rather, we imply that given the limitations imposed by modern reservoir

simulators, the choice of a three-phase model is not the greatest concern in predicting the effectiveness of a particular VRR. In both the core-scale and reservoir-scale models, it has been shown that the three-phase model does not affect the optimal VRR. Models based off real data and real rock properties might require the modified three-phase models discussed in the literature, if gas or oil trapping was significant for example.

Appendix B

B. Sample Input Files

B.1. Sample STARS File

```
** 2011-11-30, 2:13 PM, delgadde
** Fine-gird coreflood design
** VRR = 0.7; base case Corey rel perms

**********************************************************************
        ** SAMPLE DAT FILE USED FOR OPTIMAL VRR STUDIES
**********************************************************************

*INUNIT       *FIELD
*OUTUNIT    *SI
*OUTSRF      *WELL *DOWNHOLE *COMPONENT *ALL      *MASS
*OUTSRF *GRID      *PRES *SW *SO *SG *VISO *VISG *KRW *KRO *KRG
**       OUTPRN *GRID *SO *SG *PRES *VISO

**********************************************************************
                ** RESERVOIR AND K-VALUES DESCRIPTION
**********************************************************************

*GRID CART 91 9 9
*DI     *CON  0.005407978
*DJ     *CON  0.007290761
*DK     *CON  0.007290761
*DEPTH *TOP          1         1         1         4300
*POR   *CON  0.25
*PERMI         *CON  250
*PERMJ         *EQUALSI
*PERMK         *EQUALSI
*END-GRID

*MODEL 3 3 3 1
```

```
*COMPNAME       'WATER'  'OIL'   'GAS'
**              -----    --------   ------
   *CMM         18.02      385.5    16.0
   *PCRIT       3206.2     140      667.2
   *TCRIT       705.4      1100     -116.59

   *MASSDEN     62.4     58.706      38
   *CP          1.e-6    1.e-6       1.e-6
   *CT1         1.e-4    1.e-4       1.e-4

   *CPL1        100      132.5       100

   *KV1         0.0      0.0         7.9114E+4
   *KV4         1.0      0.0         -1583.7
   *KV5         0.0      0.0         -446.8

   *AVG         0.02       0.02          0.02
   *BVG         0.0        0.0           0.0

*VISCTABLE
**      Temp H20  Oil        Gas
        59    0       100          3
        68    0       100          3
        77    0       100          3
        100     0       100          3


*PRSR 1500
*TEMR 75
*PSURF 14.7
*TSURF 75

**********************************************************************************
                                        ROCKFLUID
**********************************************************************************

** Base Case Relative Permeability Curves (Sgc =0)

SWT
**$       Sw        krw        krow
0.3       0         1
0.36      0.005011872   0.560188001
0.42      0.024681355   0.293085902
0.48      0.062716077   0.140617451
0.54      0.121545247   0.060232637
0.6       0.203063099   0.022097087
```

```
0.66    0.308850192   0.006476345
0.72    0.440276486   0.001330966
0.78    0.598559007   0.000143108
0.84    0.784797791   3.16228E-06
0.9     1         0

SLT
**$ Sl  krg     krog      Pc
0.4     0.627   0
0.46    0.535341985   0.000398107
0.52    0.448644679   0.004202444
0.58    0.367210086   0.016680623
0.64    0.291403267   0.04436127
0.7     0.221677976   0.094732285
0.76    0.158619847   0.176081712
0.82    0.103026613   0.297394776
0.88    0.056080585   0.468280373
0.94    0.019827481   0.698915275
1       0         1

**************************************************************************
                                INITIAL
**************************************************************************
*VERTICAL *OFF

*SW *CON 0.3
*SO *CON 0.7

*MFRAC_OIL 'OIL' *CON 0.6318
*MFRAC_OIL 'GAS' *CON 0.3682

*PRES CON    1500
*TEMP        CON    75

**************************************************************************
                                NUMERICAL
**************************************************************************

** Depending on the rel perms/oil composition, may need to adjust these parameters

*DTMAX 0.01
*CONVERGE *TOTRES *TIGHT
*MINPRES 15
*NORTH 60
*ITERMAX 100
```

```
**************************************************************************
                                    RUN
**************************************************************************

*TIME0
*DTWELL     0.0001
*WELL        'INJ'
*INJECTOR   'INJ'
*INCOMP     WATER        1        0        0
*TINJW       75

*OPERATE   MAX  BHW  0.000157596  **Found by multiplying 'OP ' value by VRR
*MONITOR   MIN   BHP   16      SHUTIN
**         rad  geofac  wfrac  skin
**GEOMETRY  I  1.28E-3  0.249  1.  0.
*PERF'INJ'
**$ i j k
   1 5 5   1000

*WELL        'OP '
*PRODUCER 'OP '

*OPERATE   MAX  BHL   0.000225136                  ** 1/10th PV/hr
*OPERATE   MIN   BHP   16      *CONT          *REPEAT

**         rad  geofac  wfrac  skin
**GEOMETRY  I  1.28E-3  0.249  1.  0.
*PERF'OP '
**$ i j k
   91 5 5   1000

WSRF WELL TIME
TIME  0.01
TIME  0.011
TIME  0.012
TIME  0.013
TIME  0.014
TIME  0.015
TIME  0.02
TIME  0.025
TIME  0.03
TIME  0.035
TIME  0.04
TIME  0.045
TIME  0.050
TIME  0.055
```

```
TIME  0.06
TIME  0.065
TIME  0.07
TIME  0.075
TIME  0.08
TIME  0.085
TIME  0.090
TIME  0.10
TIME  0.2
TIME  0.3
TIME  0.4
TIME  0.5
TIME  0.6


*STOP
```

B.2. Sample IMEX File

```
**********************************************************************
**
**            *IO
**
**********************************************************************

RESULTS SIMULATOR IMEX
**Black Oil Model
**to simulate reduced VRR production schemes
**Base case Corey-generated rel perms
**VRR=0.7
**Grid and well locations taken from  Hongmei Li's Eclipse files


** Specifies the title for the run
*TITLE1
'3D SIMULATION MODEL FOR A 50X50X50 REGUL'

** Specify units used in the model (metric, field, lab)
*INUNIT *FIELD
**METRIC
*OUTUNIT *FIELD

** Outputs to CMG irf and mrf files
**WSRF        *WELL         *TIME
*OUTSRF      *WELL *DOWNHOLE
*WSRF         *GRID*TIME
```

```
*OUTSRF *GRID     *SO *SG *SW          *PRES *KRO *KRW *KRG *VISO *VISW
*VISG

** Outputs to CMG out file
*OUTPRN     *GRID*NONE
*OUTPRN     *WELL         *BRIEF
*OUTPRN     *RES  *EXCEPT      *HCPV


**********************************************************************
**
**           *GRID
**
**********************************************************************

*INCLUDE 'HongmeiLiGrid.str'       ** See Hongmei Li 2008

**********************************************************************
**
**           *MODEL
**
**********************************************************************

*MODEL *BLACKOIL

*DENSITY *OIL 58.6137
*DENSITY *GAS 0.0410687
*DENSITY *WATER 62.3074
*PVT BG 1
14.7    1.2906200 1.00016         1         98.6538         0.02
163.23  14.916000 1.00264         0.0883630 86.0276         0.02
311.76  29.700700 1.00534         0.0453997 75.0174         0.02
460.29  45.799200 1.00829         0.0301822 65.4163         0.02
608.82  63.394800 1.01153         0.0224067 57.044          0.02
757.35  82.706600 1.0151          0.0176972 49.7433         0.02
905.88  103.99800 1.01905         0.0145482 43.3769         0.02
1054.41 127.59100 1.02344         0.0123024 37.8253         0.02
1202.94 153.88000 1.02835         0.0106272 32.9843         0.02
1351.47 183.35300 1.03387         0.0093360 28.7628         0.02
1400.21 193.81800 1.03584         0.0089757 27.4989         0.02
1500    215.24398 1.03987336684448 0.0083162 24.9111982970866 0.02
*BOT 1
1400.21 1.03584
1500    1.03333
*VOT 1
1400.21 27.4989
```

1500 27.4989
*REFPW 14.7
*BWI 1
*CW 4E-05
*VWI 0.916101
*CVW 0

****
**
** *ROCKFLUID
**
****

*ROCKFLUID

*RPT 1

SWT
**$ Sw krw krow
0.3 0 1
0.36 0.005011872 0.560188001
0.42 0.024681355 0.293085902
0.48 0.062716077 0.140617451
0.54 0.121545247 0.060232637
0.6 0.203063099 0.022097087
0.66 0.308850192 0.006476345
0.72 0.440276486 0.001330966
0.78 0.598559007 0.000143108
0.84 0.784797791 3.16228E-06
0.9 1 0

SLT
**$ Sl krg krog Pc
0.4 0.627 0
0.46 0.535341985 0.000398107
0.52 0.448644679 0.004202444
0.58 0.367210086 0.016680623
0.64 0.291403267 0.04436127
0.7 0.221677976 0.094732285
0.76 0.158619847 0.176081712
0.82 0.103026613 0.297394776
0.88 0.056080585 0.468280373
0.94 0.019827481 0.698915275
1 0 1

```
**********************************************************************
**
**          *INITIAL
**
**********************************************************************

*INITIAL
*VERTICAL *BLOCK_CENTER *WATER_OIL_GAS

*REFDEPTH 0.0
*REFPRES 1800
*DWOC 1000
*DGOC 0
*PB *CON 0

**********************************************************************
**
**          *NUMERICAL
**
**********************************************************************

**NUMERICAL
**NORTH 60
**ITERMAX 100

**********************************************************************
**
**          *RUN
**
**********************************************************************

*RUN
*DATE 2012 1 1

*GROUP 'G1' *ATTACHTO 'FIELD'
*GROUP 'INJ' *ATTACHTO 'FIELD'
*WELL 'P3' *ATTACHTO 'G1'
*XFLOW-MODEL 'P3' *ZERO-FLOW
*WELL 'P2' *ATTACHTO 'G1'
*XFLOW-MODEL 'P2' *ZERO-FLOW
*WELL 'P1' *ATTACHTO 'G1'
*XFLOW-MODEL 'P1' *ZERO-FLOW

*WELL 'I1' *ATTACHTO 'INJ'
*XFLOW-MODEL 'I1' *ZERO-FLOW
*WELL 'I2' *ATTACHTO 'INJ'
```

```
*XFLOW-MODEL 'I2' *ZERO-FLOW

*PRODUCER 'P1'
*OPERATE *MAX *BHF 1000
*OPERATE *MIN *BHP 300          *CONT          *REPEAT
*GEOMETRY *K 0.25 0.37  1.0 0.0
*PERF *GEOA  'P1'
 27 41 5 1.0
 27 41 6 1.0
 27 41 7 1.0
 27 41 8 1.0
 27 41 9 1.0
 27 41 10 1.0
 27 41 11 1.0
 27 41 12 1.0
 27 41 13 1.0
 27 41 14 1.0
 27 41 15 1.0
 27 41 16 1.0
 27 41 17 1.0
 27 41 18 1.0
 27 41 19 1.0

*PRODUCER 'P2'
*OPERATE *MAX *BHF 1000
*OPERATE *MIN *BHP 300          *CONT          *REPEAT
*GEOMETRY *K 0.25 0.37  1.0 0.0
*PERF *GEOA  'P2'
 20 29 24 1.0
 20 29 25 1.0
 20 29 26 1.0
 20 29 27 1.0
 20 29 28 1.0
 20 29 29 1.0
 20 29 30 1.0
 20 29 31 1.0
 20 29 32 1.0
 20 29 33 1.0
 20 29 34 1.0
 20 29 35 1.0

*PRODUCER 'P3'
*OPERATE *MAX *BHF 1000
*OPERATE *MIN *BHP 300          *CONT          *REPEAT
*GEOMETRY *K 0.25 0.37  1.0 0.0
*PERF *GEOA  'P3'
```

```
 26 15 11 1.0
 26 15 12 1.0
 26 15 13 1.0
 26 15 14 1.0
 26 15 15 1.0
 26 15 16 1.0
 26 15 17 1.0
 26 15 18 1.0
 26 15 19 1.0
 26 15 20 1.0
 26 15 21 1.0
 26 15 22 1.0
 26 15 23 1.0

*INJECTOR   'I1'
*INCOMP      *WATER
*OPERATE *MAX *BHW 1050
*OPERATE *MAX *BHP 6000
*GEOMETRY *K 0.25 0.37  1.0 0.0
*PERF *GEOA  'I1'
 33 50 16 1.0
 33 50 17 1.0
 33 50 18 1.0
 33 50 19 1.0
 33 50 20 1.0
 33 50 21 1.0
 33 50 22 1.0
 33 50 23 1.0
 33 50 24 1.0
 33 50 25 1.0
 33 50 26 1.0
 33 50 27 1.0
 33 50 28 1.0
 33 50 29 1.0
 33 50 30 1.0
 33 50 31 1.0
 33 50 32 1.0
 33 50 33 1.0

*INJECTOR   'I2'
*INCOMP      *WATER
*OPERATE *MAX *BHW 1050
*OPERATE *MAX *BHP 6000
*GEOMETRY *K 0.25 0.37  1.0 0.0
*PERF *GEOA  'I2'
 27 1 5 1.0
```

27 1 6 1.0
27 1 7 1.0
27 1 8 1.0
27 1 9 1.0
27 1 10 1.0
27 1 11 1.0
27 1 12 1.0
27 1 13 1.0
27 1 14 1.0
27 1 15 1.0
27 1 16 1.0
27 1 17 1.0
27 1 18 1.0
27 1 19 1.0
27 1 20 1.0
27 1 21 1.0

*TIME 180
*TIME 360
*TIME 540
*TIME 720
*TIME 900
*TIME 1080
*TIME 1260
*TIME 1440
*TIME 1620
*TIME 1800
*TIME 1980
*TIME 2160
*TIME 2340
*TIME 2520
*TIME 2700
*TIME 2880
*TIME 3060
*TIME 3240
*TIME 3420
*TIME 3600

*STOP

Appendix C

C. Grid Size Refinement

When considering our base case, core-scale model we considered various grid sizes. We sought to make observations on a fine scale so we needed a generous amount of cells. Given the sheer number of simulations we were required to perform, we also did not want a grid so fine our results took an excessive amount of time to generate. We chose a grid with a total of 7371 active cells, with dimensions 91 by 9 by 9 cells. To test the sensitivity of our model to grid refinement, we simulated the five cases introduced in section 3.2 on two other core-scale models with identical volumes. The results of our simulations on a model with 15 by 2 by 2 cells, for a total of 60 active cells, are shown in Figure C-1.

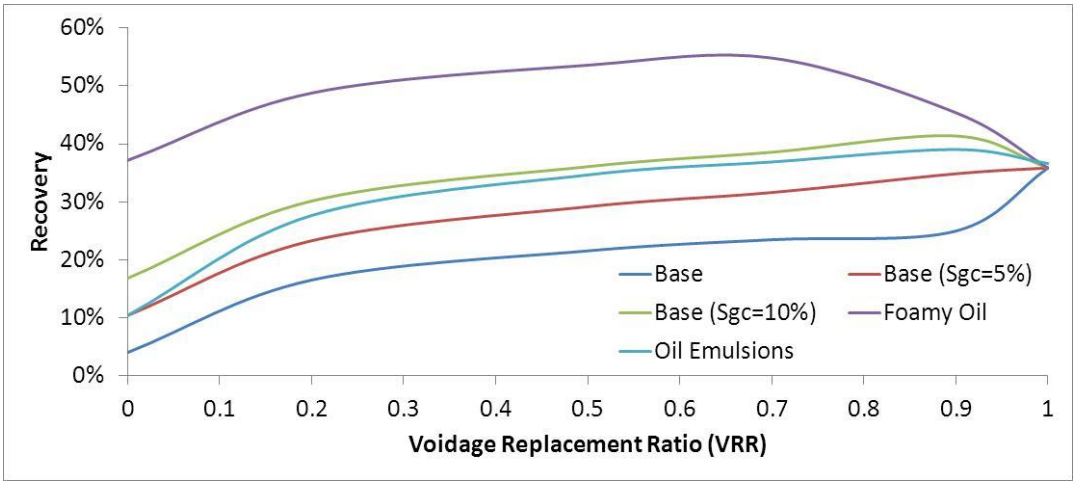

Figure C-1: Recovery as a function of VRR at 0.6 days for five cases in coarse-grid model.

Even our coarse-grid model yields acceptable results as shown in Figure C-2. The difference in recovery for every simulation is less than 2%. In general, the fine-scale model yields slightly more optimistic recoveries, but the differences are negligible. A finer-scale model was also used with dimensions 121 by 11 by 11 cells, for a total of 14641 active cells. The results using this finer-scale model were virtually identical to that of the base case model, as expected.

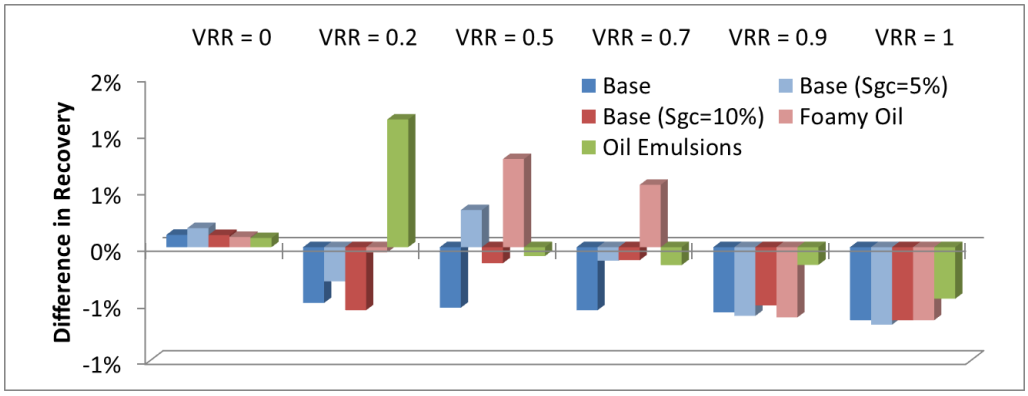

Figure C-2: Difference between the recovery found using the coarse-scale model and the recovery found using the fine-scale, base case model for various VRR.

The difference between our coarse, base, and finer grid models is negligible or slight when we consider homogeneous cores, as expected. Whether our base case model captures heterogeneity just as well as a finer scale model is not intuitive. Thus, we introduced a model that is 182 by 18 by 18 cells in dimension, for a total of 58968 active cells. Note the model is refined by a factor of 8 when compared to our base case, as each dimension is twice as large as the original case. The model was made in a likeness to the one discussed in section 3.3.7, with impermeable cells in either the i or j direction. The volume of this model and the base case model is identical, as well as the volume of the impermeable walls in both the cul-de-sac model presented in section 3.3.7 and the current model; i.e., the only difference between this new model and the previous cul-de-sac model is the refinement of the model. Figure C-3 shows the results of our sensitivity to the five cases introduced in section 3.2 on the refined cul-de-sac model.

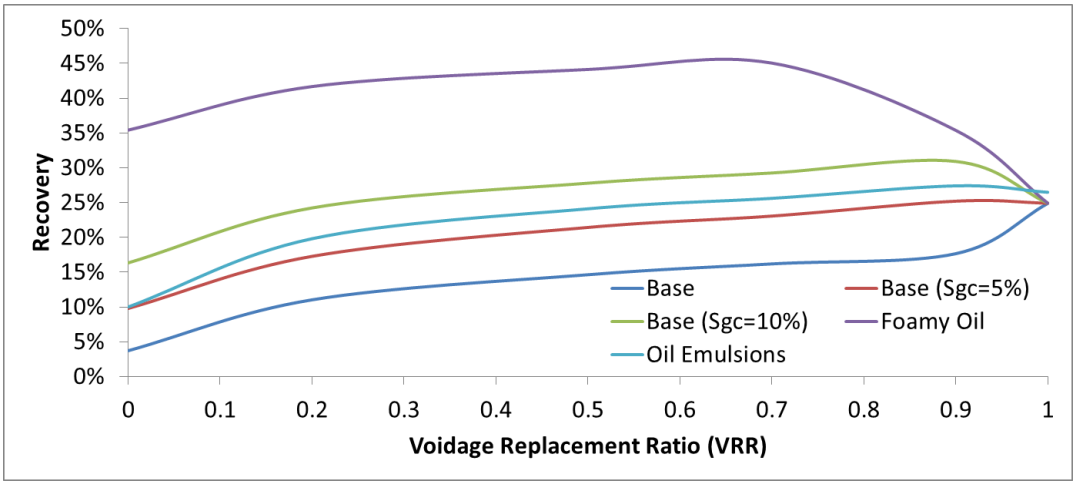

Figure C-3: Recovery as a function of VRR at 0.6 days for five cases in the refined cul-de-sac model.

The differences between the results found using the refined cul-de-sac model and the cul-de-sac model presented in section 3.3.7 are shown in Figure C-4. Notice the differences are relatively small in most cases and increase with the VRR. Given that recovery generally increases with the VRR, the fact the difference in recovery is highest at higher VRR's is not surprising at first glance. What is surprising is the variance is not directly correlated with the magnitude of the recovery. For example, the 10% critical gas saturation case has the highest recovery at a VRR of 0.9 for both models, but the largest variation between results occurs at a VRR of 1, just as with all the other cases. The foamy oil case has the lowest recovery at a VRR of 1, and yet still has the largest discrepancy between the results of the two models at a VRR of 1. There does not seem to be a correlation between variations between the results of the two models and gas mobility, as evidenced by the differences associated with the three cases with varying critical gas saturations.

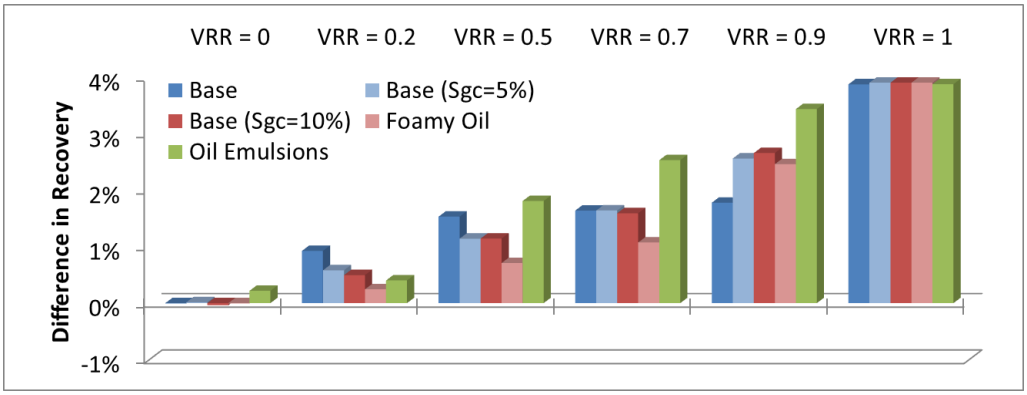

Figure C-4: Difference between the recovery found using the refined cul-de-sac model and the recovery found using the original cul-de-sac model presented in section 3.3.7 for various VRR.

From Figure C-4, our original model potentially makes a VRR less than 1 appear slightly more attractive than it deserves. The refined cul-de-sac model does not affect the optimal VRR, however. The differences between the results of the two models are slight, never exceeding 4%, and given that the refined cul-de-sac model is more prone to numerical errors due to the cells' smaller size, and because it takes significantly longer to simulate, the original discretization of the cul-de-sac model is appropriate and accurate.